CONDITION MONITORING OF HIGH EFFICIENCY HEATING, VENTILATION AND AIR CONDITIONING SYSTEMS

A Dissertation
Presented to
The Academic Faculty

by

Chen Jiang

In Partial Fulfillment
Of the Requirements for the Degree
Doctor of Philosophy in the
School of Electrical and Computer Engineering

Georgia Institute of Technology
August 2017

CONDITION MONITORING OF HIGH EFFICIENCY HEATING, VENTILATION AND AIR CONDITIONING SYSTEMS

Approved by:

Dr. Thomas G. Habetler, Advisor
School of Electrical and Computer Engineering
Georgia Institute of Technology

Dr. Sheldon M. Jeter
School of Mechanical Engineering
Georgia Institute of Technology

Dr. Ronald G. Harley
School of Electrical and Computer Engineering
Georgia Institute of Technology

Dr. Stephen Fedigan
Kilby Lab
Texas Instruments

Dr. Maryam Saeedifard
School of Electrical and Computer Engineering
Georgia Institute of Technology

Date Approved: 06/20/2017

To

my father, Demin Jiang,

my mother, Meidan Chen,

my wife, Jiaying Huang.

献给我亲爱的父亲，母亲和妻子

ACKNOWLEDGEMENTS

It is great honor for me to spend five years on my PhD journey in Georgia Tech. I must admit that it is a challenging and exciting process and cannot be completed without the help of advisors, teachers, colleagues, family and friends. I am so deeply grateful to you for constant guidance and support.

I want to say thank you to my advisor Dr. Thomas G. Habetler for his continual support and guidance. His invaluable suggestions have helped me a lot when I met difficulties.

I also want to thank Dr. Ronald G. Harley and Dr. Maryam Saeedifard for helpful comments and for serving on my proposal and thesis committee.

I would like to acknowledge Texas Instruments for providing the financial support for my PhD studies. I also would like to thank Dr. Stephen Fedigan, Dr. Rajan Narasimha and Dr. David Magee from Texas Instruments for their constant suggestions on my Phd projects.

I want to thank Dr. Sheldon M. Jeter for his immense help on mechanical engineering branch of my thesis.

I must also thank the machinists Louis Boulanger, who support a lot on my laboratory experimental setup. I would also like to thank Deborah King for patiently putting up with my frequent requests of procurement and conference travelling.

I am very thankful for all the colleagues in my power research group. I wish to especially thank Dr. Dawei He, Dr. Nan Liu, Dr. Hao Chen, Yi Du, Dr. Lijun He, Dr. Liang Du, Dr. Jie Dang, Dr. Yi Deng, Dr. Zhaoyu Wang, Dr. Dongbo Zhao, Dr. Liangyi Sun, Dr. Heng Yang, Dr. Rui Fan, Dr. Zheyu Tan, Liyao Wu, Sufei Li, Shen Zhang, Qichen Yang, Bai Cui and Chanyeop Park for their invaluable input and countless enlightening conversations.

Most of all, I am eternally grateful for my parents and my wife for the love and encouragement they gave me throughout my life.

TABLE OF CONTENTS

LIST OF TABLES

LIST OF FIGURES

SUMMARY

The objective of the proposed research is to increase energy efficiency in HVAC (Heating, Ventilation and Air conditioning) systems. Energy consumption has increased rapidly in recent decades. This has elevated concerns of a future energy crisis, and heavy negative environmental impacts. An air handler, or air handling unit, is a device used to condition and circulate air as part of a HVAC system. The operation of air handlers account, on average, for 40% of an industrial site's total energy consumption. The air handler in the HVAC system has electrical and mechanical components that can experience problems from time to time. Airflow blockage and a failure of a blower motor are two of the most common problems in air handlers.

Airflow blockage is detected utilizing a current-based condition monitoring method, which analyzes the static pressure of the fan blade, load torque, and the fan motor speeds. For most air handlers, the unbalanced load of the blower wheel is created by unevenly distributed contaminants on the blades. The traditional current-based condition monitoring method is conducted on a brushless DC, or BLDC, fan motor, followed by a stray flux spectrum analysis, which increases reliability in detecting an unbalanced load condition. Static eccentricity and dynamic eccentricity are two of the main faults commonly found in the rotor of a BLDC motor. An improved method for detecting static eccentricity is proposed based on a comparison between the positive sequence current and negative sequence current. Finally, a current-based nonintrusive condition monitoring method is established for refrigerant level detection. A thermal model of a compressor is analyzed under insufficient refrigerant level conditions to explore the mathematical relationship between refrigerant level and stator winding resistance. An undercharged detection algorithm is proposed with a detailed analysis of temperature threshold settings. This algorithm can be easily implemented on the original HVAC system to increase the system's reliability and efficiency, and to reduce

the labor cost of refrigerant level detection.

CHAPTER 1

BACKGROUND AND PROBLEM STATEMENT

Energy consumption has increased rapidly in recent decades. This has elevated concerns of a future energy crisis and heavy negative environmental impacts. The global contribution of energy consumption in residential buildings has increased to 20%, while in commercial buildings it has increased to 40% in developed countries. Most of this energy consumption goes into in heating, ventilation, and air conditioning systems, or HVAC systems for short. A heat pump is a typical HVAC device which has attracted a great deal of attention from researchers recently. Technically, a heat pump is a mechanical-compression cycle refrigeration system with both heating and cooling modes. Installation of this type of system typically includes two parts: an indoor unit, called an air handler, and an outdoor unit, similar to a central air conditioner, but referred to as a heat pump. A compressor circulates refrigerant that absorbs and releases heat as it travels between the indoor and outdoor units [1]. According to the research, the operation of air handlers accounts for 40% of an industrial site's total energy consumption [2]. Thus, increasing energy efficiency in air handlers is the primary objective of this work [3].

Roughly 50% of all commercial HVAC systems in operation have significant faults. A fault might decrease the system's efficiency by roughly 20%, causing the unit to run longer so that it can meet space cooling load demands [4]. The average evaporator airflow of a commercial AC unit is 15-25% less than optimum commissioned values. It has been demonstrated that 34% of residential air conditioners have undercharge problems and 35% of commercial rooftop units' dampers fail within several years of installation. In addition, about 50-67% of residential and commercial air conditioners are either have airflow issues or improperly charged [4].

Some other typical faults include:

• Liquid-line restriction

• Condenser and evaporator fouling

• Low refrigerant charge

• Refrigerant overcharge

• Compressor valve leaks

• Noncondensable gas in the refrigerant

Automated fault detection and diagnostics systems can address these faults by identifying them as they occur. They can communicate the fault to the owner or maintenance personnel if systems are of sufficient severity. This can eliminate reduce peak electricity demand, diagnostic labor, scheduled maintenance costs and wasted energy. Generally, the fault detection and diagnostics system work by measuring a subset of temperatures, pressures, and humidity levels in several stages of the HVAC system [4]. Automated comparisons of what these values should be in a given system against their actual values can provide useful indicators of fault conditions.

First, the embedded fault detection and diagnostics system in each device's controller has been proven to be convenient and accurate, due to specifically tailored algorithms. However, this requires additional sensor and communications hardware beyond what is traditionally fielded, and adds to the system's upfront cost. Embedded fault detection and diagnostics systems offer continuous, dedicated monitoring, which allows for the recording and reporting of faults as they occur. This ensures that repairs are performed in a timely manner. The National Institute of Standards and Technology has developed a set of algorithms for detecting faults in air-handling units and variable-air-volume boxes that has been integrated into some control units. These higher-end units have alarms for several conditions such as fouled coils, incorrect damper positions, and leaking valves [4].

Next, fault detection and diagnostics systems offer continuous monitoring and feedback on system faults by sending sensor information to a data server that continuously monitors connected systems and reports faults. The algorithms of fault detection and diagnostics systems on the server can be continuously updated independent of the data coming from the sensors.

Although the use of fault detection and diagnostics systems does typically result in reduced electricity use, these savings are usually small in comparison to the typical monthly operating costs of a business at a commercial site. It can also provide several other significant monetary benefits that amortize over the life of the system. These benefits, beyond reduced electricity use, include elimination of preventative maintenance services, increased system lifetime, and reduced repair labor and parts. Reduced maintenance and repair labor is another key benefit. Generally, labor costs are high, while replacement component costs are low. If the fault detection and diagnostics system can diagnose the problem, repair personnel can more quickly and efficiently address these faults. Emergency service calls should also be reduced by catching developing faults before they become severe, allowing the owner to schedule service calls at typical nonemergency rates. The California Energy Commission's Title 24 now provides credits for the use of fault detection and diagnostics systems in packaged rooftop units. Other regulations will likely include these systems as well, as it become more widely studied and recognized.

Fault detection and diagnostics systems can increase the reliability of HVAC systems. Reliability is defined as the probability that the system (under steady state conditions) will still work at a time t, with no maintenance work done. The reliability is a function of the number of components that can fail. A system with more components gives, in most cases, a lower reliability. Among all of the different parts in an HVAC system, the ventilation system has the lowest reliability. This indicates that there are

more failures in the ventilation system than in others [4].

1.1 Introduction to Air Handlers

An air handler, or air handling unit, is a device used to condition and circulate air as part of a HVAC system. According to the Federation of European Heating, Ventilation and Air-conditioning Associations, air handlers can be applied in many different conditions, such as office buildings, cleanrooms, and swimming pools. Before 1970, the requirements for air handlers were basically moderate humidity and temperature adjustment, but other requirements such as low acoustic noise were added, and are explained in the literature [5]. Because of these new requirements, today's air handlers consume large amounts of energy that account for almost 44% of the energy used by the whole HVAC industry. The structure of a typical air handler is illustrated in Fig. 1.1.

An air handling unit is usually a large enclosure containing a centrifugal fan or blower wheel, heating or cooling elements, and filter racks or chambers. Air handlers usually connect to a ductwork ventilation system that distributes the conditioned air through the building and returns it to the air handler. Air from a room is sucked through the inlet and filtered to be dust-free, before passing through the heating and cooling coil to adjust the temperature. An evaporator inside is used to reduce the temperature. Finally, the air is accelerated by the centrifugal force from the wheel blade which propels the air continuously towards the outlet. The speed and quantity of the air is controlled by the blower, which can typically operate at a variety of set speeds allowing a wide range of air flow rates. Nowadays, to ensure all of the operation monitoring and emergency detection technology is working, the user interface communicates with the variable speed gas furnace via the use of several wires. This communication helps guarantee comfortable air temperature and flow, alongside troubleshooting and

diagnostic capability.

The system under evaluation in the current research is a high efficiency 2 ton variable speed heat pump with a seasonal energy efficiency ratio of 20. The seasonal energy efficiency ratio, or SEER, defines the efficiency of a heat pump. In the U.S., the SEER is the ratio of cooling in British thermal unit (BTU) to the energy consumed in watt-hours. The higher the unit's SEER rating, the higher the energy efficiency. Substantial energy savings can be obtained by using more efficient systems. For example, by upgrading from SEER 9 to SEER 13, the power consumption is reduced by 30%.

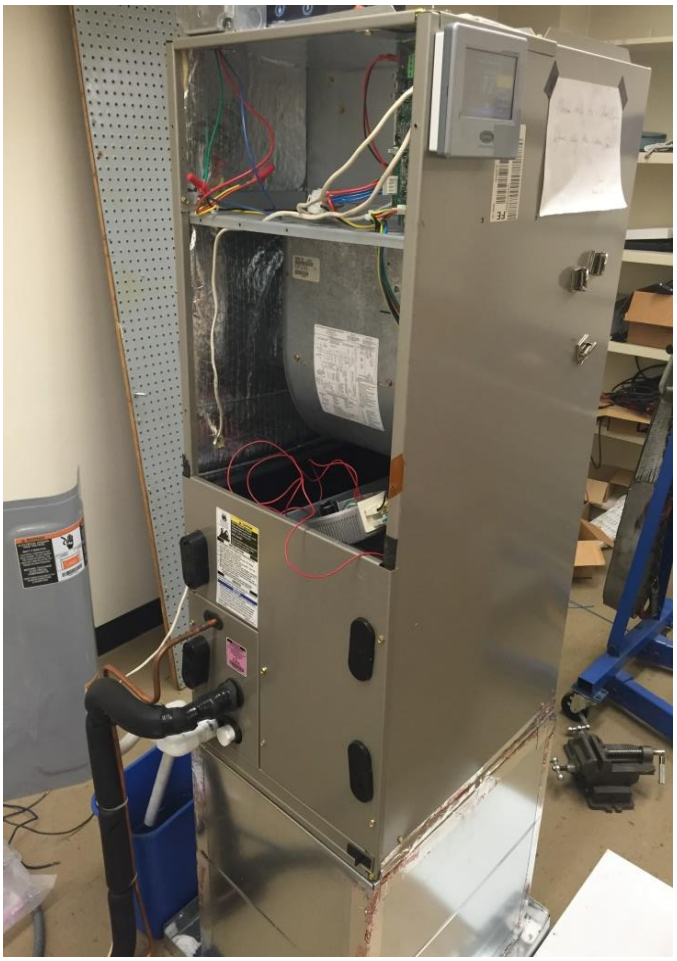

Fig. 1.1. Air handler

1.2 Introduction to the Outdoor Unit

Heat pumps have both a heating and cooling mode, while air conditioners have only a cooling mode. The relevant extra components in heat pumps which differentiate them from air conditioners give them different controls and a refrigeration circuit. Although there are many types of heat pumps and air conditioners, the basic way in which they work is generally the same.

The key difference between a heat pump and an air conditioner is the heat pump reverses the process of refrigeration. This process moves the heat in the opposite direction than an air conditioner would. That is, when in air conditioning or cooling mode, the heat pump moves heat to the outside from the inside, while in heating mode, it moves the heat inside from the outside. Refrigerant then absorbs heat from the air. It then moves the heat in the desired direction. The reversing valve accomplishes this process by reversing the refrigeration flow [6].

There is an issue worth noting regarding the tipping point. When the refrigerant is colder than the temperature of the air outdoors, it absorbs this heat. If the temperature outdoors is 45° F, the refrigerant needs to be 35° F to absorb enough heat to be effective. The metering device in the condenser causes a pressure drop on the part of the refrigerant, which drops the temperature of the refrigerant. This usually results in the refrigerant being colder than the outdoor air temperature, and allows it to absorb heat from air that is 45°F or colder to approximately 38°F. When the outdoor air temperature is colder than 38°F, the heat pump will struggle to absorb enough heat to effectively provide heating for indoor comfort. This is the tipping point, or the temperature at which the heat pump fails to provide satisfactory heating.

Heat pumps should have a means of turning the condenser off when the unit reaches its tipping point and stops being able to produce effective heat for indoor

comfort. Many heat pumps are installed without the means of turning the condenser off when they reach their tipping point. There are two methods that can be applied to turn the heat pump off when the tipping point is reached: using an outdoor thermostat to turn off the heat pump condenser when it reaches the tipping point, or the use of an indoor thermostat to read the outside temperature via a remote temperature sensor [6].

The experimental outdoor unit that is the object of this research is shown in Fig. 1.2-1.3. The fan of the outdoor unit is driven by a three-phase brushless DC motor similar to the fan motor in the air handler. It propels the air out of the outdoor unit to exchange heat with the outdoor air.

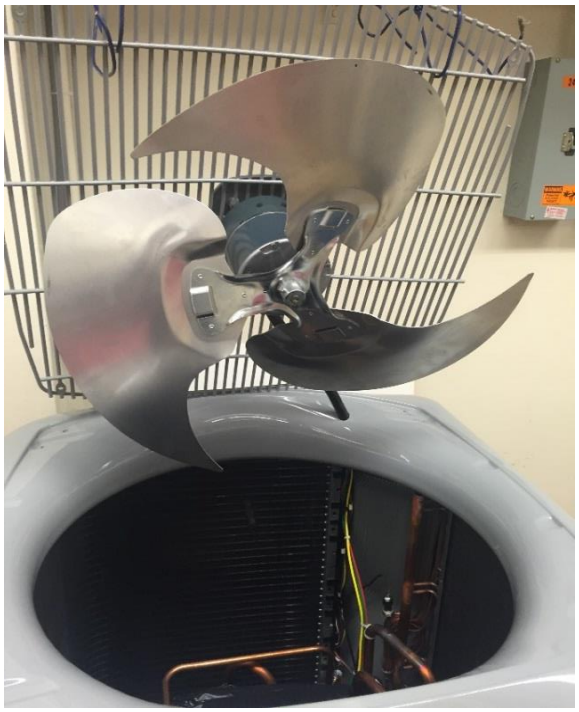

Fig. 1.2: Fan of outdoor unit

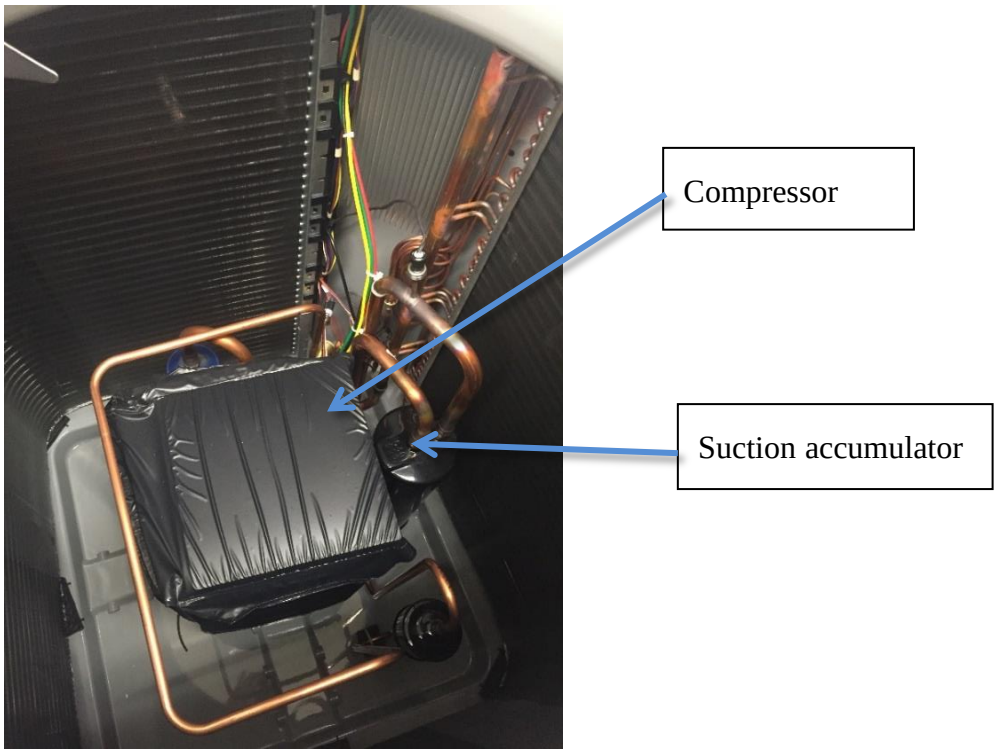

Fig. 1.3: Top view of outdoor unit

The suction accumulator in Fig. 1.3 is used to prevent liquid refrigerant flood-back to the compressor. Accumulators are commonly used on heat pumps, transport refrigeration systems, low-temperature supermarket refrigeration systems, and in any situation where liquid refrigerant is a concern. To better understand the principal of outdoor units, a detailed diagram is shown in Fig. 1.4. The refrigerant goes into the accumulator from the suction service valve through a reversing valve, which connects to both the indoor unit and outdoor unit. This reversing valve can regulate the direction of the refrigerant flow to ensure low-pressure, low-temperature gas refrigerant from either side entering the compressor. Once the refrigerant accesses the compressor through the accumulator, it can be compressed into high-pressure, high-temperature gas.

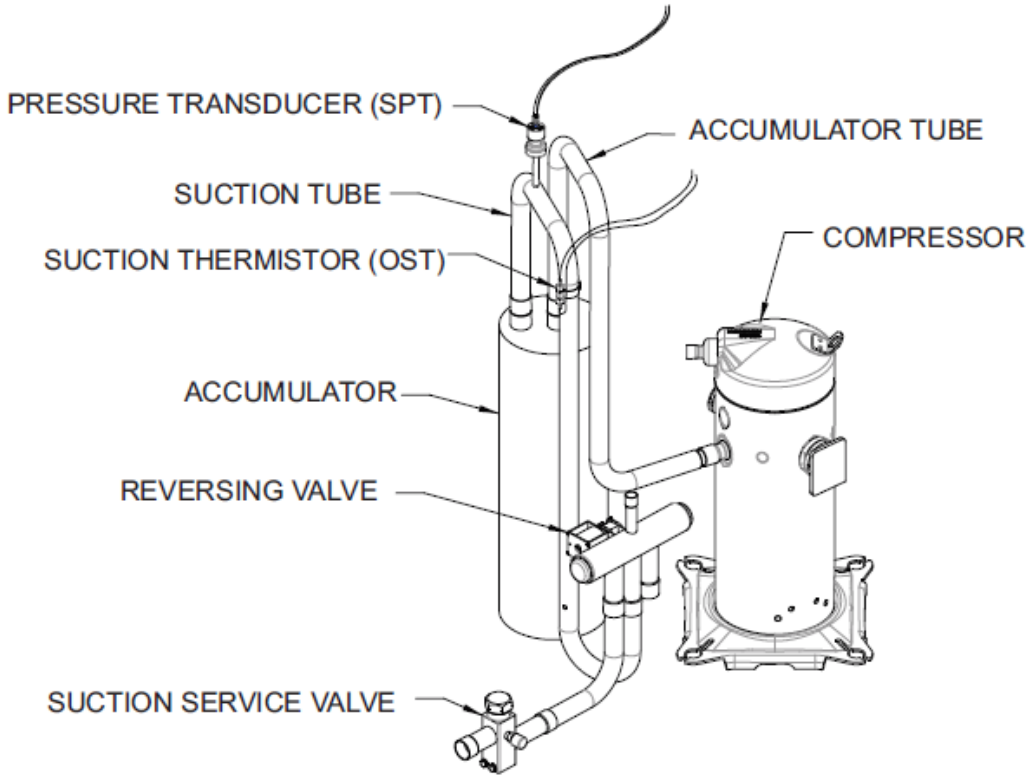

Fig. 1.4: Outdoor unit configuration

The outdoor unit in the lab uses a 5 VDC output low pressure transducer that provides a 0--5 VDC data for interpretation and a 0 to 200 psig range of pressure at the suction tube by the control board. Signals used by the control board are for:

- Low pressure cut out
- Loss of charge management
- Compressor overall envelope management
- Oil circulation management
- Lubrication management

The variable speed heat pump controller is a serially communicating device that receives capacity demands from the user interface and communicates the corresponding speed requests to the inverter drive, which directs the compressor to run at the demanded speed.

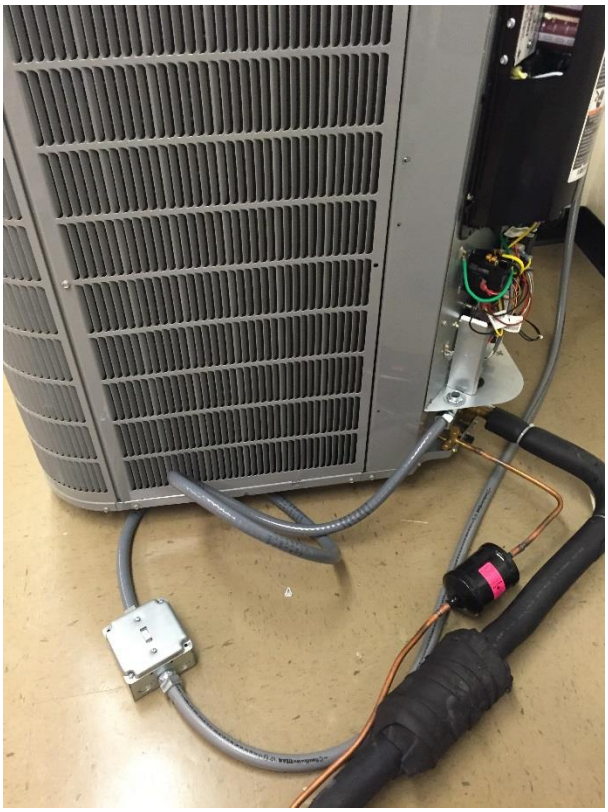

Fig. 1.5: Suction line and discharge line

1.3 Common Faults of Air Handlers

The air handler in the HVAC system has electrical and mechanical components that can experience problems from time to time. Some of the most common problems with air handlers can be fixed by identifying the problem with the system itself, although some of the issues listed need the attention of a professional HVAC technician. The HVAC technician have all the tools and parts available to make an efficient and fast repair.

1.3.1 Airflow Blockage

Since the air handler is the central unit that moves the air throughout the ductwork, it is important to make sure that objects like dirty or clogged air filters do not obstruct the air flow. A regular air filter maintenance schedule helps to maintain good

air flow throughout the duct system. It also helps keep the air handler components inside clean and free of debris and dust. With good filter maintenance, people do not have to worry about a dirty evaporator coil or any other components clogging up with dust or debris. Dusty and dirty components sometimes can lead to serious issues, including some which could cause an air conditioner to freeze up, as well as other major issues. Maintaining a good air filter maintenance schedule is easy, especially with a digital thermostat. Many of the newer digital thermostats have air filter change reminders. Good filter maintenance can prevent a number of future problems. Dirty filters can lead to issues, including water damage to the home. In the worst situations, serious problems can occur.

1.3.2 Failure of Blower Motor

The next most common problem that can occur with an air handler is a failure of the blower motor, whether it is the blower motor at fault or something else that causes the blower motor to fail. A failure could be caused by a variety of issues, including a bad relay, control board, the blower wheel being placed in the wrong position, or a fault in the blower motor itself. Thus, it is a substantial problem that requires the attention of professional HVAC technicians and researchers [7].

1.3.3 Frozen Evaporator Coil

Another common problem with air handlers can result from an issue with the air filter. In some cases, someone may neglect to install an air filter in the air handler or duct system. This might mean that some air handler components, especially the evaporator coil, could become clogged with debris and dust. In this case, the coil would need to be cleaned with coil cleaner. This is the main issue that could lead to a frozen evaporator coil. This will lead to a lack of cooling, and can even cause other problems.

In some cases, it can even damage the compressor because of liquid refrigerant returns to it. There are many other reasons for an evaporator coil to freeze, but a dirty evaporator coil is the most common cause, and fortunately it is something that can be controlled. Thus, to prevent this problem, it is very important to make sure there is a clean furnace filter in the HVAC system [7].

1.4 Condition Monitoring Methods

Condition monitoring is the process of monitoring a parameter of the conditions of machinery, such as vibration, temperature, etc., in order to identify a significant change indicative of a developing fault. It is a major component of predictive maintenance. The use of condition monitoring allows maintenance to be scheduled, or other actions to be taken to prevent failure and avoid its consequences. Condition monitoring has a unique benefit in that conditions that would shorten the normal lifespan of machinery can be addressed before they develop into a major failure. Condition monitoring techniques are normally used on rotating equipment and other machinery (pumps, electric motors, internal combustion engines, and presses), while periodic inspection using non-destructive testing techniques and fit for service evaluation are generally used for stationary plant equipment such as steam boilers, piping, and heat exchangers [8]. A Condition monitoring flowchart is shown in Fig. 1.6.

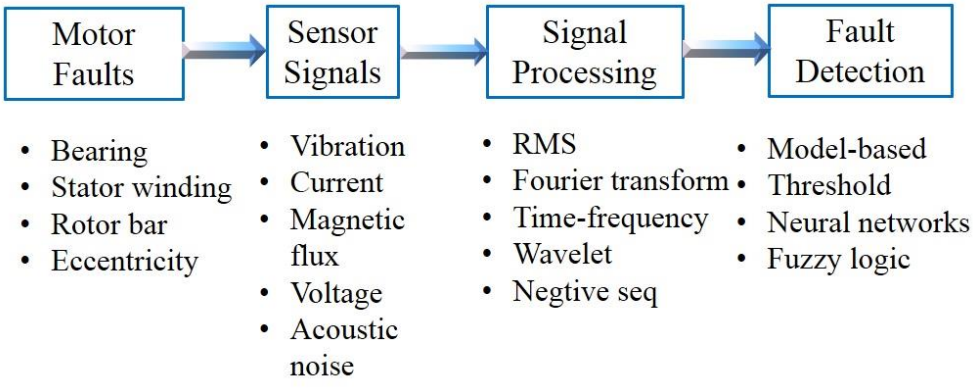

Fig. 1.6:Condition monitoring flowchart

CHAPTER 2

LITERATURE SURVEY

In this chapter, a literature survey is conducted on condition monitoring of electrical motors, airflow blockage of air handler units, unbalanced load of BLDC motors, static eccentricity of BLDC motors and winding temperature of PMSMs. In addition, a literature review of stray flux detection in relation to induction machines is presented. The development and application of stray flux detection methods are presented in detail. A comparison with stator current detection is presented, relating to stator insulation failure, bearing faults, eccentricity and broken rotor bars/end-rings. Although the stray flux method nowadays is used mostly for induction machines, its potential application to PMSM and BLDC is included as well.

2.1 Condition Monitoring of Electrical Motors

The condition monitoring method is widely used in fault detection of different kinds of electrical motors in recent years, since the stability and reliability of a motor system plays a more important role in the motor control industry. Manufacturers now are very interested in adding fault diagnostics modules to existing systems. The most well-known technique is called motor current signature analysis, which focuses on the characteristic frequency harmonics of the motor [9]. Apart from this, vibration, speed, torque, and temperature signals can be analyzed to estimate the condition of the system. In addition, automated tools such as neural networks and fuzzy logic-based systems are used to replace human involvement.

The major faults of electrical machines can broadly be classified as the following:

(1) Stator faults resulting in the opening or shorting of one or more turns of a

stator phase winding

(2) Abnormal connection of the stator windings

(3) Broken rotor bar or cracked rotor end-rings in ACIMs

(4) Static and/or dynamic air-gap irregularities

(5) Bent shaft (akin to dynamic eccentricity) which can result in a rub between the rotor and stator, causing serious damage to stator core and windings

(6) Shorted rotor field winding

(7) Bearing and gearbox failures

Of the above types of faults: 1) bearing; 2) the stator or armature faults; 3) the broken rotor bar and end ring faults of induction machines; and 4) the eccentricity-related faults are the most prevalent ones and, thus, demand special attention [9]. These faults produce one or more of the following symptoms:

(1) Unbalanced air-gap voltages and line currents

(2) Increased torque pulsations

(3) Decreased average torque

(4) Increased losses and reduction in efficiency

(5) Excessive heating

For the purpose of detecting such fault-related signals, many diagnostic methods have been developed so far. These methods to identify the above faults may involve several different types of fields of science and technology. They can be described as follows [9]：

(1) Electromagnetic field monitoring, search coils, coils wound around motor shafts (axial flux-related detection)

(2) Temperature measurements

(3) Infrared recognition

(4) Radio-frequency emissions monitoring

(5) Noise and vibration monitoring

(6) Chemical analysis

(7) Acoustic noise measurements

(8) Motor-current signature analysis

(9) Model, artificial intelligence, and neural-network-based techniques.

2.2 Condition Monitoring of Airflow Blockage in Air Handlers

According to the time of occurrence, the airflow faults in air handlers can be classified as either commissioning faults, or operational faults occurring at installation, or those occurring later during the operational life of the machine. The first type of fault is more difficult to detect, since over 90% of fault detection and diagnoses need comparisons between the initial condition and the faulty condition. Moreover, these faults usually occur in different parts of the air handler, such as the ducts, fans, and control systems. Among these faults, blockage and leakage of the ducts, and insufficient airflow are of the most severe faults [5].

Since the basic requirement for an air handler is to moderate temperature and adjust humidity, the above problems may result in failing to supply appropriate air quality to the occupants, and at the same time, cause a waste of energy in the process of functioning. A series of surveys show the existing prevalence of these problems. To detect these faults, numerous methods have been proposed in the literature. Anemometers are commonly employed to estimate airflow in ducts, with propellers measuring the rotational speed of their blades, or with hot-wire types, and both methods measure the air speed directly [10]. However, sensitivity and single-point measurement

are the main weaknesses of these methods. An indirect approach measures the dynamic air pressure instead of air speed. It exploits the relationship of equation (2.1).

$$V = \sqrt{\frac{2p_w}{\rho}} \tag{2.1}$$

In equation (2.1), ρ is the air density and p_w is dynamic air pressure. However, this method is similarly limited by the single-point measurement problem. A flow plate or true-flow grid [11] is used to compensate the above drawbacks through measuring the average air pressure by inserting a series of tubes into the duct. Pressure measurements of relatively high accuracy can be used. However, due to the high cost, difficulty to install, and sensitivity to bias, these have not been widely utilized. Other less common approaches are demonstrated in [12] and [13], where CO_2 or ozone is injected at one point in a duct and the concentration is measured on the other side of the pipeline to determine the flow of air. In [14], the acoustic spectrum and transfer function of the duct are measured by sensors and exploited to pinpoint any blockage. Most of these conventional methods above are either not reliable enough or expensive. Recently, a new idea has been proposed [15] that is based on measurements of the currents and the voltages at the terminals of the motor to then identify faulty mechanical behavior based on these observations. The principal benefit associated with the use of these electrically-based fault detection and diagnosis techniques is that electrical instrumentation is often easier to install, more reliable, and less expensive than comparable mechanical instrumentation, and at the same time smart sensors have been widely utilized in today's energy management systems. The work in [15] is a preliminary attempt and still suffers the drawbacks of being difficult to practically apply, thus proving of limited contribution and only applicable to offline tests.

2.3 Condition Monitoring of Unbalanced Load of BLDC Motors

According to some previous research, an unbalanced load can be created by mounting a series of set screws to one side of the circular disk (load). As the unbalanced disk rotates, the set screw pulls outward as a result of the centrifugal force. The rotor is therefore being pulled continuously outward with a force that is dictated by both the mass of the set screw, as well as the position of the set screw on the blade. Such an unbalanced condition causes slight dynamic eccentricity besides vibration and torques pulsating. The set screws are added to the disk under the designed position and mass. Based on this analysis, there should be a clear increase in the principal sidebands seen in the frequency domain, which shows that a mechanically unbalanced rotor can be detected by monitoring the principal sideband frequencies that occur around the fundamental frequency.

References [16], [17] present a method for detecting faults utilizing the stator current spectrum in a BLDC motor under dynamic operating conditions. Specific characteristic frequencies can be used as an index to show unbalanced torque and dynamic eccentricity. The technique proposed in [18] evaluates the imbalance-specific modulation of the electric power in an induction motor. Reference [19] further examines the effect of changing the load of the motor on detecting load unbalance and shaft misalignment in both the current and vibration spectra. It shows that the spectral components associated with mechanical conditions do not always linearly change as the load varies.

The stray flux of an electrical machine is a residual and undesirable effect which does not participate in the process of generating electromagnetic torque. However, stray flux can be used for machine monitoring. A new experimental procedure for using the

stray flux as an indicator for a stator winding fault is provided in [20]. In another reference related to the stray flux of an induction machine, the external flux sensors are used to detect the rotor fault and unbalanced voltage detection [21][22]. The comparison between the effect of stator current and the stray flux spectrum on the mechanical fault of an induction motor is presented in [23][24].

2.4 Condition Monitoring of Static Eccentricity of BLDC Motors

Because of the wide range of applications of BLDC motors, the fault diagnosis of BLDC has become an important research hotspot. For those BLDC motors in operation, rotor faults account for most faults [9]. Static eccentricity and dynamic eccentricity are two of the main faults in the rotor of a BLDC motor. In an ideal machine, the rotor is center-aligned with the stator bore and the rotor’s center of rotation is the same as the geometric center of the stator bore. Rotor eccentricity will occur if the air gap changes as the BLDC motor rotates. In the case of static eccentricity, the position of the minimum radial air gap length is fixed in space. Typical causes of static eccentricity include stator core ovality, or incorrect positioning of the rotor or the stator at the commissioning stage. Dynamic eccentricity occurs when the center of the rotor is not at the center of rotation and the minimum air gap revolves with the rotor. When the eccentricity becomes large, the resulting unbalanced radial forces can cause a stator-to-rotor rub, which can result in damage to the stator and rotor. In the case of static eccentricity, this is a steady pull in one direction. This makes the unbalanced radial forces in static eccentricity difficult to detect unless special equipment is used, which is impractical for motors in service. Static eccentricity in an induction motor can be detected from the magnitude of the principal slot harmonics in the motor's current

spectrum. However, in a BLDC motor, no principal slot harmonics are produced in the current spectrum, as the rotor is smooth and is comprised of magnets that span an entire pole arc [25].

There has not been much research done into fault detection for static eccentricity in BLDC, because it is difficult to detect compared to dynamic eccentricity. In BLDC motors, the relative permeability of a magnet is equal to that of air. Therefore, the BLDC motors have relatively large air gaps. Hence, any physical shift causing a change in air gap length has a negligible effect on the flux distribution. Reference [26] proposes a method for detecting static eccentricity in induction motors by observing the negative sequence current. It also comes up with a method of separating the negative sequence components from their positive sequence counterparts using qd-axis current spectra in a newly selected rotating reference frame. Reference [25] uses the negative sequence current as an indicator for static eccentricity. A transient simulation of the complete BLDC motor drive is carried out in Matlab to observe any change in the negative sequence current. Reference [27] provides a control method for the BLDC motor in the presence of static rotor eccentricity. Most of the previous research into detecting static eccentricity focuses on negative sequence current change in BLDC motors. In reference [28], an improved method is proposed based on the comparison between the positive sequence current and negative sequence current. A BLDC motor with static eccentricity in the air handler is tested in the experiment.

2.5 Online Estimation of Winding Temperature of PMSMs

The temperature of PMSM is the key factor reflecting the motor’s condition. In this section, only the online estimation of stator winding temperature will be considered. The most common method to measure the temperature of PMSM winding

is to use a battery-powered infrared sensors and slip rings. Although using these instruments is a relatively direct method of measuring temperature, the cost, extra effort of mounting the sensor and reliability of these sensors and circuits are a concern in the long run [29] [30][31][32].

Recently, more indirect temperature estimation methods have been developed. The online estimation of winding temperature of PMSM mainly includes the signal injection method [33] and the electrical machine model estimation method [35]. For both methods, the temperature dependence of resistance can be exploited so the main issue becomes online resistance estimation. The main drawback of these two methods is the small contributions from the resistive voltage drop to the total terminal voltage in a high-efficiency, high-power machine.

$$\frac{R_s(t)}{R_0} = \frac{T(t)+k}{T_0+k} \tag{2.2}$$

The temperature is calculated by the equation (2.2), where k is the temperature coefficient. The T_0 is the reference environment temperature. For a typical rotor with aluminum bars of 62% volume conductivity, k is 225. For copper bars, k is 234.5.

Lee proposes a method of injecting a controllable DC bias into the input current and obtaining the DC voltage and current bias, then calculating the stator winding resistance by DC bias [33]. This method commonly causes torque ripple which are not desired in applications. Methods using an electrical motor model always exploit a Kalman filter or the recursive least square method to estimate the winding resistance or impedance, which is a sign of temperature change. Nikola Z. Popov proposes a method without added signal injection, providing a PWM pulse as input interference with a carrier-wave frequency from 10 kHz to 100 kHz, the change of input impedance giving a response to the change of winding temperature, with the temperature error using this method less than 8° C [34]. A 3rd order EKF algorithm is

used in the rotating reference frame to estimate the winding resistance and the permanent magnet flux [35]. By using EFK to estimate winding resistance, the motor angle and speed are also required, so an extra rotor position sensor should be installed.

In addition, there is another temperature estimation method based on a thermal model of PMSM [36]. The temperature in the winding heads (end-winding) is of particular importance, since it typically significantly exceeds the one in the stator slots. Using this method, one would use a low order thermal model to monitor the temperature in different places of the winding and the permanent magnet. The model parameters are estimated solely based on experimental data.

2.6 Condition Monitoring Based on Stray Flux

Induction motors are widely used in different industry applications which can experience various kinds of faults in stators and rotors. Due to its importance for the diagnosis of motor faults, the classical condition monitoring method focuses on the stator current spectrum and is well researched and presented. This section, rather, presents a review of stray flux detection in relation to induction machines. The development and application of stray flux detection methods are presented in detail. A comparison with stator current detection is presented, relating to stator insulation failure, bearing faults, eccentricity and broken rotor bars/end-rings. Although the stray flux method nowadays is used mostly for induction machines, its potential application to PMSM and BLDC is included as well.

The advantage of stray flux detection includes its non-invasive measurement and simple implementation. Compared with winding current signature analysis, which under some circumstances cannot discriminate between different faults such as eccentricity and stray flux, the analysis is much more sensitive, robust and reliable, and

thus is suited to initial fault detection on the part of an induction machine. Moreover, its results are more informative, and includes helpful information such as the location of defects in an induction machine.

However, the placing of the external flux sensor leads to greater difficulties in relation to repeatability. For the purposes of monitoring, this method takes into account that the diagnosis is always carried out from a reference signal, with the machine running under appropriate conditions. Thus, for efficient diagnostics, it is necessary to always attach the magnetic flux sensor in the same position. Also, the threshold values of these axial flux harmonics, which can distinguish a faulty motor from a healthy motor, are not easy to predetermine because several factors, especially the sensor location and motor model, affect them. For this reason, it is advisable to collect a reference measurement of the flux for each healthy motor to determine, experimentally, the relative distribution of these harmonic components. Moreover, the result of the stator current analysis cannot be directly used as a reference value for axial fluxes. The stator current spectra are quite alike for similar motors, hence, the spectrum of one motor can be quite reliably used as a reference value for another similar motor. In the axial flux spectra, there are so many differences among the various motors that it is better to set a reference measurement for each machine.

Flux analysis is used mostly for induction motors, hence for PM synchronous motor faults, with the permanent magnet as a flux source, the stray magnetic field from the motor can be included in the magnetic circuit of the motor. It has been shown that mesh and the related frequencies that cannot be easily identified in stator current show up in the EMF stray flux spectrum [37]. Stray flux detection can be widely exploited to diagnose other faults in PMSM.

2.6.1 External Magnetic Field Analysis

Methods based on the analysis of external magnetic fields were developed in the 1970s by Penman [38]. The drawback of these methods is tied to the difficulty of modeling a magnetic field that strongly depends on the electromagnetic behavior of the stator yoke and of the motor housing, which have an important shielding effect [39]. Some approaches need simple geometries [40,41,42,43], but these methods, based on simplified geometry and under particular hypotheses, can hardly be exploited for electrical machines. External magnetic fields can be studied using axial and radial decomposition, according to most papers.

Reference [44] includes some research from a theoretical point of view. 2D and 3D finite element models are used, the difficulty being in the magnitude difference of the magnetic field between the inside and outside of the machine. Nevertheless, with a proper geometric representation, the stray fields have been obtained with an acceptable accuracy. This encouraging result will allow the design of electromagnetic shields around the machine. Another paper proposes two approaches to compute the magnetic stray field created by a faulty electrical machine. The first one is based on the homogenized FEM method. The second one is based on the combination of an analytical expression for the magnetic field in the air gap with an integral method. Both methods can save significantly on CPU time and memory [45]. Reference [46] also presents a theoretical approach to stray flux analysis with a three-phase squirrel-cage induction machine for stator and rotor electrical faults detection. The stray flux is analyzed at a point outside the machine using the Biot-Savart law, taking into account the effect of the end-windings for the stator and the end-ring segments for the rotor squirrel-cage.

In reference [47], Kokko states that the determination of the complex 3D pattern of this leakage flux is difficult but not necessary. When it comes to the threshold setting, since the condition monitoring of motors by axial leakage flux is based on the relative

changes in certain flux frequency components, their absolute amplitude values are not required [48]. Recently, some researchers also present FEM followed by the Neuro Fuzzy Logic method to statistically analyze different kinds of motor faults [49,50].

2.6.2 Development of Stray Flux Detection Instrument

Measuring magnetic leakage flux is straightforward, with circular search coils placed on the rear end of the machine, concentric with the shaft. These coils generate a voltage proportional to the rate of change of the leakage flux [51]. In addition to search coils and hall sensors, some other sensors such as optical fiber and radio frequency sensors are utilized for the monitoring of the electrical machine [52], [53]. An integrated fluxgate sensor is implemented to detect magnet defect faults [54]. In recent years, researchers have developed new magnetic flux detection devices to increase sensitivity and accuracy of condition monitoring systems. A "C-shape" flux probe has been developed which can be installed for different machine sizes. Nonetheless, these search coils are based on Faraday's Law of Induction and cannot measure static magnetic fields [55]. Other instruments, such as giant magnetoresistance (GMR) sensors, make static flux and point measurements possible, and are extremely useful for condition monitoring. Besides this, they have very high resolution and sensitivity. Giant magnetoresistance sensors have been applied to the nondestructive testing and evaluation of ferromagnetic or electrical conductive materials. They have the proven advantages of high sensitivity and spatial resolution, linearity, and frequency responses to magnetic fields [56], [57]. They have already been applied in the inspection of different depths and orientations of cracks in plates, bearings and rails.

2.6.3 Stator Insulation Monitoring and Failure Detection

Winding failures are a major fault, accounting for over 45% of total machine failures. In the literature, many condition monitoring techniques based on different failure mechanisms and fault indicators have been developed. Machine current signature analysis is a very popular and effective method at this stage. However, it is extremely difficult to distinguish different types of failures, and it is hard to obtain local information if a non-intrusive method is adopted. Typically, some sensors need to be installed inside the machines to collect key information, which leads to the disruption of machine operation and additional costs.

Some authors recommend using stray flux to detect stator winding insulation failure. The main factors are sensor type, sensor direction and sensor quantity. FEM is the basic method of building a 2D or 3D machine model together with some statistical analysis. Reference [56] presents a new non-invasive monitoring method based on giant magnetoresistance sensors to measure stray flux leaking from the machines. It is focused on the influence of potential winding failures on the stray magnetic flux in induction machines. Finite element analysis and experimental tests on a 1.5-kW machine are presented to validate the proposed method. With time-frequency spectrogram analysis, it is proven to be effective in detecting several winding faults by referencing stray flux information. The novelty lies in the implementation of giant magnetoresistance sensors and analysis of machine faults. Some other novelties are introduced by using different flux probes in different positions around the machine and the statistical evaluation of the experimental results [58]. This analysis has revealed important variation in some harmonic components, especially in the axial body flux collected by the sensor designed and constructed in the laboratory. The tests in load and no-load conditions have shown significant similarities, even if the stator current gives interesting diagnostic information only when the motor is loaded. Hence, especially at no-load, stray flux seems more efficient for this fault diagnosis. In addition, the increased efficiency regarding fault detection and the possibility of detecting the

azimuth position of the short-circuit fault inside the stator is offered by a system of two coil sensor series connected, and one pole shifted around the motor [59]. Considering power supply harmonics, it is possible to easily detect the stator winding faults in the low-frequency range of the flux spectrum with low-frequency resolution [79].

2.6.4 Bearing Fault Detection

The percentage rate for bearing faults is approximately 35-55% regarding all causes of machine failure [60], [61]. Some authors have even presented much higher percentages for bearing faults, e.g. Immovilli [62] asserts that it is up to 90% for small machines. Therefore, bearing faults are an oft-investigated issue in the field of electric machine diagnosis [63]. Approximately 40% of premature bearing failures are caused by inadequate or improperly used lubricants [64]. The most common indicators for potential bearing problems are increased temperature and a high vibration or noise level of the machine [65].

Two types of bearing faults are usually distinguished. The first are single point defects and the second is generalized roughness. In the case of single point defects, the characteristic spectral components in a vibration signal can be predicted for inner ring, outer ring, rolling element and cage faults. These frequencies can also appear in the stator currents around the fundamental harmonic [66]. Although they are usually clearly visible using vibration analysis, in the case of stator current it is difficult to observe due to low amplitude and noise disturbance [62]. Signal processing methods have been applied, but the results are still not clear. In contrast to single point defects, generalized roughness does not produce a characteristic frequency, but rather specific frequency bands.

A stray flux based bearing fault diagnosis method has been implemented in

several papers, most of which use several search coils and flux probes. Some experimental measurements are carried out by means of a current probe and by means of various flux probes, in different positions [48], [67]. Comparisons are conducted to find the main advantages, which are the simplicity and the flexibility of the custom flux probe with its amplification and filtering stage. The flux probe can be easily positioned on the machines and adapted to a wide range of power levels. An industrial probe such as an Emerson (M-343F-1204type) is implemented in [48], which has several turns wound around a circular air core. This probe has to be mounted on the fan end of the machine and can be used to measure only the leakage axial flux. Other custom flux probes, like the one consisting of a semicircular ferrite core with 44 mm outer and 40 mm inner diameters, are utilized to detect the winding fault. The main advantage of this cheap (only a few Euros) flux probe over the industrial ones is its small size, which enables the measurement of the stray flux anywhere around the machine [48].

2.6.5 Air Gap Eccentricity Detection

Generally, up to 10% is permissible and should not have a significant influence on motor characteristics and lifetime [68], [69]. However, a higher level of eccentricity gives rise to unbalanced magnetic pull and therefore noise, vibration and excessive bearing wear occur [70], [71], [72].

For machine monitoring purposes, the classical motor current signature analysis has shown its weakness in distinguishing eccentricity occurrence in the presence of other mechanical faults. Although Park's vector approach can cover this drawback, the high cost due to its requirement in using three current sensors and an advanced processing technique make it less desirable in an industrial setting. Moreover, the detection of dynamic eccentricity in a stator current around the principal slot harmonic is effective only for some combinations of numbers of pole pairs and rotor slots [73].

The experimental results have revealed the potential of a simple search coil for the detection and the distinction of eccentricity, even in the presence of similar mechanical faults [74]. Dynamic eccentricity produces low frequency air gap flux components. However, they can be observed in the stator current only with mixed eccentricity. Unlike motor current signature analysis, measuring the stray flux allows the detection of purely dynamic eccentricity or dynamic eccentricity under mixed eccentricity with a minimal effect of static eccentricity [75]. This feature can be understood as an advantage of this method, because the same frequency components are presented in a stator current only if both types of eccentricity exist together, and it is not easy to distinguish them. A drawback of this method is the relatively significant impact of stator yoke saturation [75]. A new approach to detecting eccentricity faults is presented in this paper, by monitoring the slot leakage flux of the stator. In order to measure the slot leakage flux, two placements of search coils in the stator slot are applied [76]. Most of the papers related to this part pay attention to measured motors with static, dynamic and mixed eccentricities, as well as the healthy ones. Measurements were carried out for four types of loads: no load, half-load, full load and overload [77].

CHAPTER 3

CONDITION MONITORING OF AIRFLOW BLOCKAGE IN AIR HANDLERS

3.1 Introduction

In this chapter, airflow blockage is detected utilizing a current-based condition monitoring method. This eliminates the need for an airflow sensor which increases cost and decreases reliability. A current based constant airflow algorithm is applied to continuously control the speed of the fan motor to accommodate the change of the load torque, relating to the air pressure change at the inlet or outlet of the air handler. This chapter first lists the airflow values under different blockage conditions to verify that the constant airflow algorithm is implemented. Then, the proposed current-based frequency domain analysis is conducted, focusing on the fundamental frequency component, showing speed changes of the fan motor under different airflow blockage conditions.

3.2 Constant Airflow Control

Traditional fan motors are controlled to run at a constant speed by setting a fixed voltage frequency. When an airflow blockage happens, the volume of air moved by the blower wheel will also vary, which changes the static pressure on the blades of the blower wheel. Then the speed drops accordingly with an increase of load pressure. Recently, a constant airflow control has become an important criterion for manufacturers in selecting a blower wheel drive because of higher demand for system efficiency based on government environmental policies [78]. Constant airflow control

also provides better humidity and temperature control, which can raise comfort level for residents. A constant air flow algorithm is implemented in the high-efficiency HVAC system to regulate fan motor speed by detecting the airflow blockage conditions. The basic control principle is discussed below.

For the BLDC motor inside the air handler, two airflow blockage conditions with the same airflow rate are discussed, to maintain constant airflow. However, the motor shaft torque and the speed of the fan motor are different under these two conditions, while a dynamic balance situation is achieved to maintain constant airflow conditions. The equation (3.1) expresses the relationship between motor shaft torque and the speed of fan motor, where T is the motor shaft torque, and ω is the speed of fan motor.

$$\frac{T_1}{\omega_1} = \frac{T_2}{\omega_2} \tag{3.1}$$

The key idea of the above equation is to maintain a constant ratio of the motor shaft torque and speed of fan motor, regardless of the static air pressure of the blower wheel blades. The fundamental frequency components of the stator current can be exploited to detect airflow blockage conditions.

3.3 Constant Airflow Verification

A preliminary experiment is conducted to examine whether there is a constant airflow control algorithm implemented in the system. The airflow is sucked from the bottom of the air handler to the outlet at the top through a blower wheel. The airflow speed is measured by an anemometer at the outlet at five different positions (shown in Fig. 3.1). The inlet is blocked in different percentages to simulate airflow blockage conditions caused by a dirty filter or blower wheel, as can be seen in Fig. 3.2.

According to the experiment results in Table 3.1, the airflow is nearly the same, considering the accuracy of the air flow probe under three different fan speed levels which can be set using the UI (User Interface). These results show clearly that the constant airflow control algorithm is implemented inside the air handler by regulating the fan motor speed to control the airflow speed as a blockage happens.

Table 3.1: Airflow speed (m/s)

Blockage percentage / Fan speed level	0%	30%	50%	70%	85%
Low	0.2	0.1	0.2	0.1	0.1
Medium	0.5	0.5	0.6	0.6	0.6
High	1.1	1.2	1.2	1.2	/

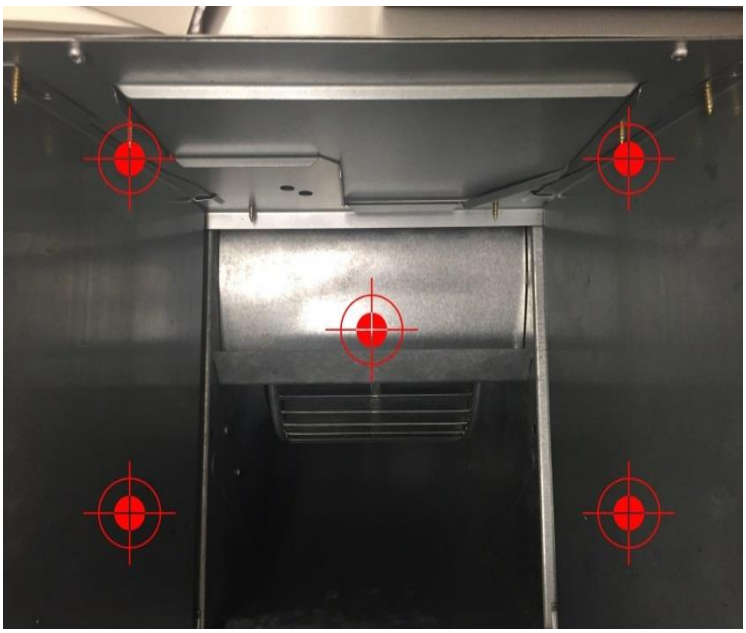

Fig. 3.1: Outlet of air handler (top view)

Fig. 3.2. Inlet of air handler

3.4 Airflow Estimation

3.4.1 Data Acquisition

The blower wheel and fan motor are detached as shown in Fig. 3.3 and Fig. 3.4. There is an extension line added between the controller and the motor which is used to measure the stator current. Based on Fig. 3.3, the whole motor drive is sealed inside, and the fan motor is a typical three-phase six-pole eighteen-slot BLDC motor (1/2HP, 120V/240V AC single-phase input, 50/60Hz).

Fig. 3.3: Detached blower wheel

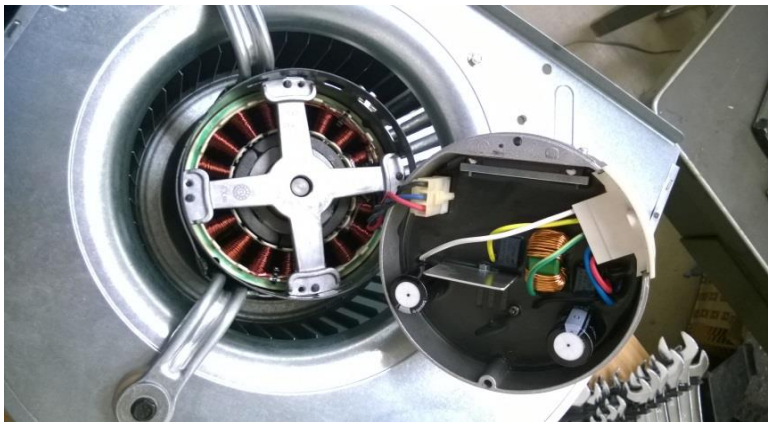

Fig. 3.4: Detached fan motor

One current probe (Tektronix TCP303), illustrated in Fig. 3.5, is used to measure the three phase currents. The current signal inputs to an oscilloscope via a computer interface.

Fig. 3.5: Current probe (Tektronix TCP303)

The datasets are collected from a single-phase current (Phase A or Phase B) of the BLDC motor. The current data detected with different airflow open areas can be

classified into 15 groups (Durations: 5s 10s 20s; Airflow Open Area: 85% 70% 50% 30% 0%) with settings in Table 3.2.

Table 3.2: Current detection settings

Duration	Sampling Frequency	Airflow Open Area
5 s	5000Hz	85% 70% 50% 30% 0%
10 s	2500 Hz	85% 70% 50% 30% 0%
20s	1250 Hz	85% 70% 50% 30% 0%

3.4.2 Theoretical Analysis of the Trapezoidal BLDC Motor Control

The trapezoidal control method, which is also known as 120-degree inverter control, is implemented in this BLDC fan motor. At each commutation state, only two of the three phases are energized, as is shown in Fig. 3.6. This control method has some advantages. The most significant strength is that since only one phase current at a time needs to be controlled, no more than one current sensor is needed for the current loop control. Thus, only one shunt resistor is necessary to put in the line inverter input to control the current.

BLDC motors have a trapezoidal back EMF waveform. In order to obtain optimal torque, a trapezoidal shape current is controlled to energize the motor. The combination of DC current at each commutation state with a trapezoidal back EMF makes it possible to produce a constant torque situation. When it comes to the torque ripple, according to Fig. 3.6, since the current cannot be established instantaneously in a motor phase, the main torque ripple is produced at a commutation point [36].

Compared with other well-established control methods, such as field oriented control and 180-degree inverter control, this trapezoidal control method is much simpler and easier to implement. So, it is widely used in a HVAC system where control accuracy requirements are not so high, and cost effectiveness is more important.

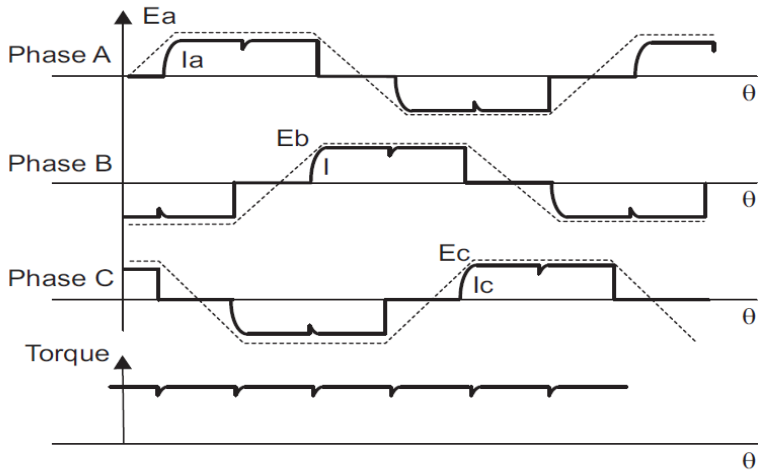

Fig. 3.6: Three phase current and back-EMF waveform under trapezoidal control

Sensorless speed control of BLDC motors is realized by measuring the time between successive zero crossings of the back-EMF waveform, as can be seen in Fig. 3.6. The commutation point is delayed by 60 degrees after the zero-crossing point. The frequency and amplitude change under different blockage conditions in Fig. 3.7 and Fig. 3.8 reflect the torque and speed change of the fan motor.

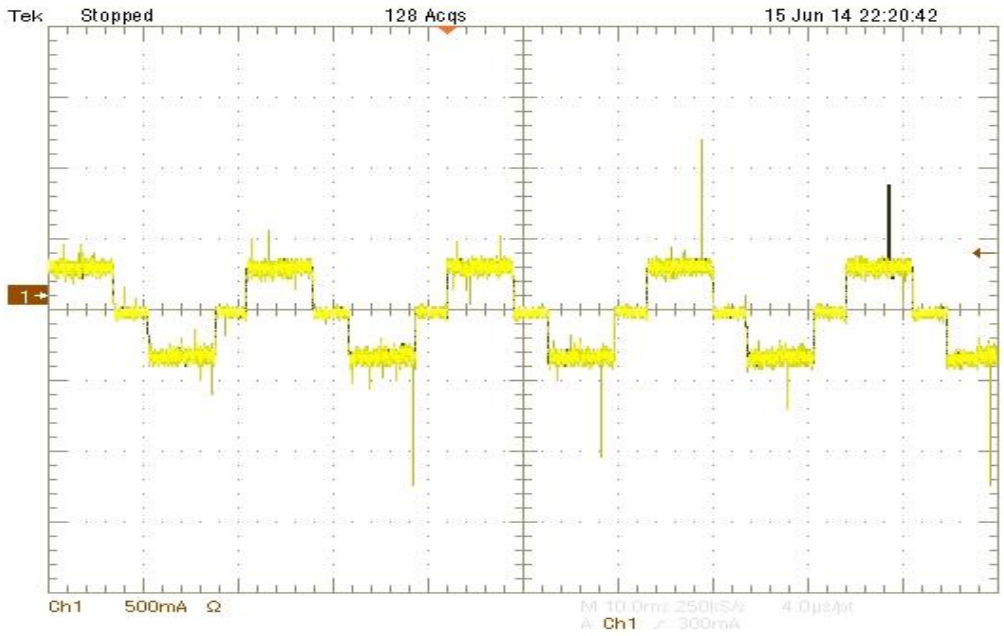

Fig. 3.7: 0% blockage condition (normal condition)

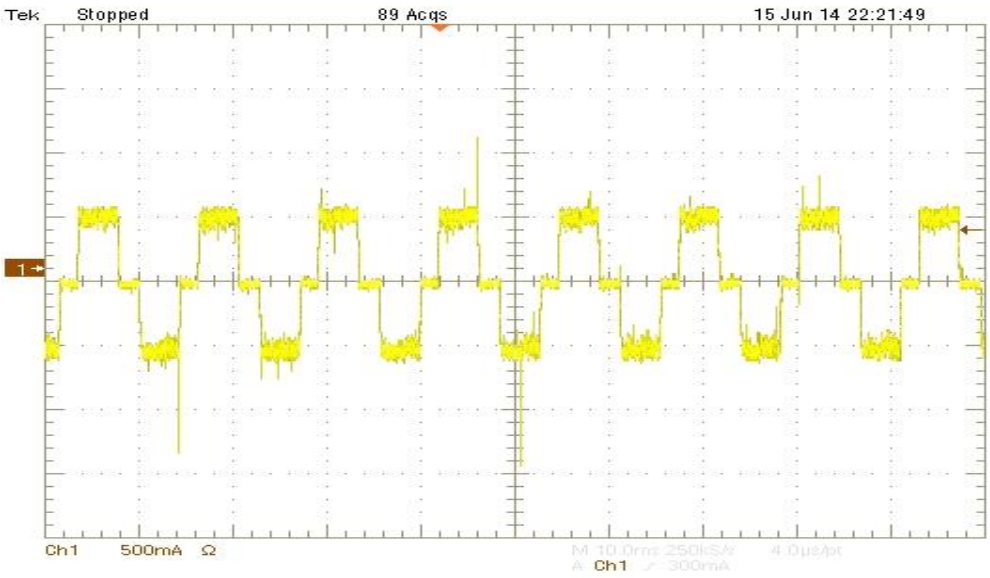

Fig. 3.8: 70% blockage condition

3.4.3 Experiment Results and Analysis

Three groups of FFT results based on three different FFT settings are compared. Since the fundamental frequency component is the only one of interest, the

sampling frequency and resolution are not so sensitive to the results. FFT with a 1.25 kHz sampling frequency and the highest resolution of 0.05 Hz is selected to examine the variation of fan motor speed. All of the important FFT setting parameters are listed in Table 3.3.

Table 3.3: Stator current FFT settings

Speed level	Medium
Sampling frequency	1.25k
Sampling point	25000
Sampling duration	20s
Frequency resolution	0.05Hz

The medium speed level of 46 HZ is selected if there is no airflow blockage in the system. The fundamental frequency increases significantly as the blockage percentage increases, based on FFT analysis of stator current in the Fig. 3.9-3.12. The speed information with respect to blockage percentage is summarized in Table 3.4.

Table 3.4: Data under different conditions

Blockage Percentage	0%	30%	50%	70%	85%
Motor Speed(Hz)	46	54	63	82	95

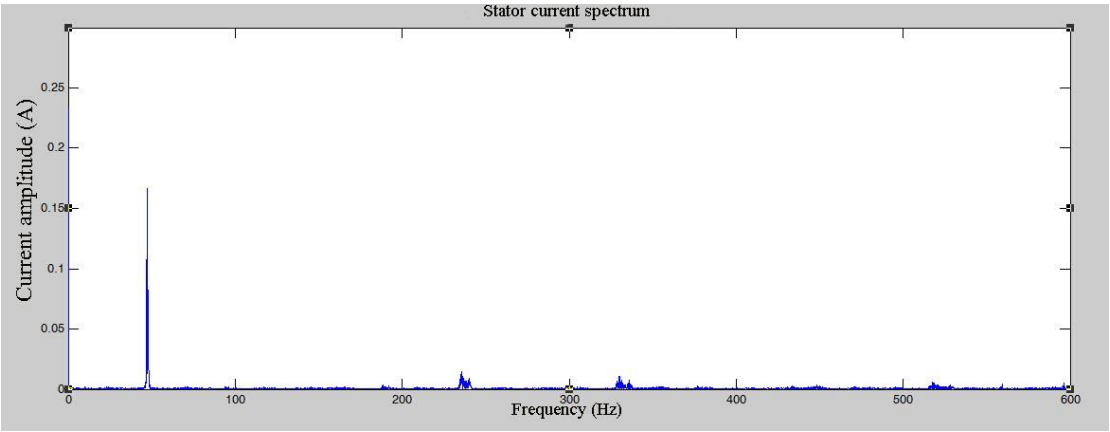

Fig. 3.9: Stator current spectrum under 0% blockage condition

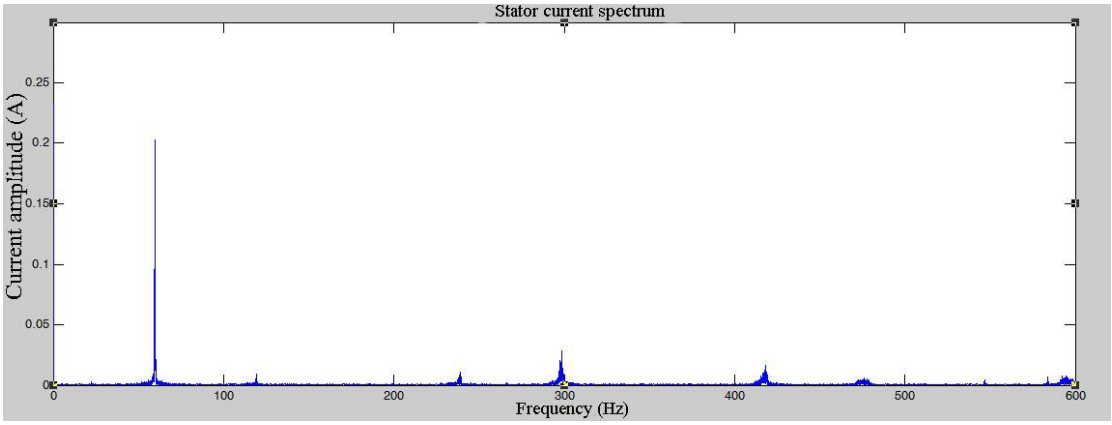

Fig. 3.10: Stator current spectrum under 50% blockage condition

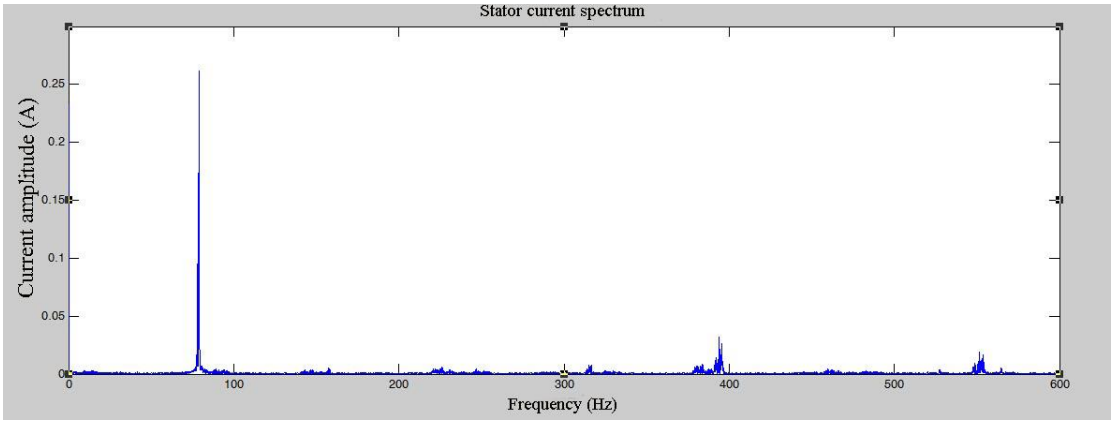

Fig. 3.11: Stator current spectrum under 70% blockage condition

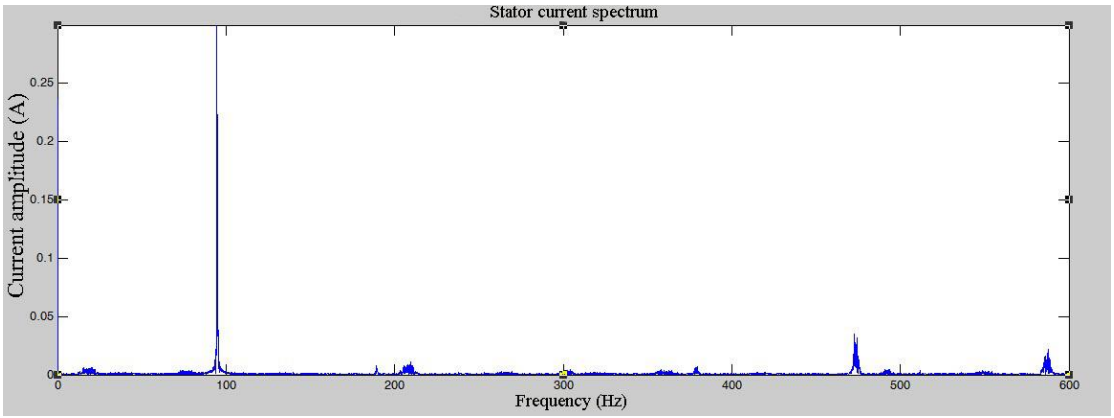

Fig. 3.12: Stator current spectrum under 85% blockage condition

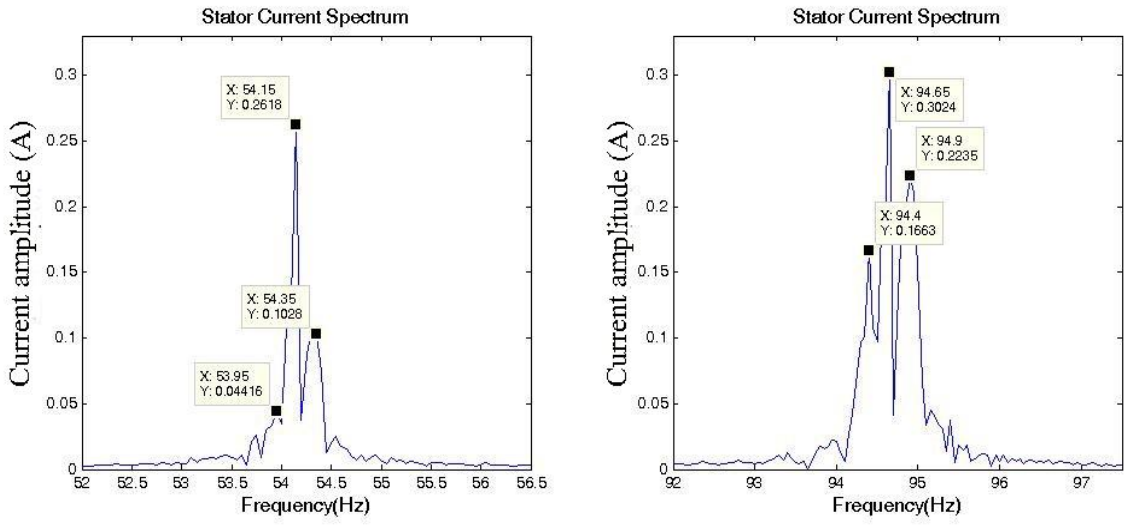

Fig. 3.13: Stator current spectrum under 30% and 85% airflow blockage

More attention should be paid to the amplitude change under different blockage

conditions. In Fig. 3.13, 30% and 85 % airflow blockage conditions are further compared. The amplitude of the fundamental component increases from 0.26 to 0.3 A because the airflow blockage raises the static pressure of the blower wheel so that load torque increases. This also can be utilized to detect the airflow variation, although speed change is more noticeable when compared to the load variation.

3.5 Conclusions

In this chapter, airflow blockage conditions are monitored by merely focusing on stator current variation. This method can successfully eliminate the cost and reliability issues of airflow sensors. For most high efficiency HVAC systems, constant airflow control is a basic feature which can continuously control the speed of the fan motor to accommodate the change of the load torque relating to the pressure change at the inlet or outlet of the air handler. This constant airflow control algorithm is verified under different blockage conditions. Then the main target becomes to estimate airflow variation by detecting fan motor speed. The results of the experiment show that the fundamental frequency increases significantly as the blockage percentage increases. More attention is paid to the amplitude change under different blockage conditions. This also can be utilized to detect the airflow variation because of the load change. However, the speed detection method is more straightforward and effective for a HVAC system implemented with a constant airflow algorithm.

CHAPTER 4

CONDITION MONITORING OF UNBALANCED LOADS OF FAN MOTORS IN AIR HANDLERS

4.1 Introduction

For most air handlers, the unbalanced load of a blower wheel is created by the unevenly distributed contaminants on the blades. In the experiment, the dirt and other contaminants are emulated by adding some weights to the inner side of the blade. The traditional current-based condition monitoring method is conducted followed by a stray flux spectrum analysis. The proposed stray flux spectrum could increase reliability in detecting an unbalanced load condition.

4.2 Theoretical Analysis of Unbalanced Load Detection

4.2.1 Stator Current Analysis

A pulsating load and an unbalanced load have similar effects on the magnetic field of the BLDC motor. This can be encountered in applications such as reciprocating compressors. The frequency in the BLDC stator current affected by such an unbalanced load is given by:

$$f_{vth} = f_e \mp k \cdot f_r \tag{4.1}$$

Where f_{vth} is the harmonic frequency as a result of the pulsating load, f_e is the fundamental frequency, and f_r is the mechanical rotor frequency.

Past research in the area of BLDC motor diagnosis has shown that the

unbalanced load torque can enhance the severity of dynamic eccentricity regarding the BLDC motor, and eccentricity conditions affect certain characteristic frequency components in the machine stator current. Dynamic eccentricity in BLDC motors produces current components at frequencies given by

$$f_{de} = f_e \mp \frac{2mf_e}{P} \tag{4.2}$$

where f_{de} is the dynamic eccentricity frequency, f_e is the fundamental frequency, P is the number of poles and *m* is any integer. Hence, current components at the rotating frequency sidebands of f_{de} can be monitored to detect the presence of dynamic eccentricity.

Thus, for some cases like a broken blade of a blower wheel or unevenly distributed contaminants on the blades, both kinds of frequency components should be found in the stator current spectrum, and the component $f_e \mp \frac{2mf_e}{P}$,when *m* equals to 1, should be more prominent in the spectrum, because both faults can produce this quantity.

According to the equation (4.1) and (4.2), the most outstanding side frequency components of the BLDC fan motor in the lab are located at the 2/3rd and 4/3rd of the fundamental frequency. However, because of a dynamic eccentricity in the system, the 1/3th and 5/3th of fundamental frequency component can be observed as well, and the corresponding *m* is equal to 2 in equation (4.2).

4.2.2 Stray Flux Analysis

The stray flux of a BLDC motor is a residual and undesirable effect which does not participate in the process of generating electromagnetic torque. The stray flux is the magnetic flux that radiates out of the machine due to the inherent machine dissymmetry. In fact, it will be difficult to quantify the magnitude of the stray flux, since it is related

to the place where it is sensed around the machine body [79].

However, by observing the change of the stray flux spectrum at some characteristic frequency points near the BLDC motor under different unbalanced load conditions, the severity of faulty conditions can be determined. When the load is unbalanced, the magnetic field of the BLDC motor is not a perfect circle, so additional stray flux appears outside the motor. It has been shown in [80] that the unbalance fault in the induction motor could be detected by the examination of rotational frequency harmonics that appear in the axial stray flux spectrum, for instance, at $f_r, 2f_r, 3f_r$ where f_r is rotational frequency of the induction motor. For a BLDC motor, the rotational harmonics reflecting the asymmetry can be $2f_e$ because an unbalanced load produces even harmonics in the system.

4.3 Experiment Results and Analysis

4.3.1 Current Spectrum Analysis

As mentioned in Chapter 3, the current probe (Tektronix TCP303) and Pearson Current Monitor (model:110A; 0.1V per Amp) are used to measure the phase current which is illustrated in Fig. 4.1.

Fig. 4.1: Current probe (Tektronix TCP303) and Pearson Current Monitor

The unbalanced load of the BLDC motor is realized by adding a different number of weights to the inner edge of the blade in the blower wheel. Two weights (30g each, calculated based on the mass of the fan blade) are added in Fig. 4.2.

Fig. 4.2. Weights on the blade

The motor driving the blower wheel in the air handler is a three phase, six pole BLDC motor. The datasets are collected from one phase current of the BLDC motor. Practically, in order to get the characteristic harmonic component which is caused by the dynamic eccentricity and unbalanced load in this air handler, the effect of low frequency mechanical oscillation noise and high frequency oscilloscope noise need to be well filtered. The mechanical oscillation harmonics are caused by unbalanced load vibration. A group of sampling indexes, including sampling time and resolution, are tested and selected to detect the unbalanced load condition of the blower wheel motor. Most of the high frequency noise signals, including some of the mechanical oscillations, are removed. The FFT settings are shown in Table 4.1, including sampling time and resolution (sampling frequency：625 Hz, sampling points：800), aiming to avoid over-sampling. Then the FFT with Hanning Window is applied to the stator current spectrum under different conditions.

Table 4.1: FFT settings for unbalanced load detection

Sampling frequency (Hz)	625
Sampling points (#)	800
Frequency resolution (Hz)	0.78

Fig. 4.3-4.4 show the FFT results of normal conditions and unbalanced load

conditions with two weights (30g each) added to one blade as shown in Fig. 4.2. Fig. 4.5-4.6 are log scaled figures provided so that four side band characteristic frequency components are more evident. The side band harmonics increase significantly as an unbalanced load is added. It is clear that all the harmonics are symmetrical to the fundamental frequency.

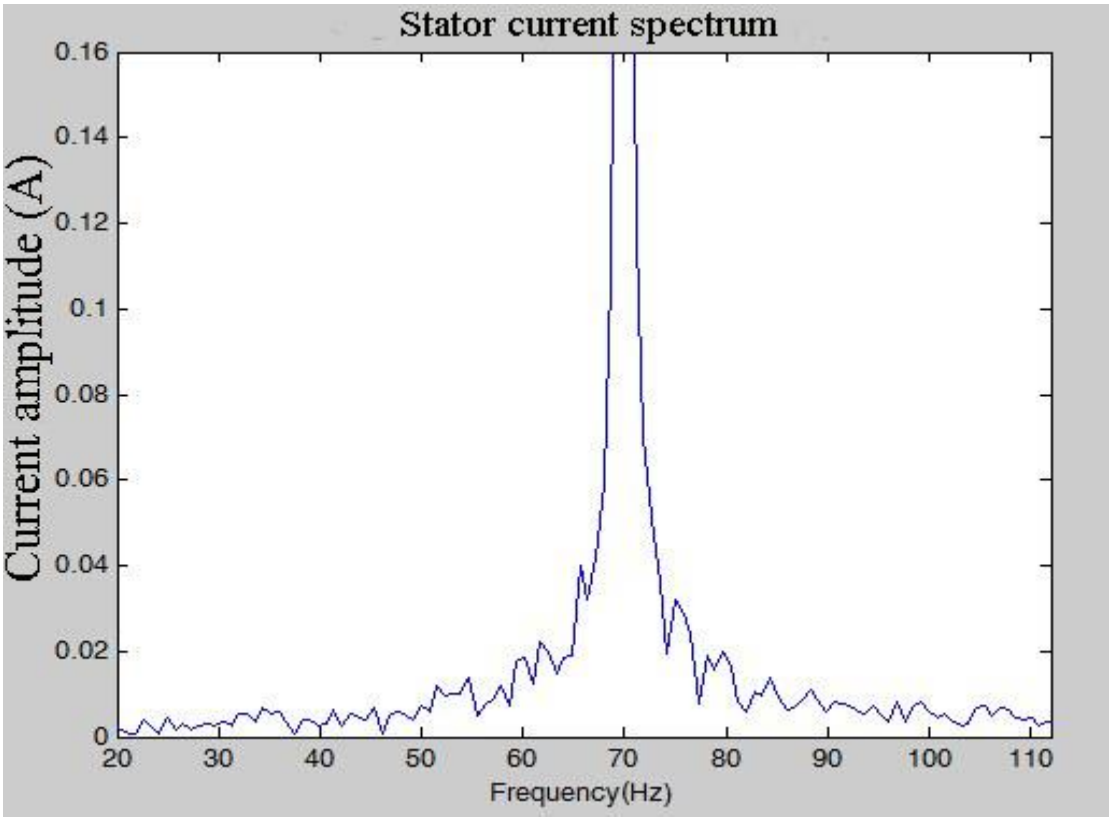

Fig. 4.3: Stator current spectrum under normal condition

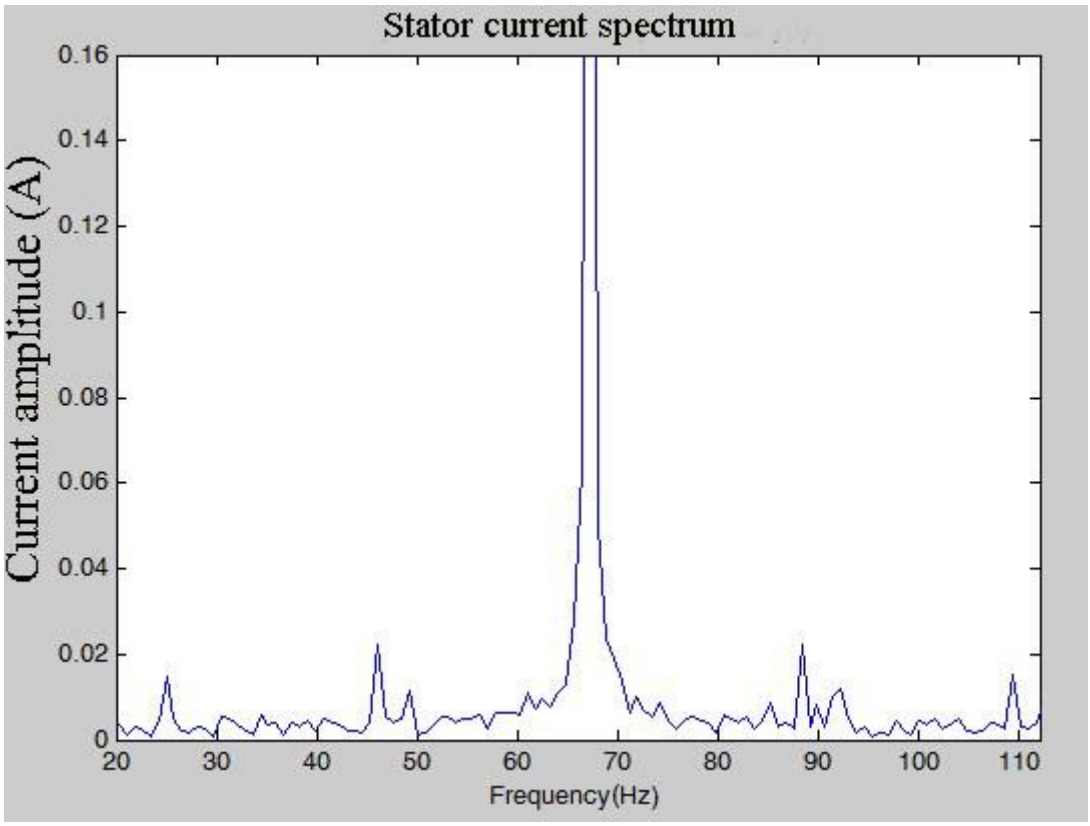

Fig. 4.4: Stator current spectrum under faulty condition (two weights added)

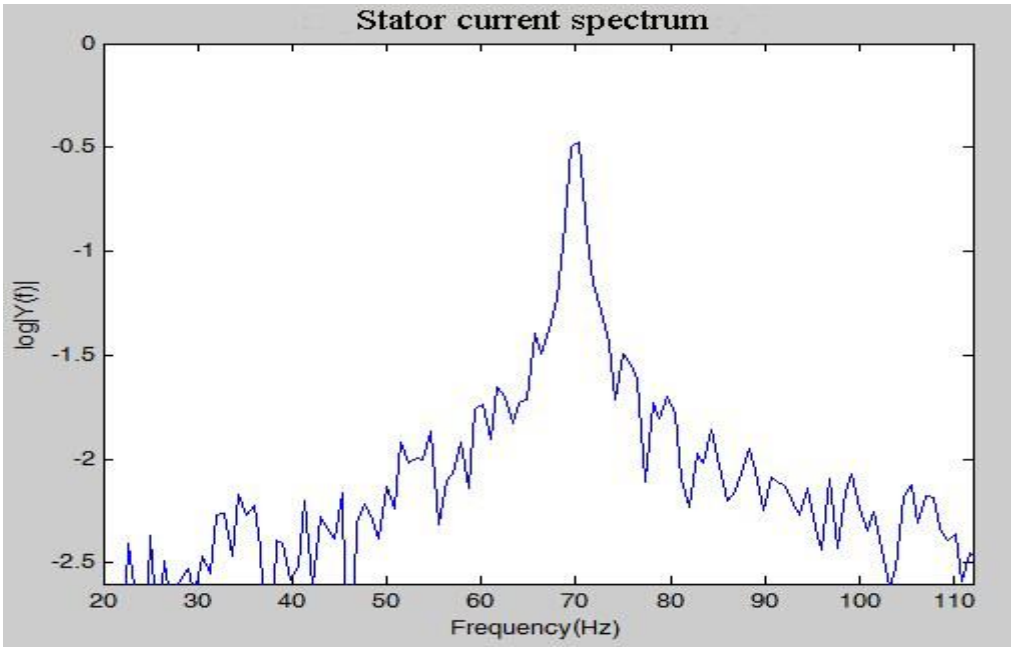

Fig. 4.5: Stator current spectrum under normal condition

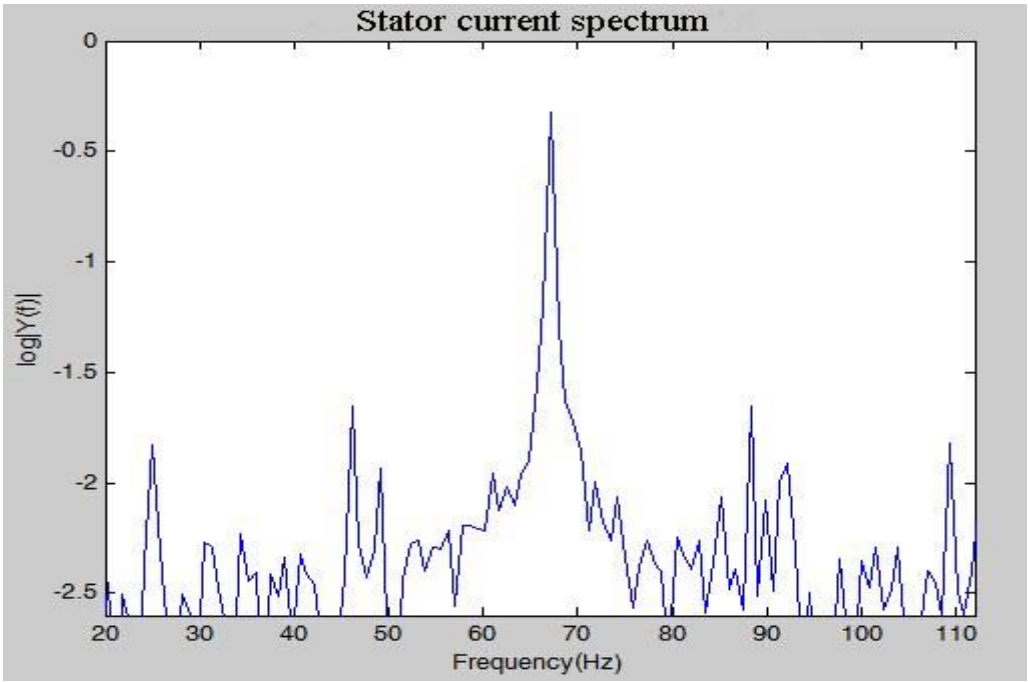

Fig. 4.6: Stator current spectrum under faulty condition (two weights added)

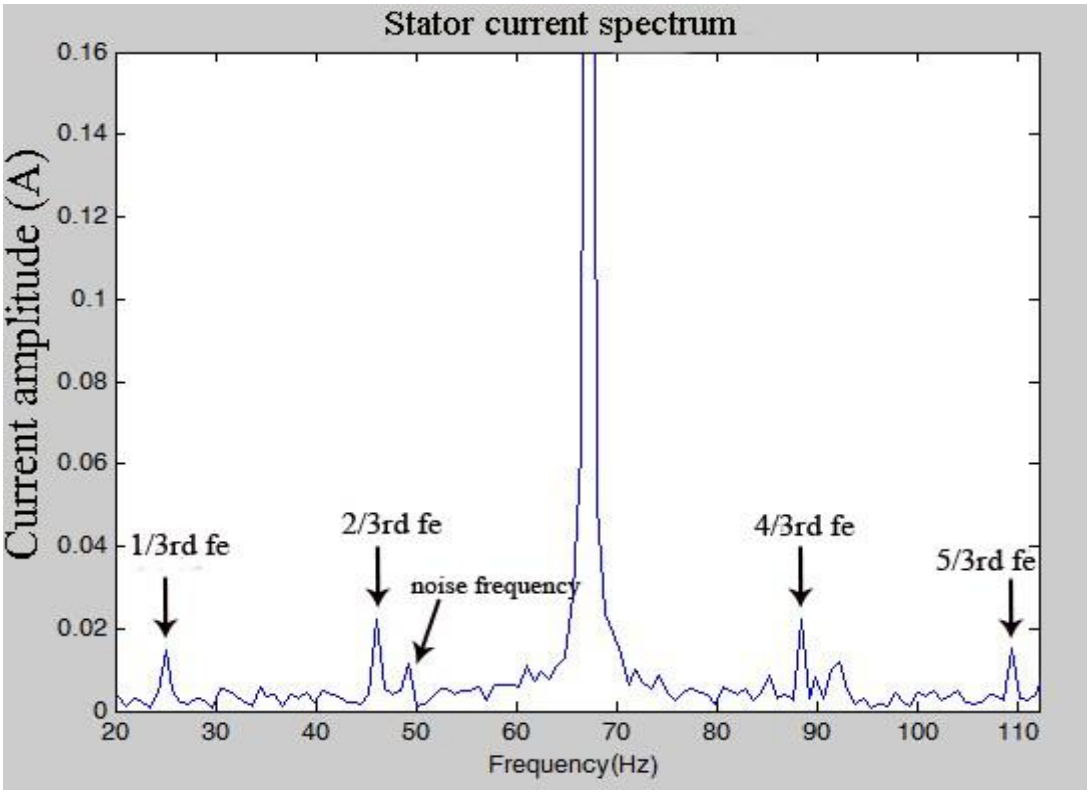

Fig. 4.7: Stator current spectrum under faulty condition (two weights added)

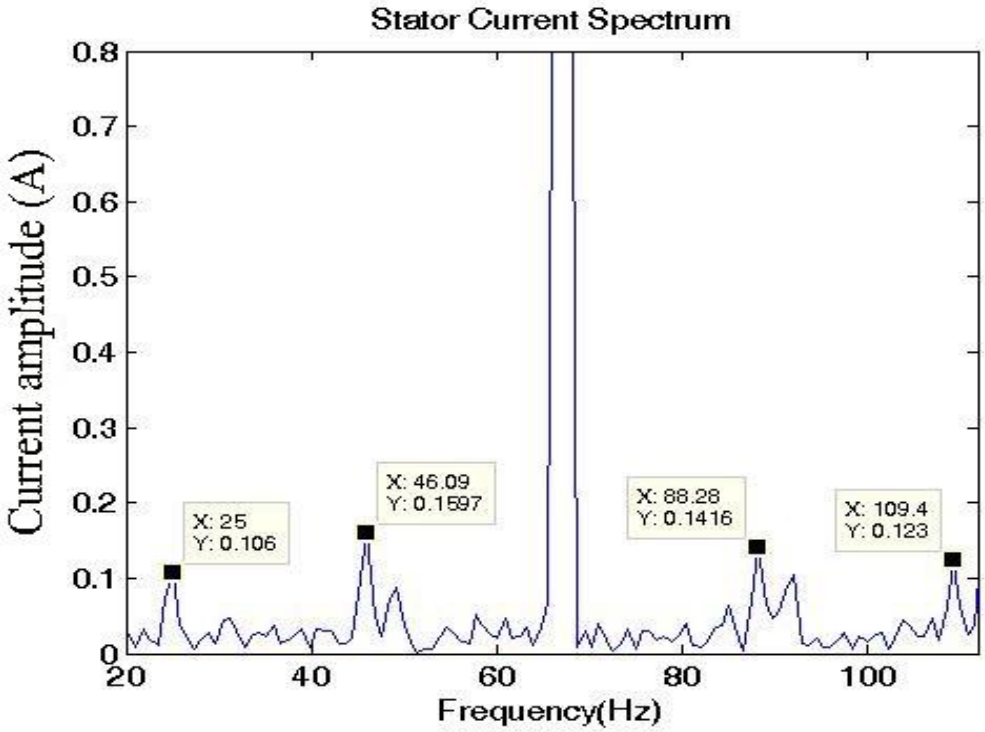

Fig. 4.8: Stator current spectrum under faulty condition (two weights added)

In Fig. 4.7-4.8, there are four side band harmonics in unbalanced load conditions. The fundamental frequency is located around 67Hz. Theoretically, the characteristic frequency should be 22.3Hz, 44.7Hz, 89.3Hz and 111.7Hz, which stands for 1/3, 2/3, 4/3 and 5/3 of fundamental frequency. Considering the low resolution of 0.78 Hz, the side band harmonics are now perfectly located in these four expected points. There are some noise frequencies near the characteristic frequency as well, which are caused by the oscilloscope and the whole HVAC system. The amplitude of these noise frequencies will vary in each FFT experiment. Sometimes, the noise frequency can have a large effect on the real FFT spectrum.

4.3.2 Stray Flux Spectrum Analysis

In the experiment, a stray flux sensor is put inside the blower as shown in Fig. 4.9. Fig. 4.10-4.11 shows the stray flux spectrums in normal conditions and unbalanced

load conditions (two weights added). Although the characteristic frequency components ($\frac{1}{3}f_e, \frac{2}{3}f_e, \frac{4}{3}f_e, \frac{5}{3}f_e$) exist in the stray flux spectrum as well, it is evident the fundamental component and second order harmonics increase because an unbalanced load induces the asymmetry and leakage of the magnetic field, and even harmonics increase. The increasing amplitude of the fundamental frequency component is also caused by the total torque variation by adding weights to the fan blade. According to Fig. 4.10-4.11, the amplitude of fundamental frequency component increases by 65%, while the amplitude of the second harmonics component increases by 102%. Considering the effect of total load change, the increasing rate of the second harmonics component vs. the fundamental frequency component can still be an indicator of an unbalanced load condition.

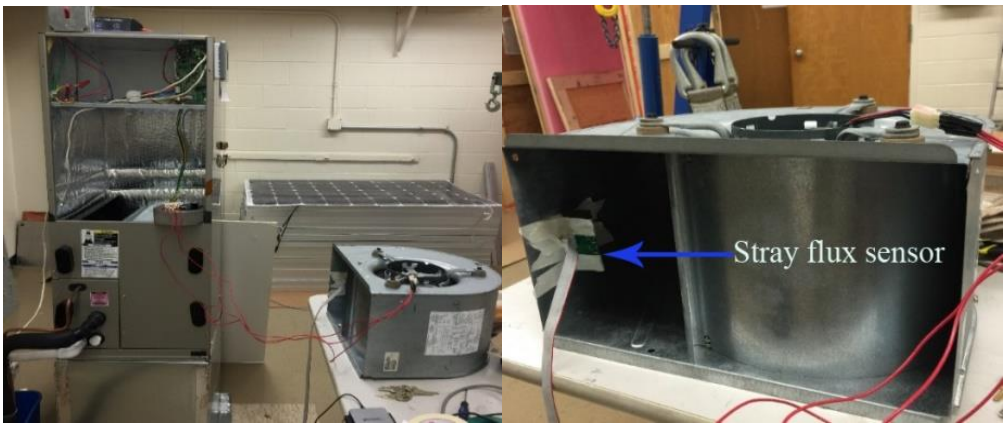

Fig. 4.9. Blower wheel and stray flux sensor

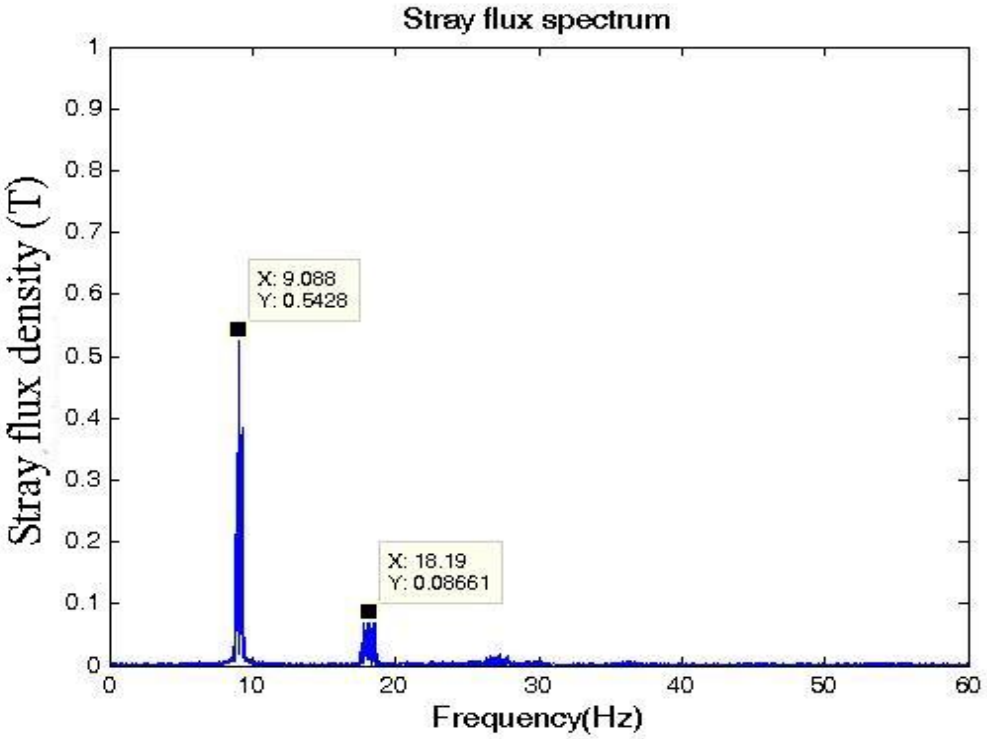

Fig. 4.10: Stray flux spectrum under normal condition

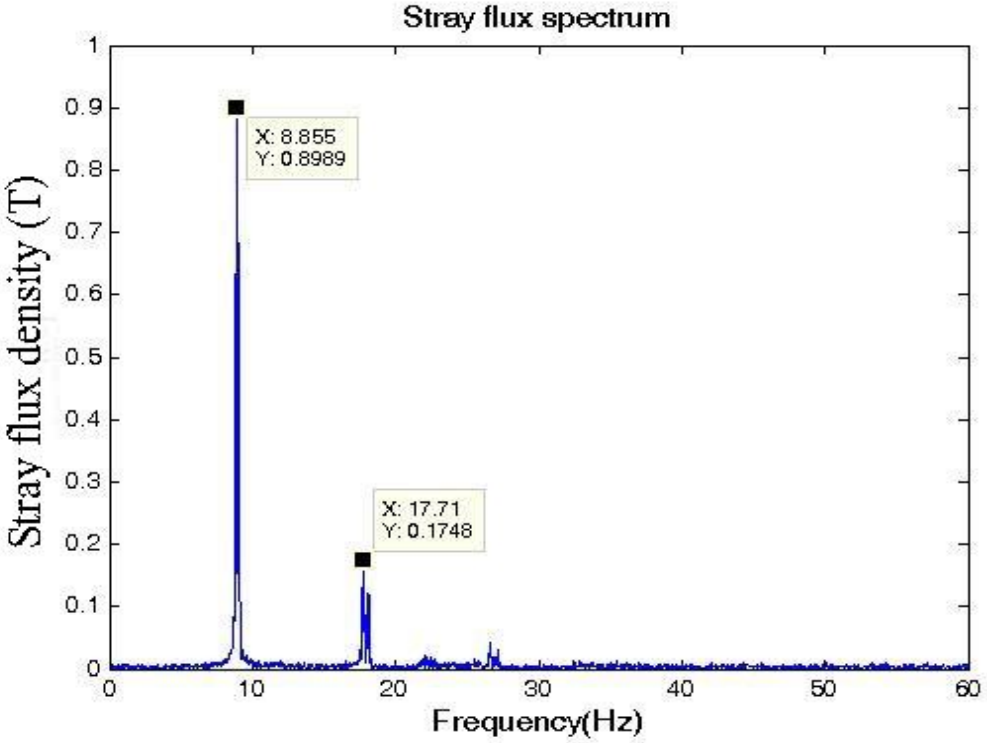

Fig. 4.11: Stray flux spectrum under unbalanced load condition

4.4 Conclusions

For most air handlers, the unbalanced load of the blower wheel is created by the unevenly distributed contaminants on the blades. In the experiment, the unbalanced load condition is emulated by adding a different number of weights to the inner side of the blade. The traditional condition monitoring method is to exploit specific characteristic frequency components which can be used as an index showing unbalanced torque and dynamic eccentricity.

The unbalanced load can create dynamic eccentricity conditions or increase dynamic eccentricity severity. The main target is to monitor the unevenly distributed contaminants on the blades or the broken blade where both can produce unbalanced conditions. Thus, characteristic frequency components of both unbalanced load conditions and dynamic eccentricity created by unbalanced loads are observed. Two levels of unbalanced load conditions are examined with one and two weights added to the inner side of one blade. Experiment results show very clearly that 2/3 and 4/3 of fundamental frequency components increases significantly with respect to the unbalanced load severity, while 1/3 and 5/3 of fundamental frequency components also increase due to dynamic eccentricity. Moreover, since the air handler is running in a relative stationary mode with three fixed preset speed levels for most of the time, the unbalanced load detection is conducted under constant speed conditions without any speed level change. For non-stationary conditions, the time-frequency/time-scale methods can be utilized to detect the faults.

A new stray flux spectrum condition monitoring method is proposed to increase the reliability in detecting an unbalanced load condition. The stray flux of an electrical machine is a residual and undesirable effect which does not participate in the process of generating electromagnetic torque. A high accuracy external flux sensor is

used to detect unbalanced load. When the load is unbalanced, the magnetic field of the BLDC motor is not a perfect circle, so additional stray flux appears outside the motor. For a BLDC motor, the rotational harmonics reflecting the asymmetry can be $2f_e$ because an unbalanced load produces even harmonics in the system. Introducing another high accuracy sensor increases the total cost of the system, so this is mainly applicable to an HVAC system of a higher importance which requires increased reliability, for example an HVAC system for a data center.

CHAPTER 5

CONDITION MONITORING OF STATIC ECCENTRICITY OF BLDC MOTORS IN AIR HANDLERS

5.1 Introduction

Because of the wide range of applications of BLDC motors, the fault diagnosis of BLDC becomes an essential problem. Rotor faults account for most of the faults affecting BLDC motors. Static eccentricity and dynamic eccentricity are two of the main faults in the rotor of a BLDC motor. In HVAC system, static eccentricity of fan motor is usually caused by incorrect positioning of the rotor or the stator at the commissioning stage or operational stage when some collision happens to the air handling unit. If static eccentricity lasts for a long time, it will create unbalanced electromagnetic field and shorten the lifespan of the fan motor. In this chapter, an improved method in detecting static eccentricity is proposed based on the comparison between the positive sequence current and negative sequence current. Compared to the traditional method, which only focuses on the change of the negative sequence of fundamental frequency current, the method proposed could be more reliable, since a

positive sequence current and harmonics current are considered as well. A BLDC motor with static eccentricity in an air handler will be tested. The effectiveness and availability are verified in both simulation and experimental results.

5.2 Negative Sequence Current Analysis

Asymmetries in three phase BLDC motors may arise due to several reasons, such as load fluctuations, unbalanced supply voltages, and static eccentricities. These asymmetries can be reflected in the negative sequence components of a stator current. One method that could be used to diagnose static eccentricity is the detection of negative sequence current components that are produced because of motor eccentricity. Static eccentricity results in unequal amounts of magnetic flux passing across stator coils. This results in an imbalance in the three phase currents, which should theoretically produce a negative sequence current.

This section briefly reviews the established negative sequence current analysis. The negative sequence current is obtained from the measurement of the three phase stator currents of BLDC motors using equation (5.1),

$$I_{a2} = \frac{1}{3}\left(I_{a,f} + \alpha^2 I_{b,f} + \alpha I_{c,f}\right) \tag{5.1}$$

where $I_{a,f}$, $I_{b,f}$ and $I_{c,f}$ are the magnitudes of the fundamental components of the three phase current signals, and α is a phase rotation operator equivalent to $e^{i2\pi/3}$ or 120°.

5.3 Analysis and Results

5.3.1 Simulation Analysis and Results

A three phase, six pole, and eighteen slot BLDC motor is built in Maxwell 2D,

as shown in Fig. 10. The model of a BLDC motor is built with different degrees of static eccentricity. The original air gap is set at 0.07 inches. The stator is shifted 0.035 inches away, which is half of the original air gap from the original point, by shrinking the designed band. For the designed model in Fig. 5.1, the air gap on the left is much larger than that on the right so that severe static eccentricity is produced in this BLDC motor. Considering the calculation time of Maxwell 2D, the simulation step is set to be 0.002s and stop time is 0.4s. The required three phase current is listed in Fig. 5.3-5.5. It can be noted that the stator current in Fig. 5.3-5.5 is not an ideal square wave because of the existence of inductance and phase switching.

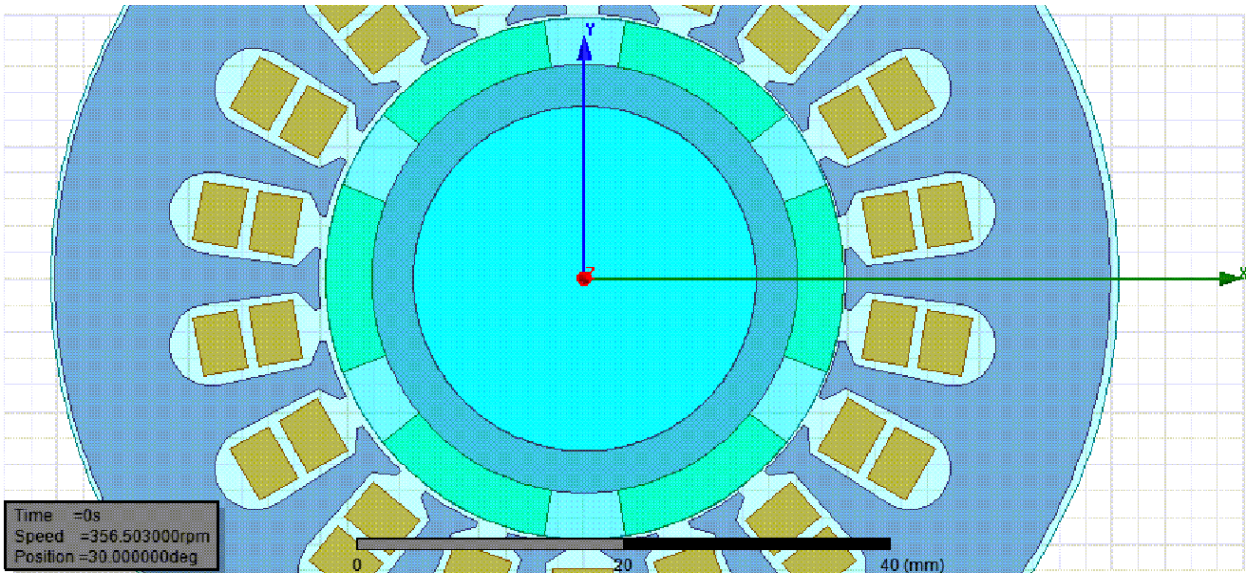

Fig. 5.1: BLDC model with static eccentricity in Maxwell

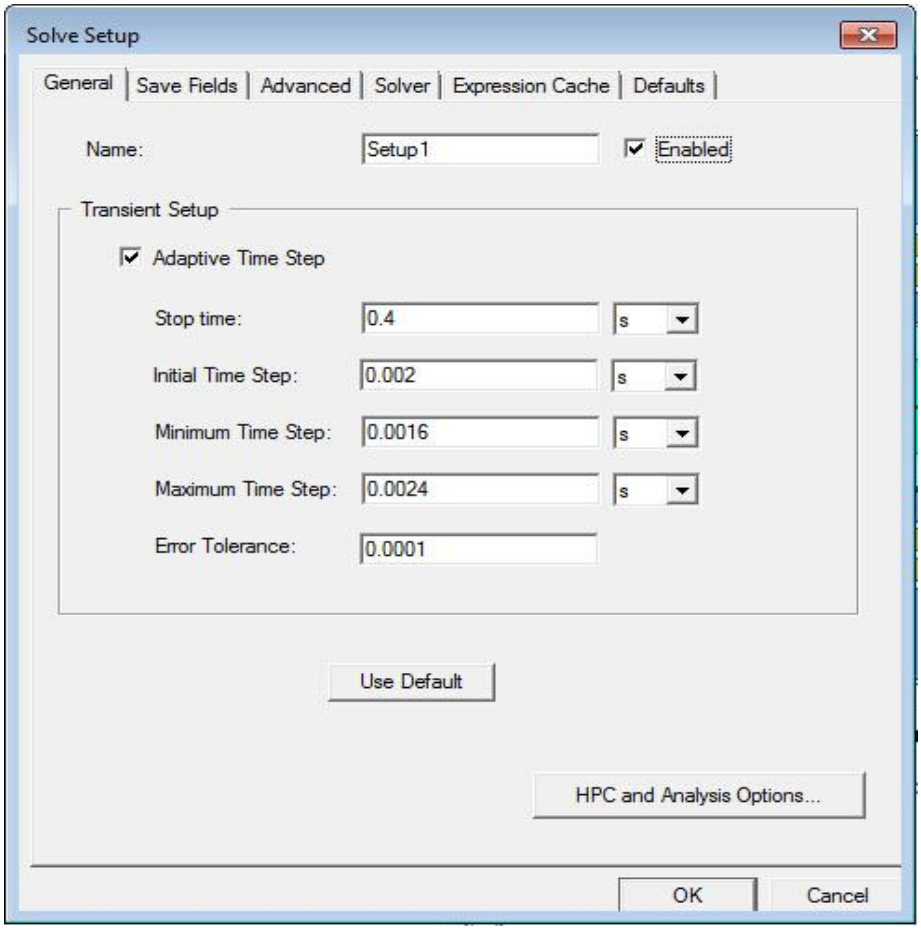

Fig. 5.2: Simulation settings

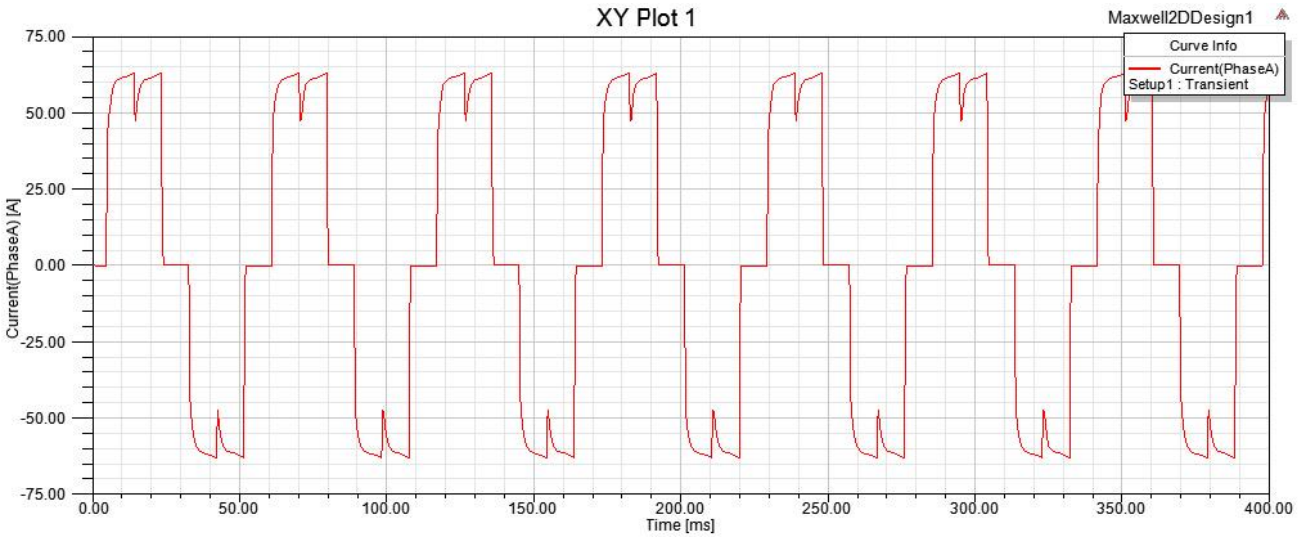

Fig. 5.3: Phase A current waveform

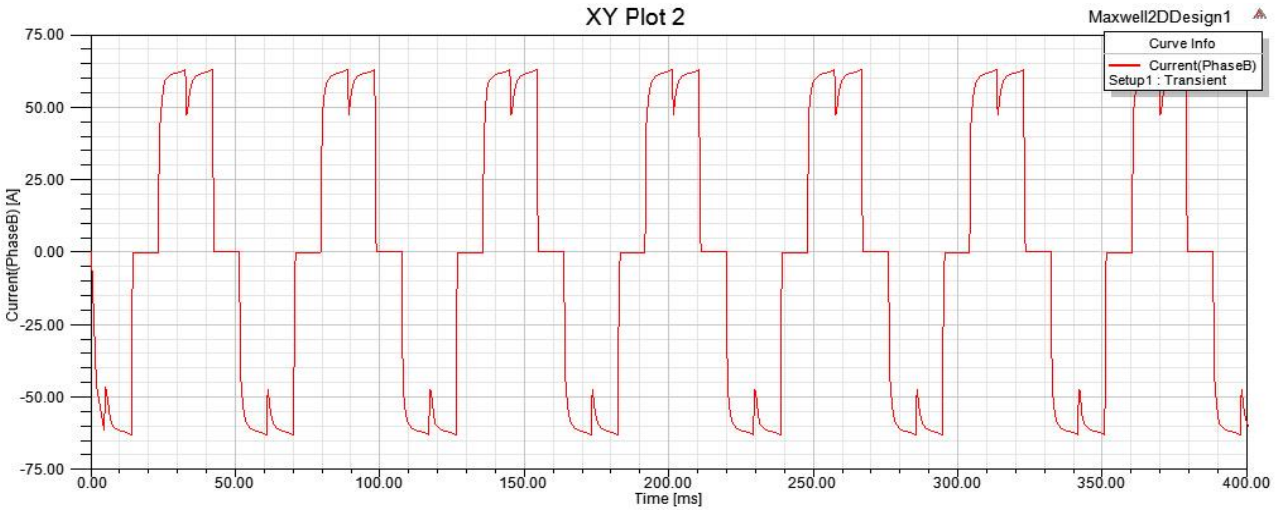

Fig. 5.4: Phase B current waveform

Fig. 5.5: Phase C current waveform

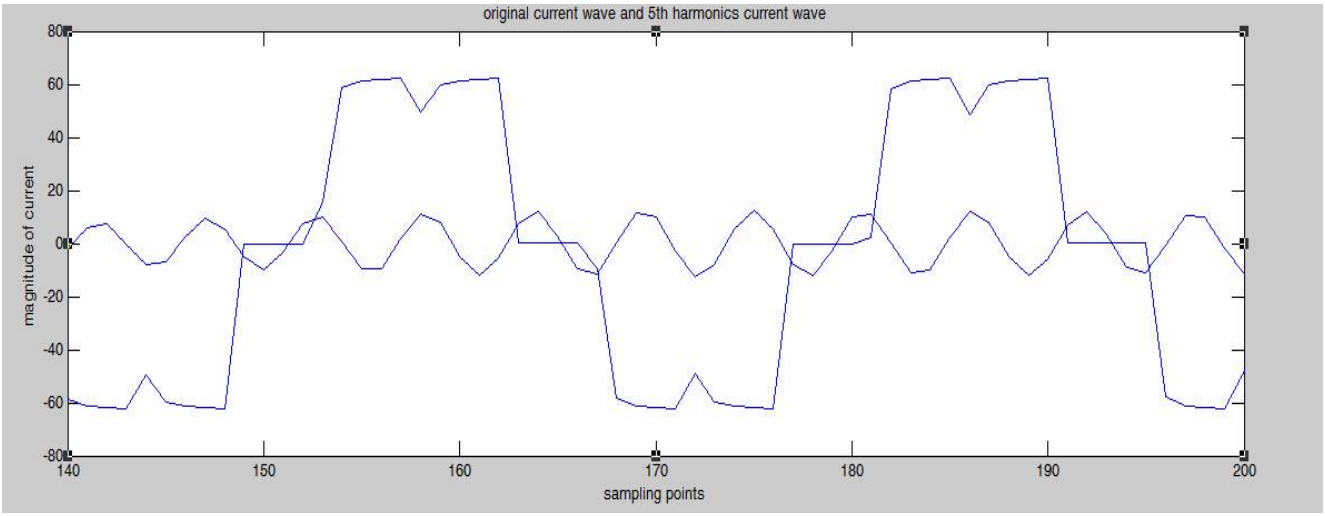

Fig. 5.6: Separated fundamental frequency and 5th harmonics

The fundamental frequency current, 5^{th} harmonics current and 7^{th} harmonics current is filtered from the three-phase current based on FFT results. These current signals at specific frequencies are utilized to calculate the positive sequence current and negative sequence current, which are listed in Table 5.1.

Table 5.1: Three phase current and positive/negative current with static eccentricity

	Current Magnitude (Amp)	Current Phase angle (deg)
Phase A	63.2692	-71.104
Phase B	66.3806	166.346
Phase C	62.3714	45.1147
Positive Seq	63.9833	-2.1098
Negative Seq	2.4488	-74.117

For an ideally designed Maxwell BLDC model, the effect of unbalanced supply voltages and load fluctuations can be eliminated. The negative sequence current is produced solely by static eccentricity. Theoretically, the negative sequence current should not be zero because of an unbalanced air gap. The simulation result verifies that the negative sequence current itself could be an indicator of static detection for BLDC motors if load fluctuations and an unbalanced supply voltage had not existed.

5.3.2 Experiment Analysis and Results

For the general air handler in Fig. 5.7, the blower wheel is driven by a three phase, six pole and eighteen slot BLDC motor (1/2HP, 120V/240V AC single-phase input, 50/60Hz). To add the static eccentricity to this BLDC motor, three different outer races outside the bearings are built. The material of the outer race has been removed at three different levels. Three new outer races shifting away from the geometrical center point with a distance of 0.005, 0.007, 0.009 inches are designed.

The air gap is measured by a feeler-gauge when the rotor is rotated every 120 degrees. Under each condition, four air gap values in each symmetrical position are measured as shown in the right bottom corner of Fig. 5.7. Thus, the designed static eccentricity condition can be ensured.

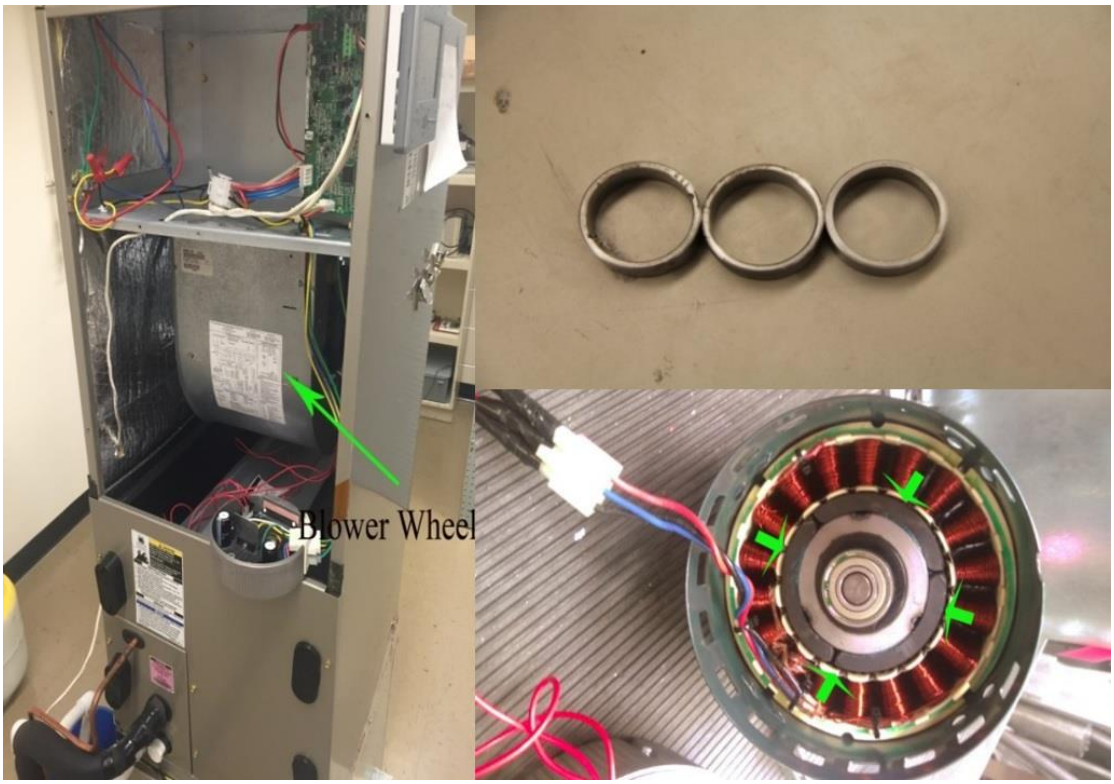

Fig. 5.7: Air handler and detached fan motor

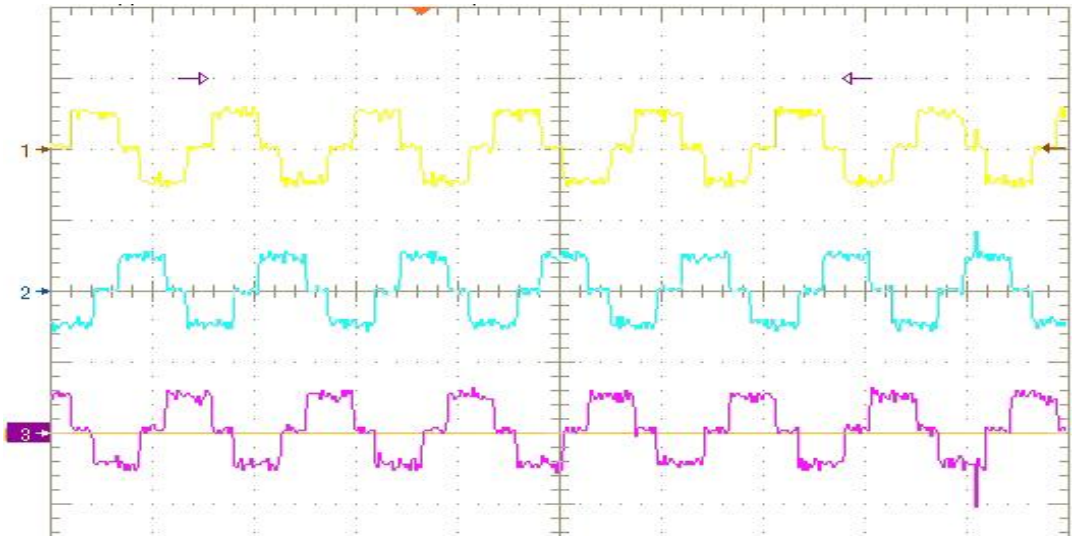

Fig. 5.8: Three phase stator current

The three phase currents of the BLDC inside the air handler are detected by current probe (Tektronix TCP303), as shown in Fig. 5.8. In order to attain a positive sequence current and a negative sequence current, the phase angle and magnitude of the three phase currents (fundamental, 5^{th} and 7th) are calculated using FFT. The original phase current, together with a 5^{th} harmonics current filtered by a specifically designed filter in Matlab, are shown in Fig. 5.9.

The positive and negative sequence components of the fundamental currents, 5^{th} harmonics current, and 7^{th} harmonics current is calculated in Table 5.2-5.7. Based on the calculation results, a negative sequence current is noticed in both normal conditions and in static eccentricity conditions. Theoretically, the negative sequence current should be zero because of the balanced air gap. However, according to the data we measured in normal conditions, the original air gaps are not perfectly equal in different directions. So, under normal conditions, there are some negative sequence currents shown in the experiment's results. The supply voltage and the load fluctuation is relatively small compared with the static eccentricity severity because of the large air gap offset implemented in the experiment. However, this issue still needs to be considered for a more accurate estimation method.

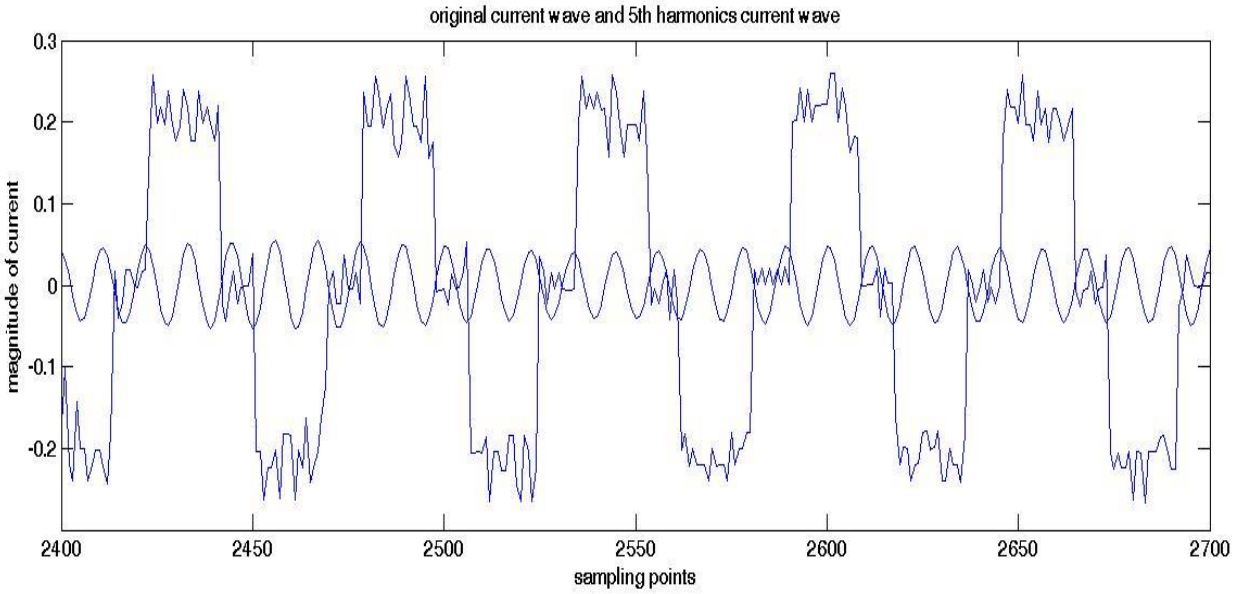

Fig. 5.9: Original phase current and 5th harmonics

Table 5.2: Positive and negative sequence components of the fundamental currents in normal condition

	Current Magnitude (Amp)	Current Phase angle (Deg)
Phase A	0.2016	-60.109
Phase B	0.2081	-179.75
Phase C	0.1912	61.7477
Positive Seq	0.2002	-0.7154
Negative Seq	0.00427	60.4158
Neg/Pos ratio (Current Magnitude)	0.0213	

Table 5.3: Positive and negative sequence components of 5th harmonics current in normal condition

	Current Magnitude (Amp)	Current Phase angle (Deg)
Phase A	0.0454	63.8447
Phase B	0.0412	-172.73
Phase C	0.0421	-58.465
Positive Seq	0.00248	2.6289
Negative Seq	0.0428	0.34326
Pos/Neg ratio (Current Magnitude)	0.0579	

Table 5.4: Positive and negative sequence components of 7th harmonics current in normal condition

	Current Magnitude (Amp)	Current Phase angle (Deg)
Phase A	0.0347	-42.599
Phase B	0.0339	-175.12
Phase C	0.034	68.6805
Positive Seq	0.0341	-7.0303
Negative Seq	0.00222	60.7607
Neg/Pos ratio (Current Magnitude)	0.0651	

Table 5.5: Positive and negative sequence components of the fundamental currents in static eccentricity condition

	Current Magnitude (Amp)	Current Phase angle (deg)
Phase A	0.2317	57.7083
Phase B	0.258	-63.197

Phase C	0.2387	177.173
Positive Seq	0.2428	-0.4962
Negative Seq	0.0083	-52.865
Neg/Pos ratio (Current Magnitude)	0.0342	

Table 5.6: Positive and negative sequence components of the of 5th harmonics current in static eccentricity condition

	Current Magnitude (Amp)	Current Phase angle (deg)
Phase A	0.0537	-58.511
Phase B	0.05	65.2599
Phase C	0.052	173.806
Positive Seq	0.0041	15.3462
Negative Seq	0.0517	-1.3532
Pos/Neg ratio (Current Magnitude)	0.0793	

Table 5.7: Positive and negative sequence components of the of 7th harmonics current in static eccentricity condition

	Current Magnitude (Amp)	Current Phase angle (deg)
Phase A	0.0416	58.0578
Phase B	0.037	-53.388
Phase C	0.0429	-168.87
Positive Seq	0.0403	7.2223
Negative Seq	0.0045	-63.46
Neg/Pos ratio (Current Magnitude)	0.1117	

The comparison of the two conditions (normal condition and static eccentricity condition) is listed in Table 5.8. The Neg/Pos ratio in fundamental frequency increases as static eccentricity appears. All of the experimental settings remain unchanged, except for the different outer races inserted into the BLDC motor. Thus, the static eccentricity could be the main factor increasing the Neg/Pos ratio. This index can be utilized to make judgments regarding static eccentricity severity. The same behavior is also noticed in the negative sequence component of the 7^{th} harmonic. For the 5^{th} harmonic, the effective index is the Pos/Neg magnitude ratio. Compared to the traditional method, which only focuses on the change of the negative sequence of the fundamental frequency current, the method proposed in this paper could be more reliable, since the positive sequence current and harmonics current which represent load fluctuations are considered as well. Since BLDC motors have relatively large air gaps, even a small change of positive sequence current may have a non-negligable effect on the fault detection of static eccentricity. It is concluded that the index Neg/Pos ratio and Pos/Neg ratio could be a more effective indicator in detecting static eccentricity in BLDC motors.

Table 5.8: Comparison of the two conditions (normal condition and static eccentricity condition)

Neg/Pos or Pos/Neg ratio (Current Magnitude)	Fundamental(Neg/Pos)	5^{th}(Pos/Neg)	7^{th}(Neg/Pos)
Normal	0.0213	0.0579	0.0651
Static eccentricity	0.0342	0.0793	0.1117

5.4 Conclusions

The fault diagnosis of BLDC becomes an essential problem because of the wide range of applications of BLDC motors. It is known that asymmetries in three phase BLDC motors may arise due to several reasons, such as load fluctuations, unbalanced supply voltages and static eccentricities. The static eccentricity detection of BLDC motors is relatively difficult compared with dynamic eccentricity. In BLDC motors, the relative permeability of a magnet is equal to that of air, leading to relatively large air gaps in BLDC motors. Hence, any physical shift causing an air gap length change has a negligible effect on the flux distribution. Most of the previous research on detecting static eccentricity focuses on the negative sequence current change of BLDC motors.

An improved method in detecting static eccentricity is proposed based on the comparison between the positive sequence current and negative sequence current. Compared to the traditional method, which only focuses on the change of the negative sequence of fundamental frequency current, the method proposed could be more reliable, since the effect of load fluctuations can be largely eliminated. According to the experiment results, this method is very effective in detecting severe static eccentricity conditions in this 1/2 HP three phase, six pole and eighteen slot BLDC motor. However, further research on this method should be conducted for all kinds of BLDC motors with different structures and power ratings.

CHAPTER 6

CONDITION MONITORING OF THE REFRIGERANT LEVEL IN REFRIGERATION SYSTEMS

6.1 Introduction

There are several faults that can occur with the outdoor units of HVAC systems, and they can exist individually or in any combination, creating a multitude of symptoms [39].

Typical faults can include:

- Under or overcharge
- Refrigerant leaks
- Restrictions in the liquid line or expansion device
- Defective thermal expansion valve or other expansion device
- Non-condensable gases in the system
- Condenser and evaporator fouling.

The difficulty with diagnosing refrigerant problems is that there can be multiple faults that are interrelated. For example, a problem with a liquid line restriction or non-condensable contaminants in the system can lead to a false diagnosis of refrigerant charge. Arriving at a correct diagnosis requires that the system be inspected for faults in a particular order using a systematic approach that considers the environmental conditions during testing and other factors.

The challenge in performing diagnostic tests is to identify the particular source of problems that affect performance so that they can be corrected. Combinations of faults can yield false clues about the conditions of refrigerant charge, and can be very

difficult to sort out. As reported by Purdue researchers, “evaluating fault detection and diagnosis is hard” and “false alarms happen” [81]. The methods in this chapter describe an attempt to significantly improve field diagnostic procedures and catch one major problem, which is refrigerant undercharge condition.

For each air-conditioning system, a specified amount of refrigerant is required for the system to operate at optimal conditions in terms of design discharge and suction pressures. Field systems usually show some variations from the specified charge conditions. Small variations are possibly due to the negligence of the field installers, which may not affect system performance significantly. However, serious performance degradation can occur when the level of charge is below a certain limit. Periodic maintenance of the system can identify and correct the problem. However, in many cases the problem may persist for a long period of time because of poor or no maintenance, resulting in lower system performance and higher energy usage [82].

Proper refrigerant charge affects both the efficiency and capacity of the system. Besides impacting energy usage and the system capacity, incorrect charge can also damage equipment. If the system is overcharged, there is a chance that liquid refrigerant will not completely evaporate and could enter the compressor cylinder from the suction point causing damage to the compressor. If there is too little charge in the system, the low suction line pressure and corresponding saturation temperature of the refrigerant can lead to the formation of ice on the evaporator, which restricts heat transfer, increases airflow resistance, and reduces airflow. This will further reduce air conditioner performance and can shorten compressor life [81].

Tests of more than 4,000 residential cooling systems in California indicated that about 34% were undercharged, 28% were overcharged, and only 38% had the correct charge. Additional field data for residential cooling systems gathered by Blasnik et al. and Proctor indicated that an undercharge of 15% is common. Temple identified how

many units of a sample of 289 were within 4°F of the nominal charge for subcooling and 8°F for superheating. Of these, 28% had an acceptable charge, 31% were high, and 41% were low. Mowris reported field measurements of 4,168 air conditioners where 72% of systems had improper refrigerant charge, and 44% had improper airflow. These studies point to the conclusion that a large percentage of systems are operating below their rated efficiencies. It should be noted that the accuracy of large sets of field measurements may be brought into question by technicians using analog pressure gauges and pipe temperature measurement instruments that might cause false undercharge diagnostics.

The impact of under and overcharge is developed from data obtained by Pacific Gas & Electric Company at their San Ramon test facility using systems with orifice and thermal expansion valves. The results verify that thermal expansion valves can mitigate the effects of undercharge, provided they are properly installed. If the thermal expansion valve's sensing bulb does not have good thermal contact with the suction line, refrigerant charge can be misdiagnosed [81].

Some previous research shows the results of some experiments where the refrigerant is insufficient [81]. Fig. 6.1 clearly reveals that both air enthalpy and refrigerant enthalpy methods yield similar results where cooling capacity decreases at charge levels down to 90%. For further reduction in charge level to 80% and below, while the refrigerant enthalpy method shows a gradual decrease in the cooling capacity, the air enthalpy method shows a drastic decrease to zero and even negative values [82].

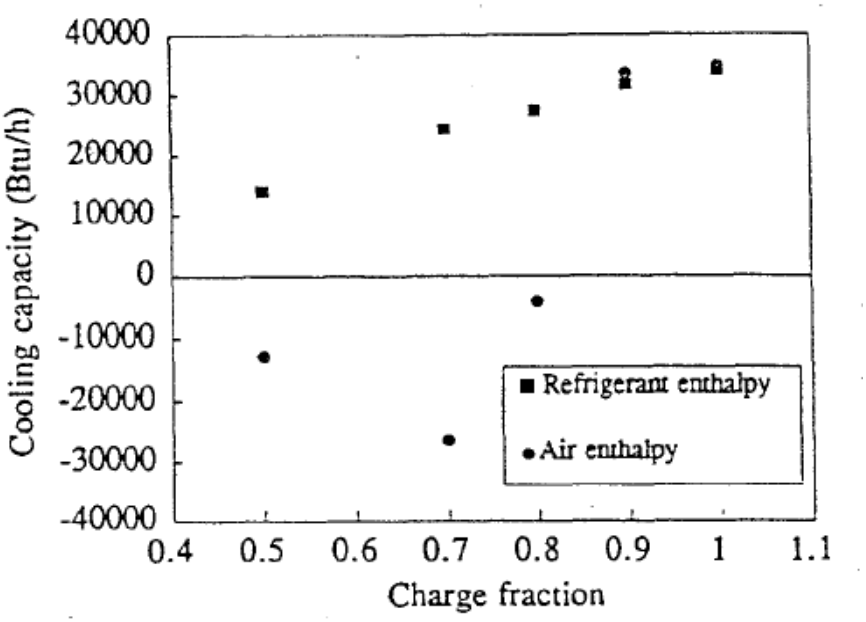

Fig. 6.1: Cooling capacity vs. charge fraction

In relation to the detection of undercharge problems, several approaches to fault detection and diagnosis have been published over the years [83-86]. In practice, for the professional HVAC technician, it is very common to use pressure gauges and temperature measurement tools to diagnose a problem by comparing the measured value with a reference value under different conditions. This is called a direct signal evaluations method, utilizing the comparison to known characteristics [83]. Some other methods, such as model-based parity-space approaches, imply the calculation of residuals, or observer-based approaches, can be used [84]**.** Benchmark tests show that often, a combination of various approaches is required to get the most reliable and accurate refrigerant level estimation results**.** For the classification task, statistical methods, such as Bayes classifiers, are mentioned [85], as well as expert systems and methods based on fuzzy logic or neural network techniques [86].

6.2 Theoretical Analysis of Condition monitoring of Refrigerant levels

6.2.1 Basic Diagram of Condition Monitoring Method

The cooling capacity is reduced when the refrigerant is insufficient. In order to adjust the temperature with the same accuracy as full charge level, the torque of the compressor is controlled to be higher than rated, thus more energy is utilized to drive the motor. As the current magnitude is higher, loss of energy on the stator and rotor resistance increases, and more heat is produced inside the motor. Because stator resistance is assumed to have a linear relationship with temperature, as the time of use increases, the stator winding resistance will increase. As a result, the magnitude of the current of the undercharged air conditioner will be higher than the fully charged one. These relationships are clarified in Fig. 6.2. Therefore, the ultimate goal of this research project is to estimate the stator winding resistance.

Fig. 6.2: Key relationship between refrigerant level and stator winding resistance

The basic diagram regarding the condition monitoring method is presented in Fig. 6.3. The back EMF constant is detected offline for the compressor motor utilizing reverse rotation when shutting down the motor. With estimated speed and measured current/voltage, the RLS (recursive least square) is conducted to estimate stator

resistance in real time. Then, the temperature can be estimated in a straightforward manner. On the other hand, temperatures at the inlet, outlet, and surface of the compressor is measured to provide more information for temperature verification.

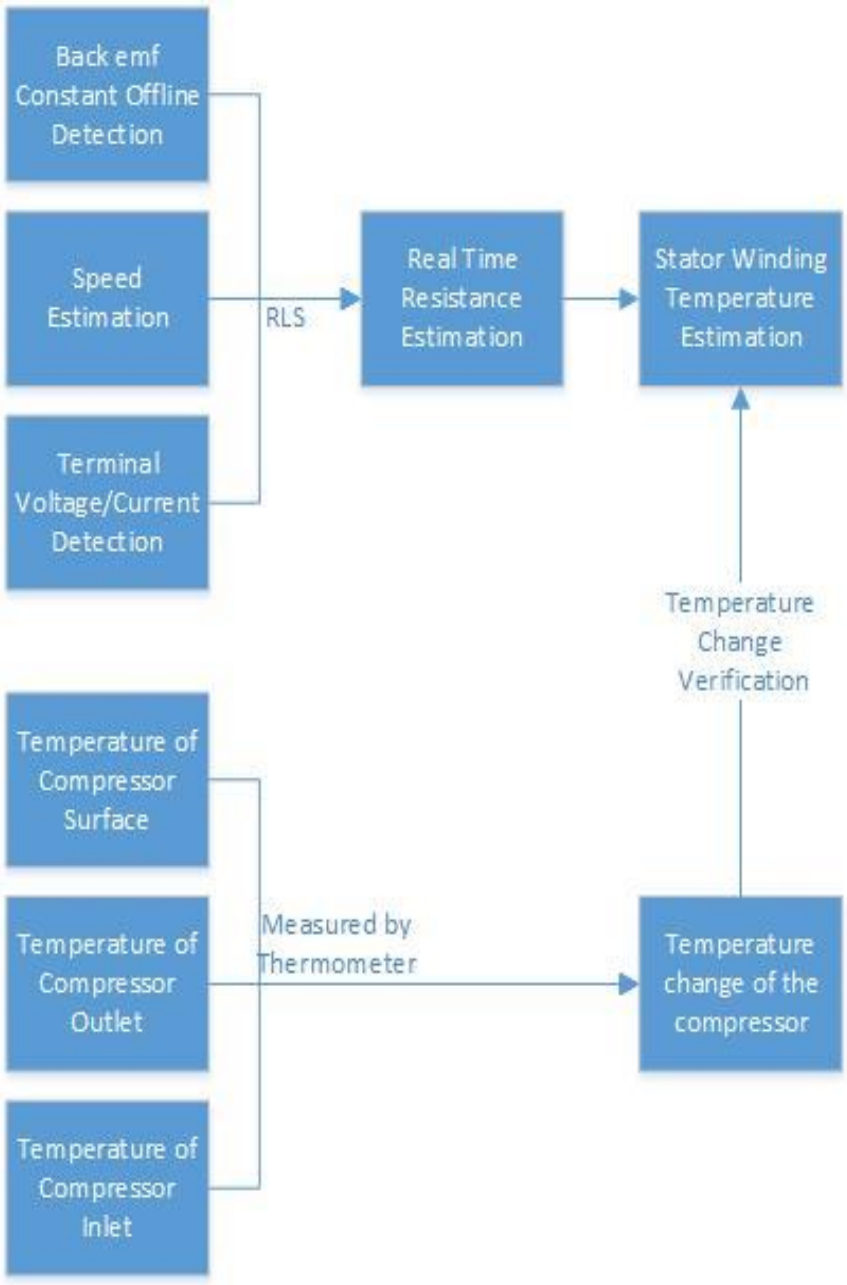

Fig. 6.3: Basic diagram of condition monitoring method

6.2.2 RLS Estimation of PMSM Stator Resistance

The RLS estimation method is applied in the research. The RLS is an adaptive filter which recursively searches for the coefficients that can minimize a weighted linear least squares cost function, relating to the input signals.

6.2.2.1 Basic Theory

According to the mathematical model of a typical PMSM under stationary reference frame, the stator current i_a, stator resistance R_a, stator inductance L_a, and terminal voltage v_a are the main variables in equations (6.1)-(6.4).

$$pi_a = -\frac{R_a}{L_a} i_a - \frac{e}{L_a} + \frac{v_a}{L_a} \tag{6.1}$$

$$L_a p i_a = v_a - R_a i_a - e \tag{6.2}$$

$$L_a p i_a = u - e \tag{6.3}$$

$$\text{Where, } u = v_a - e \tag{6.4}$$

According to the discrete state equation:

$$i_a(n+1) = A i_a(n) + B u(n) \tag{6.5}$$

$$\text{where, } A = \left[1 - \frac{R_a \Delta T}{L_a}\right],\ B = \left[\frac{\Delta T}{L_a}\right] \tag{6.6}$$

And ΔT is the sampling period.

$$i_a(n+1) = [A \quad B][i_a(n) \quad u(n)]^T \tag{6.7}$$

$$\theta = [A \quad B] \tag{6.8}$$

The unknown parameter matrix θ can be derived from known vectors by using the least square method. This method identifies the parameter matrix θ, such that the square of the prediction error reaches minimum.

$$\varepsilon = (i_a(n+1) - \theta[i_a(n) \quad u(n)])^2 \tag{6.9}$$

$$\text{Let } z = [i_a(n) \quad u(n)] \tag{6.10}$$

$$\theta(n+1) = \theta(n) + (i_a(n+1) - \theta(n) z) z^T P_c(n) \tag{6.11}$$

$$P_c(n+1) = \frac{1}{\lambda}\{P_c(n) - P_c(n)z(\lambda + z^T P_c(n)z)^{-1} z^T P_c(n)\} \quad (6.12)$$

$$R_a = \frac{(1-A)}{B} \quad (6.13)$$

$$L_a = \frac{\Delta T}{B} \quad (6.14)$$

6.2.2.2 Forgetting Factor

The smaller λ is the smaller contribution of previous samples. This makes the filter more sensitive to recent samples, which means more fluctuations in the filter coefficients. The $\lambda = 1$ case is referred to as the growing window RLS algorithm. In practice, λ is usually chosen between 0.98 and 1. The convergence speed of the RLS algorithm is also affected by the choice of λ, since a smaller value of λ leads to faster convergence while increasing the maladjustment in a stationary environment.

6.2.3 Temperature Estimation

$$\frac{R_s(t)}{R_0} = \frac{T(t)+k}{T_0+k} \quad (6.15)$$

The temperature is calculated by the equation (6.15), where *k* is the temperature coefficient. The T_0 is the reference environment temperature. For a typical rotor with aluminum bars of 62% volume conductivity, *k* is 225. For copper bars, *k* is 234.5.

6.2.4 Estimation of the Back EMF Coefficient

The back EMF coefficient is dependent on the magnetic flux density produced by the motor's magnets. All the magnets are subject to demagnetization, including reversible and irreversible demagnetization. The reversible demagnetization property is largely dependent on the material of the magnet.

Presently, there are four different magnetic materials being used in permanent

magnet motors. These four magnetic materials are: aluminum-nickel-cobalt (AlNiCo), samarium-cobalt (SmCo), neodymium-iron-boron(NdFeB), and ferrite or ceramic.

Within the temperature range, -60ºC < T < 200ºC, all four magnetic materials exhibit linear, reversible thermal demagnetization, so that the amount of magnetic flux density produced by each magnet decreases linearly with the increasing temperature of the magnet. Hence, similar to electrical resistance, the expression of back EMF coefficient, reversible linear decrease with increasing magnet temperature amounts to equation (6.16) [87]:

$$K_e(T) = K_e(T_0)[1 - B(T - T_0)] \tag{6.16}$$

The back EMF coefficient is calculated under room temperature, which provides a way to estimate the back EMF coefficient vs temperature curve. However, the change of back-EMF caused by room temperature change is extremely small.

Equations (6.17)-(6.19) describe the characteristics of PMSM:

$$v_a = R_a i_a + L_a p i_a + e \tag{6.17}$$

$$T_e = K_e \Phi_f i_a \tag{6.18}$$

$$\mathrm{e} = \mathrm{K_e}\Phi_\mathrm{f}\mathrm{w} \tag{6.19}$$

When the PMSM stops after running for a while, the i_a will be zero, so the equations become (6.20)-(6.22):

$$v_a = e \tag{6.20}$$

$$e = K_e \Phi_f w \tag{6.21}$$

$$K_e \Phi_f = \frac{U_{ab}}{2\sqrt{3}\pi f} \tag{6.22}$$

U_{ab} is the line-to-line voltage between phase A and phase B.

6.2.5 Low Refrigerant Level Detection Using a Thermal Dynamic Method

This part focuses on the mathematical relationship between refrigerant charge level and the temperature of the compressor parts. A typical refrigerant cycle is described in Fig. 6.4.

6.2.5.1 Charge Level vs. Mass Flow Rate

A thermal expansion valve is a component in air conditioning systems that controls the amount of refrigerant flow into the evaporator, thereby controlling the superheating at the outlet of the evaporator. When undercharged, the thermal expansion valve is not expected to control superheat effectively. The thermal expansion valve may be seeing vapor and liquid at its entrance. The evaporator will be starved of refrigerant and running high superheat. Undercharged systems mean less mass flow rate throughout the entire system. There is no accurate mathematical relationship between charge level and mass flow rate, since the system contains a thermal expansion valve. It generally depends on the performance of the different systems. However, the charge level and mass flow rate can be measured at the same time to solve this problem. Fig. 6.4 shows a typical refrigeration cycle with an expansion valve.

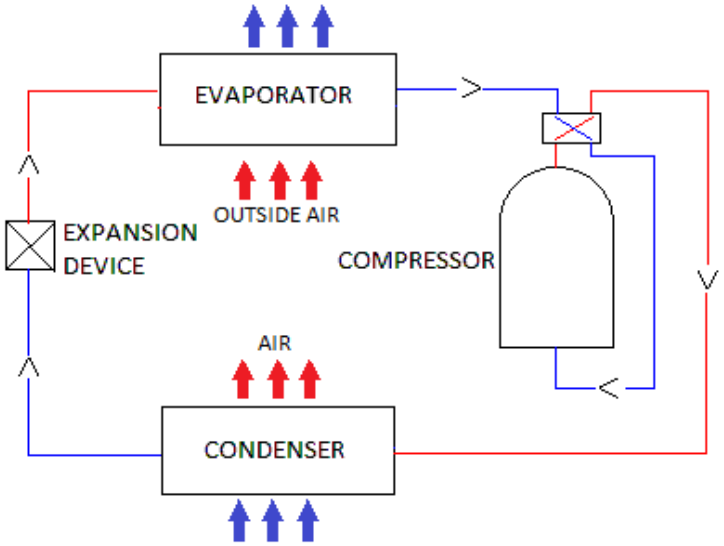

Fig. 6.4: Typical refrigeration cycle

6.2.5.2 Compressor Work Load Calculation

With a low refrigerant level, the compressor must compress much lower pressure vapors coming from the suction line to the proper condensing pressure. This requires a greater compression range and a higher compression ratio. This greater compression range from the lower evaporator pressure to the condensing pressure is what causes more compression work and generates more heat from compression. In order to further explain the process, a pressure enthalpy chart is shown in Fig. 6.5. The pressure and enthalpy variation in the four steps of the refrigeration cycle are described.

The ideal work is

$$W^* = (\dot{m})(h_{outlet} - h_{inlet}) \tag{6.23}$$

The actual work is

$$W = \frac{W^*}{\eta} \tag{6.24}$$

where W^* is the ideal work and η is the efficiency. In equation (6.23), h_{outlet} is the enthalpy at the outlet of compressor, which is a function of pressure, temperature and composition. The enthalpy at the inlet of compressor is expressed by h_{inlet}. In general, the enthalpy change will play a more important role in the ideal work equation.

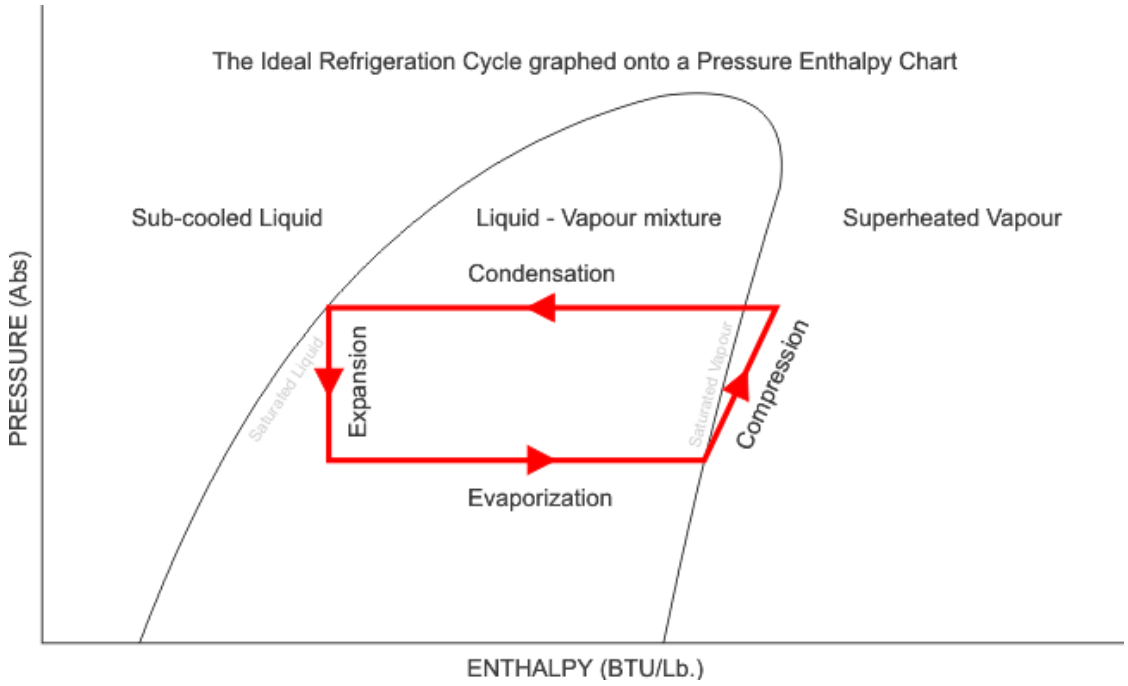

Fig. 6.5: The ideal refrigeration cycle graphed onto a pressure enthalpy chart

6.2.5.3 The Heat Transfer Calculation of a Compressor Based on Thermal Dynamic Model

The compressor of the heat pump used for the experiment is a Copeland scroll compressor. The sectioned Copeland scroll compressor is shown in Fig. 6.6. Recently, a thermal model-based temperature estimation method has been widely researched. Temperatures in different locations of the compressor were predicted using a lumped-parameter thermal model, in which the enthalpy form of the energy equation was used to describe the energy exchange for each control volume [88]. The control

volumes chosen for the analysis and the heat transfer terms involved are illustrated in Fig. 6.7. For instance, the energy balance for the suction plenum is described in the equation (6.25):

Fig. 6.6: Sectioned Copeland scroll compressor

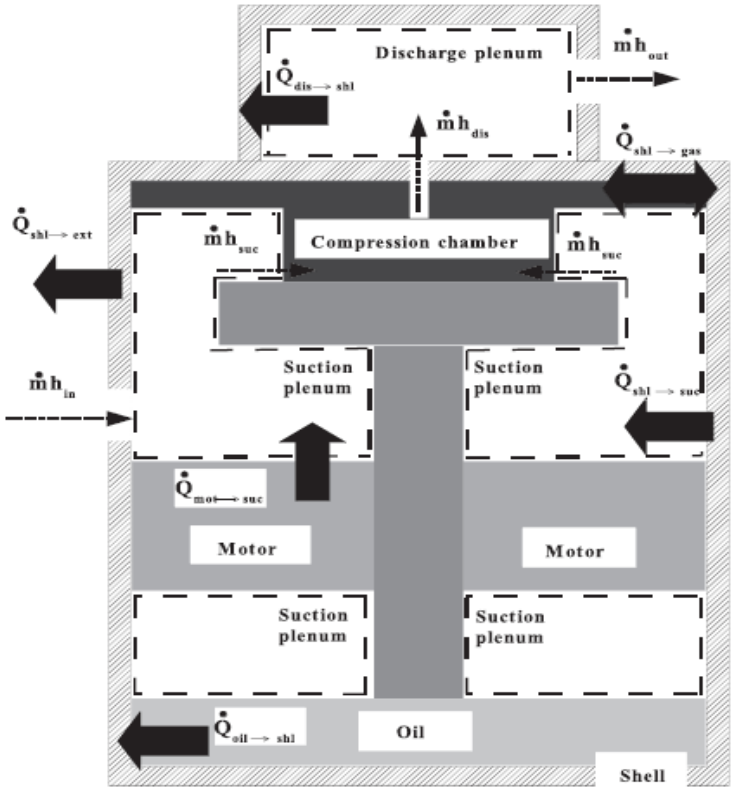

Fig. 6.7: Schematic of the compressor geometry and control volumes for energy balance

Nomenclature

Roman

h	Specific enthalpy J kg^{-1}
$\dot{m}$	Mass flow rate kg s^{-1}
$\dot{Q}$	Heat transfer W
T_c	Condensing temperature °C
T_e	Evaporating temperature °C
UA	Global heat transfer conductance W K^{-1}
$\dot{W}_{ele}$	Electrical power consumption W
$\dot{W}_{pv}$	Indicated Power W
$\dot{W}_{shf}$	Shaft Power W

Greek

η_e	Electrical efficiency
η_s	Isentropic efficiency
η_m	Mechanical efficiency
η_v	Volumetric efficiency

Subscripts

dis	Discharge
dis-shl	From discharge chamber to shell
ext	External ambient
in	Compressor inlet
mot	Motor
mot-suc	From motor to suction gas
oil	Oil
oil-shl	From oil to shell
out	Compressor outlet
shf	Shaft
shl	Shell
shl-ext	From shell to external ambient
shl-gas	From shell to compressed gas
shl-suc	From shell to suction gas
suc	Suction

Fig. 6.8: Parameter settings

$$\dot{m}h_{in} + \dot{Q}_{shl-suc} + \dot{Q}_{mot-suc} = \dot{m}h_{suc} \tag{6.25}$$

The other compression cycle equations are listed in (6.26)-(6.30):

$$\dot{m}h_{suc} + \dot{W}_{pv} + \dot{Q}_{shl-gas} = \dot{m}h_{dis} \tag{6.26}$$

$$\dot{m}h_{dis} = \dot{m}h_{out} + \dot{Q}_{dis-shl} \tag{6.27}$$

$$\dot{Q}_{shl-ext} + \dot{Q}_{shl-suc} + \dot{Q}_{shl-gas} = \dot{Q}_{oil-shl} + \dot{Q}_{dis-shl} \tag{6.28}$$

$$\dot{Q}_{mot-suc} = \dot{W}_{ele} - \dot{W}_{shf} \tag{6.29}$$

$$\dot{Q}_{oil-shl} = \dot{W}_{shf} - \dot{W}_{pv} \tag{6.30}$$

The heat transfer terms are represented through global heat transfer coefficients, as shown in the equation (6.31) for the heat transfer between the shell and the external environment.

$$\dot{Q}_{shl-ext} = UA_{shl-ext}(T_{shl} - T_{ext}) \tag{6.31}$$

Fig. 6.8 presents all the parameter settings. Fig. 6.9 gives an example of thermal resistance and elements of a typical lumped-parameter thermal model. Measurements of temperature in different regions of the compressor for the different operating conditions are allowed, to evaluate all of the global heat transfer conductances required in the model.

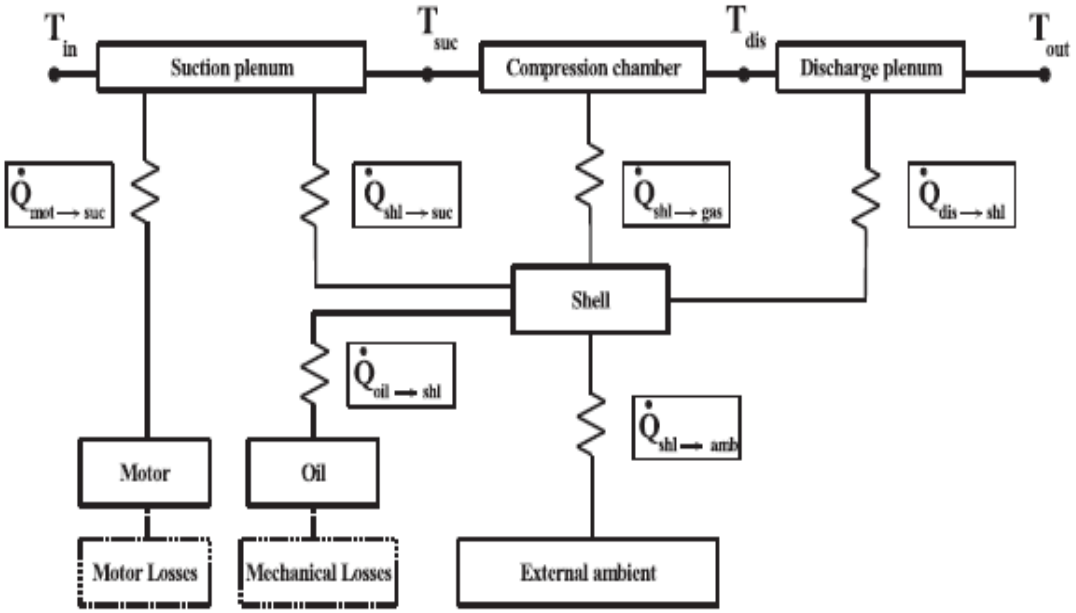

Fig. 6.9: Thermal resistances and elements of the lumped-parameter thermal model

After being calibrated, the thermal simulation model can be applied to predict the temperature of important compressor components under any operating conditions not included in the experiments. The set of equations generated by the energy balances are solved using a Newton-Raphson iterative method.

The Copeland compressor of the heat pump in the lab is totally sealed, which increases the difficulty in measuring the temperature in the different chambers and the parts inside the compressor. As a result, an estimation of thermal resistance is extremely hard to accomplish. However, for some semi-sealed compressors, or non-sealed compressors, this thermal dynamic analysis method is quite practical and the thermal model could be optimized if more data is captured in the experiment.

6.3 Experiment and Results

6.3.1 Experiment Setup

As was mentioned before, the compressor motor is a three phase PMSM. The original capacity of this heat pump is two tons and is fit for a room size of 1400 ~ 1500 square feet. The rest of the key parameters of the outdoor unit are listed in Table 6.1.

Table 6.1: Outdoor unit parameters

Capacity	2 tons
Refrigerant type	R410a
Refrigerant weight	13 lbs (5.9 kg)
Compressor power supply	208~230 V AC
Compressor motor type	PMSM
Frequency	60 Hz

Min circuit amps	23.5 A
Max fuse current	30 A
Max design/working pressure	700 PSIG
Design/test pressure gage	Hi 450 psi Low 250 psi

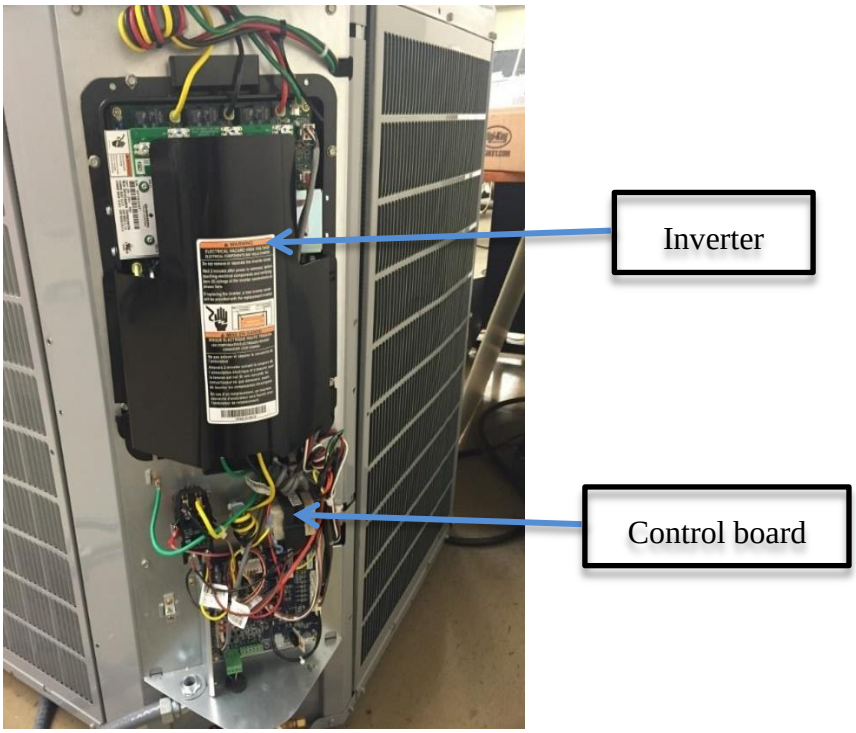

Fig. 6.10: Control board and inverter of outdoor unit

The inverter and control board are located on one side of the outdoor unit, as shown in the picture (6.10). Several pressure sensors are implemented inside to send monitoring electrical signals back to the air handler, while at the same time demonstrating real time conditions in the thermostat. The control board in Fig. 6.10 is used to control both the fan motor and the compressor in the outdoor unit.

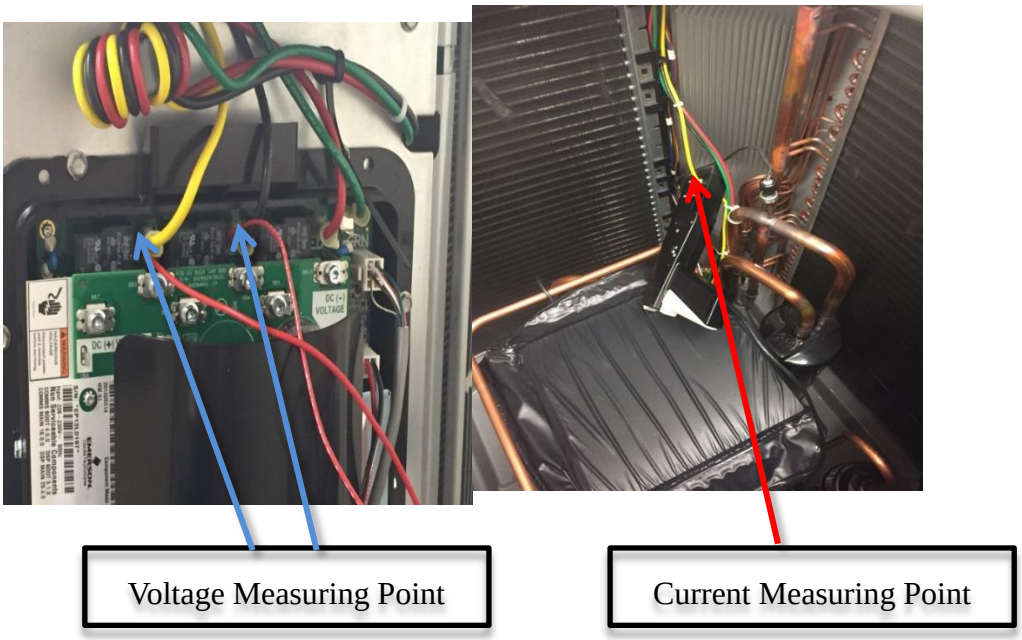

Fig. 6.11: Voltage and current measuring point in the outdoor unit.

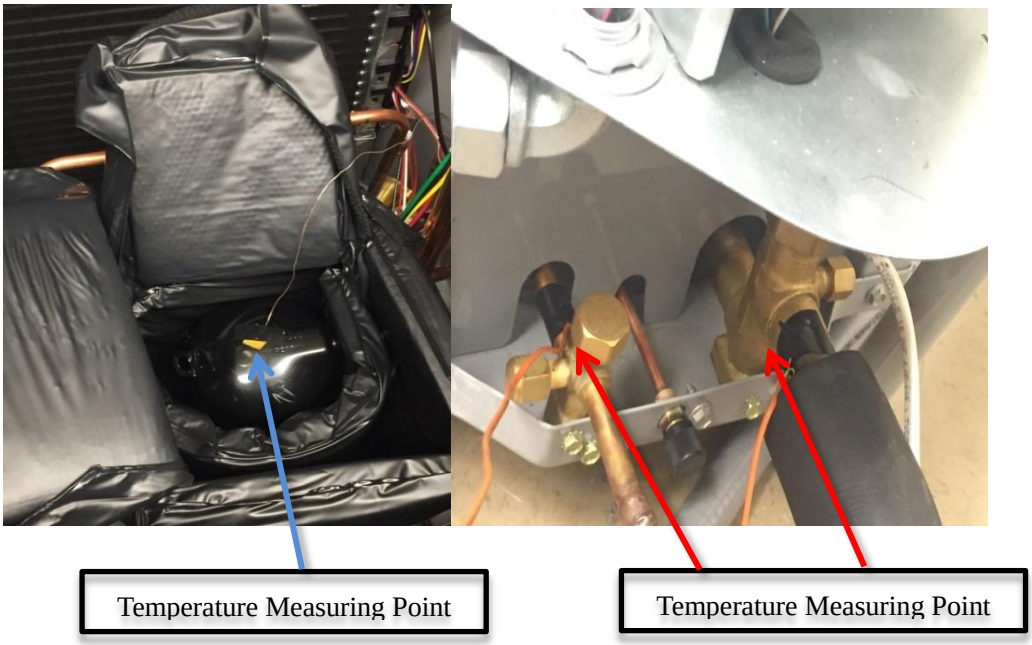

Fig. 6.12: Temperature measuring point in the outdoor unit.

For the sake of estimating the resistance of the compressor motor, single phase current and line-to-line voltage is measured in Fig. 6.11. Voltage sensing points are located exactly at the output terminal point of the inverter. For current sensing, a current sensor is placed inside the outdoor unit. A voltage sensor board is built to detect the

terminal voltage with a ratio of 135 (380V/2.8V) in Fig. 6.13. In addition, Fig. 6.12 shows that three temperature sensors are attached to the compressor surface, discharge port, and suction port to obtain extra temperature information which can be utilized to verify the trend of temperature change inside the compressor.

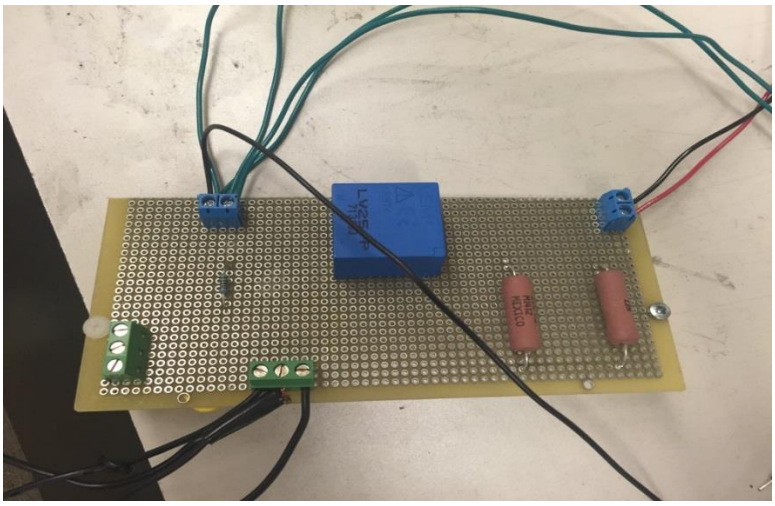

Fig. 6.13: Voltage sensor board

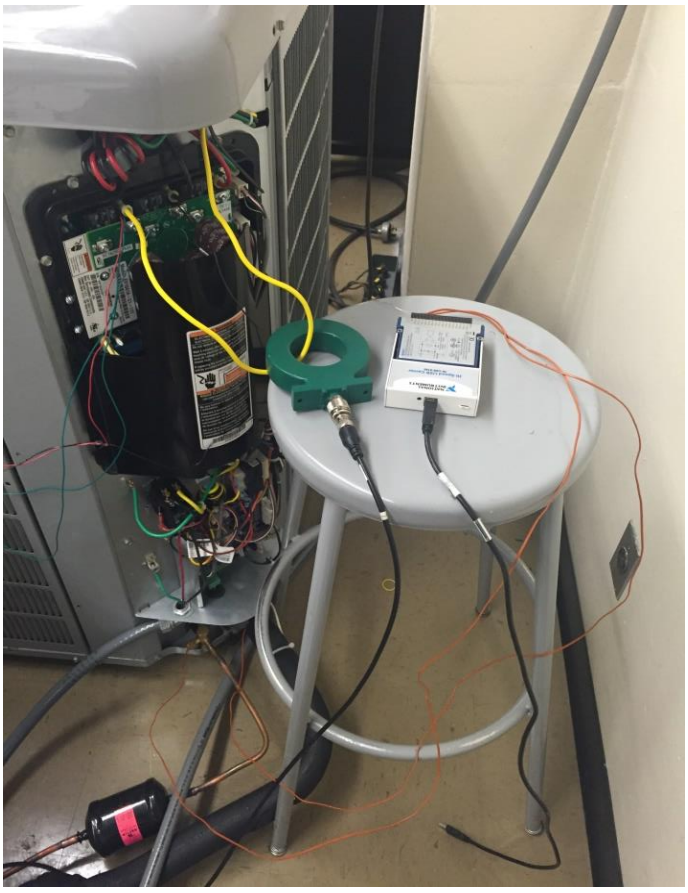

Fig. 6.14: Current probe and NI 9213 thermal couple input module

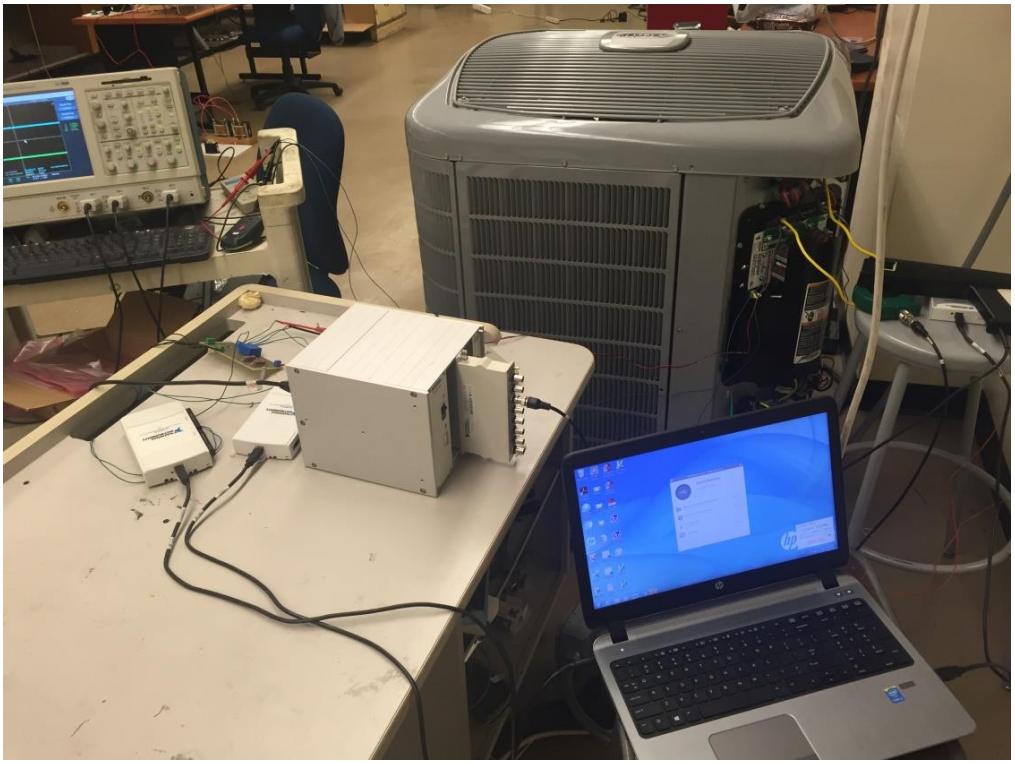

Fig. 6.15: Experiment setup

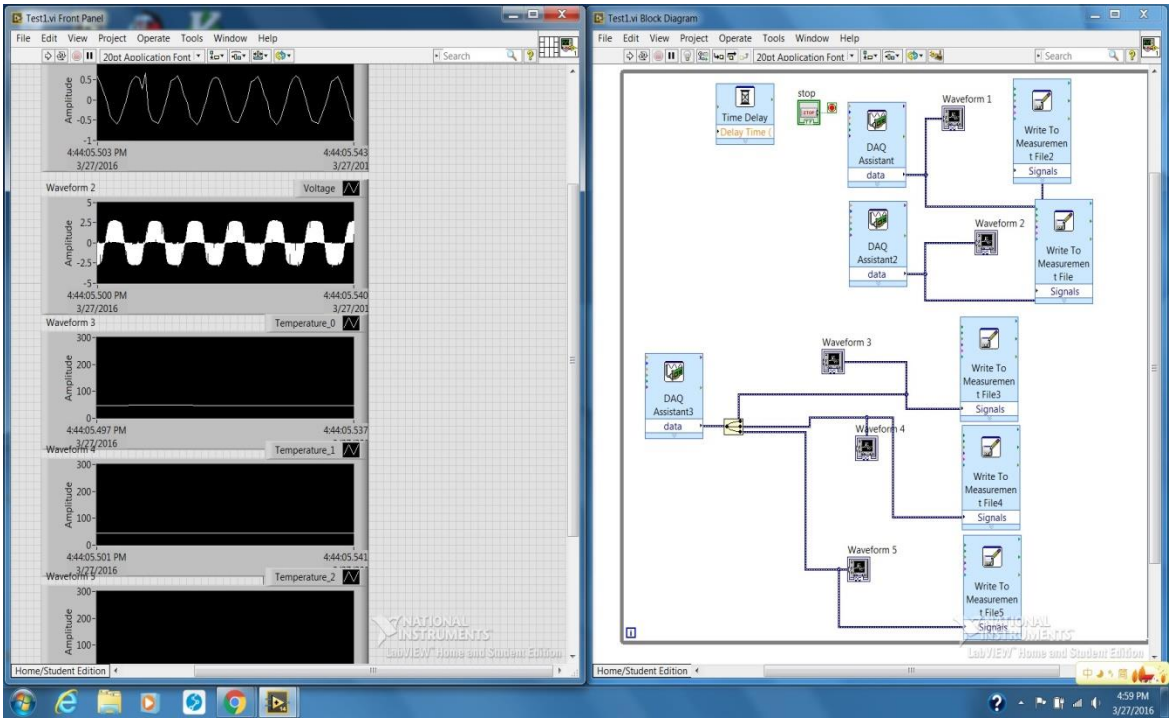

Fig. 6.16: Signal sampling screen in Labview

An NI SCXI 1140 (8-Channel Lowpass Elliptical Filter Module) is used for current filtering after acquiring signals from the current probe. The output voltage

signal is then connected to an NI 6210 module. Finally, all sensed signals including one current signal, one line-to-line voltage signal, and three temperature signals are collected by Labview for further analysis. All of the experiment setups are shown in Fig. 6.14-6.15.

The PWM frequency of voltage detection is 10kHz. The current/voltage/ temperature sampling frequencies are listed in Table 6.2.

Table 6.2: Experiment setting for current/voltage/temperature detection

Duration	**Sampling Frequency**	**Signal type**
15 minutes	2000 Hz	Current
15 minutes	40000 Hz	Voltage
15 minutes	100 Hz	Temperature

6.3.2 Data Collection

6.3.2.1 Back EMF Coefficient Estimation

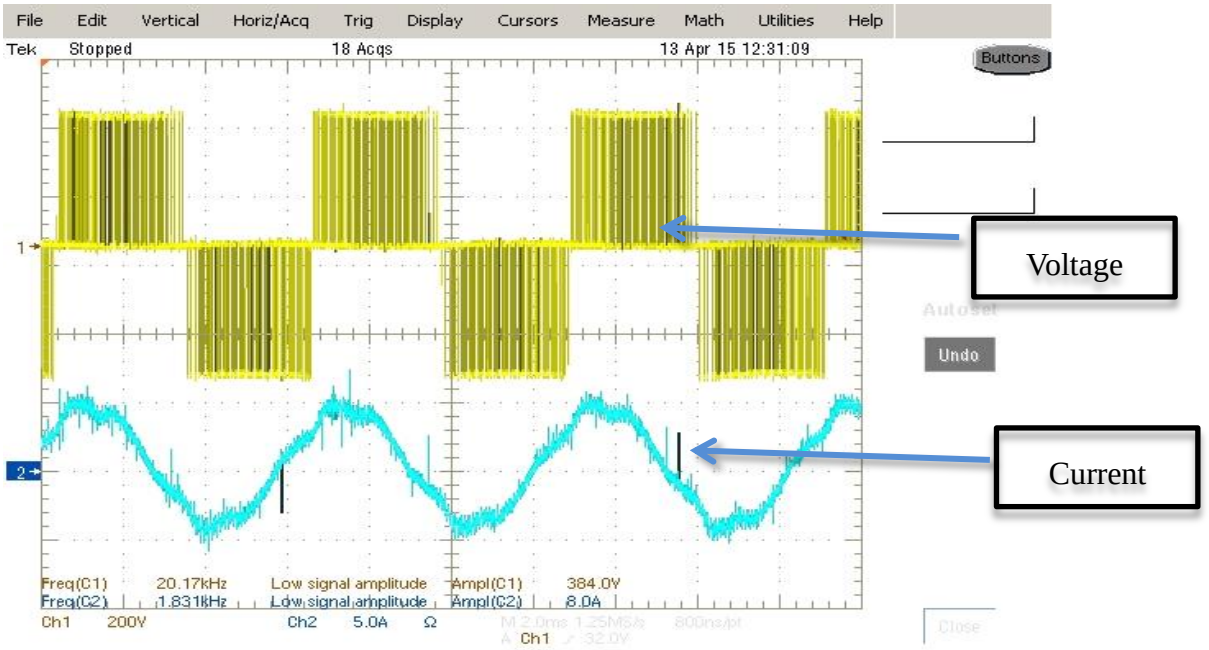

Fig. 6.17: L-L Voltage and stator current wave form under normal conditions

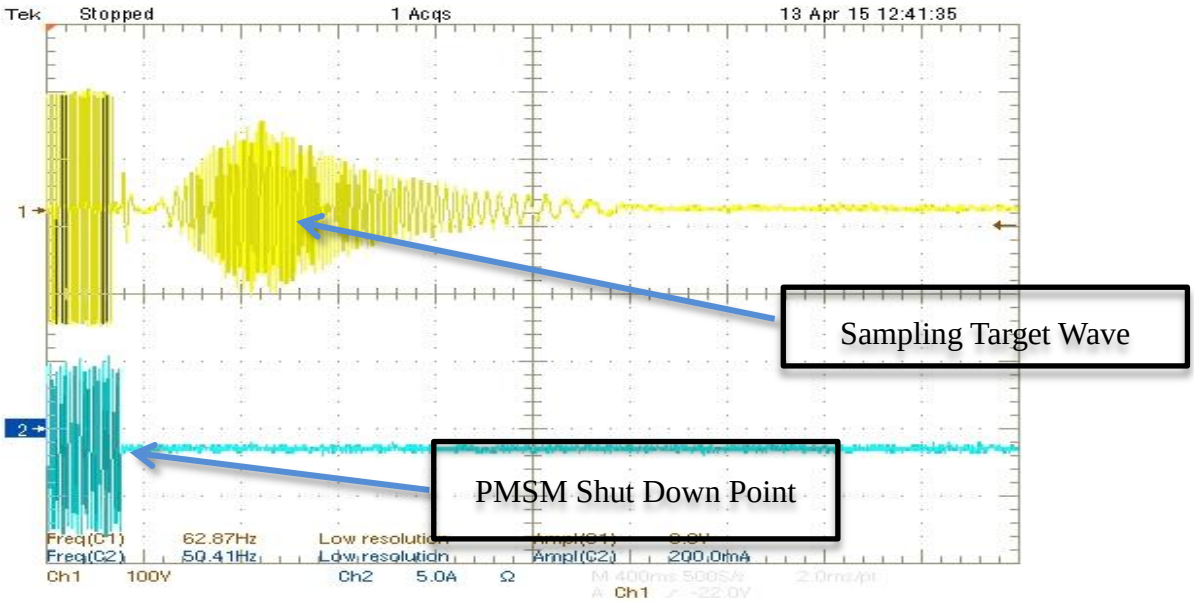

Fig. 6.18: L-L Voltage and stator current waveform during the stopping transient

According to the voltage waveform in Fig. 6.17, SPWM is conducted to control the PMSM. In Fig. 6.18, the phase voltage and current turn to zero at the PMSM shut down point while the motor speed is zero as well. Somehow, the voltage increases, which is a clear sign the compressor motor is running again. The target voltage is equal to the back-EMF of the PMSM, and the target voltage waveform appears when the motor starts to run again. The reason for this circumstance is that the PMSM inside the scroll compressor runs backwards for a short period of time after the power supply is shut off, so that the internal pressures are equalized. There is still a large amount of refrigerant in the condenser and discharging line when the system is shut off. Some of the refrigerant expands and goes backwards to the compression chamber, causing the reverse movement of the compressor motor. This momentary reversal of the direction of the scrolls has a limited effect on compressor stability and lifespan. This is also a very normal condition which can only produce noise when shutting down the system. According to [89], no matter whether it is a single-phase or three-phase model, this kind of noise can be reduced to some extent by implementing some specific devices. Table 6.3 lists the experiment results of detected line-to-line voltage and frequency in each cycle before an average back-EMF coefficient is calculated.

Table 6.3: Estimation of back-EMF coefficient

Wave cycles	1	2	3	4	5	6	7	8	9	
f(Hz)	60.4	62.5	78.1	83.3	104.2	125	41.7	27.2	18.9	
Line to line voltage (peak to peak) (V)	150	168	188	197	220	245	110	80	44	
Line to line voltage	53.0	59.4	66.5	69.7	77.8	86.6	38.9	28.3	15.6	

(RMS value)(V)										
$K_e\Phi_f$(V/rad)	0.081	0.087	0.078	0.076	0.068	0.064	0.086	0.096	0.076	0.079

6.3.2.2 Stator Winding Temperature Estimation

The temperature is estimated by equation (6.15), where *k* is the temperature coefficient and T_0 is the reference environment temperature which is 26°C. For copper bars, *k* is 234.5. A preliminary experiment is conducted to detect line-to-line resistance by multimeter as the outdoor unit is turned off. As the outdoor unit is turned off, the measured line-to-line stator winding resistance R_0 is 2 ohms under reference room temperature.

6.4 Results

Fig. 6.19-21 shows the captured start up voltage and current waveforms, which reveal the three stages of starting up the compressor motor. The startup control algorithm is probably an open loop plus closed loop control. Fig. 6.22-6.24 are FFT results based on terminal voltage and current waveform from Labview.

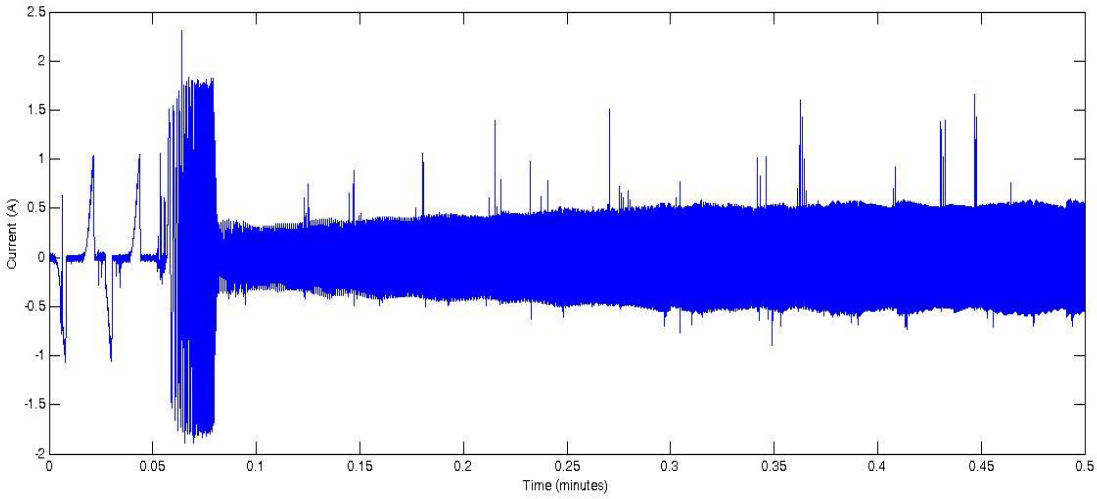

Fig. 6.19: Startup current waveform

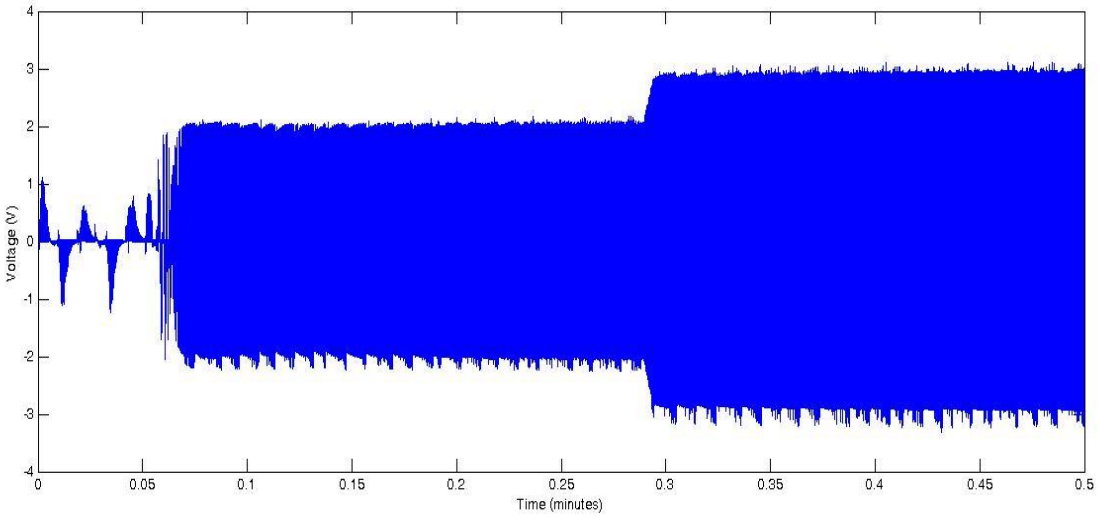

Fig. 6.20: Startup voltage waveform

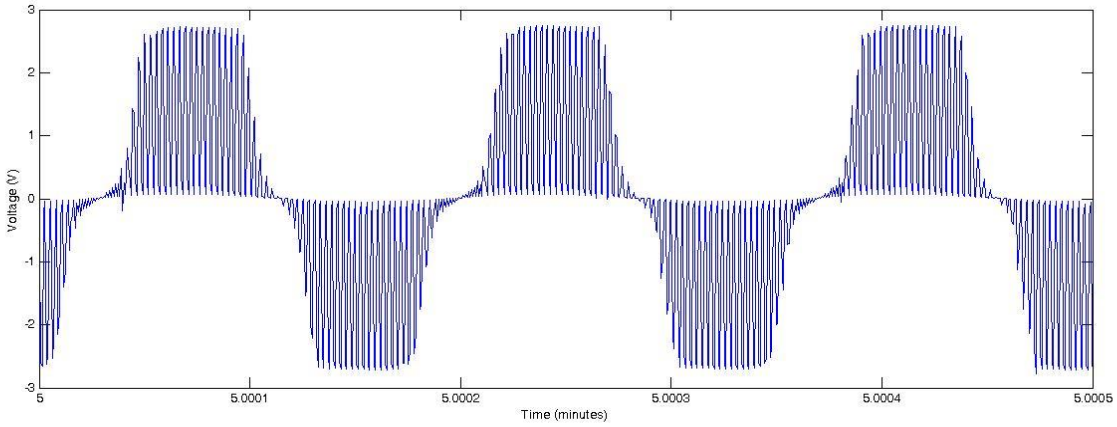

Fig. 6.21: Voltage waveform

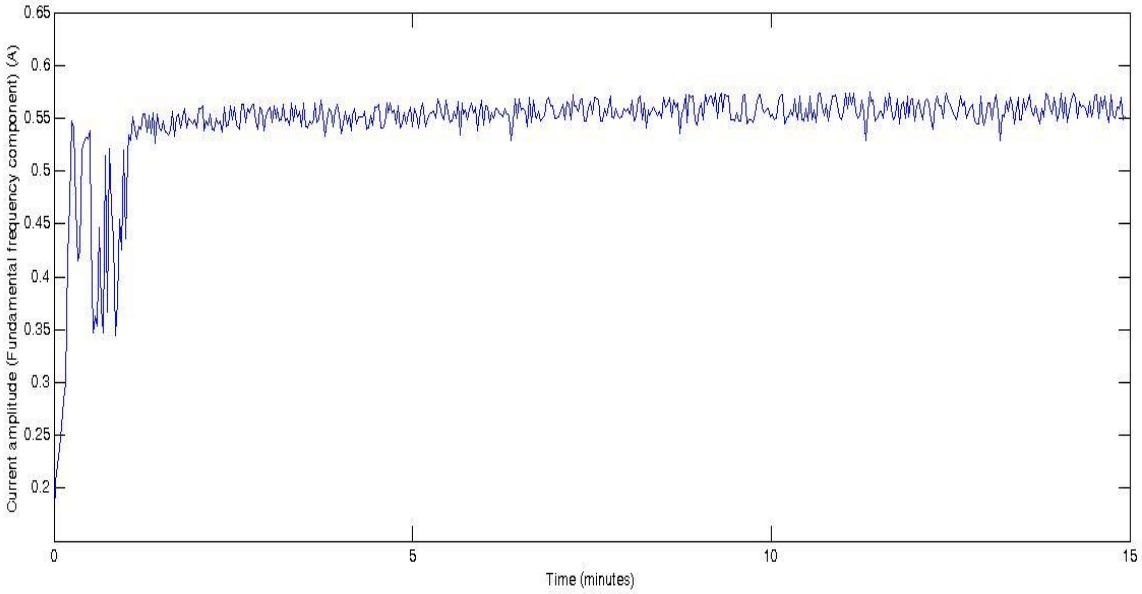

Fig. 6.22: Current amplitude (fundamental component)

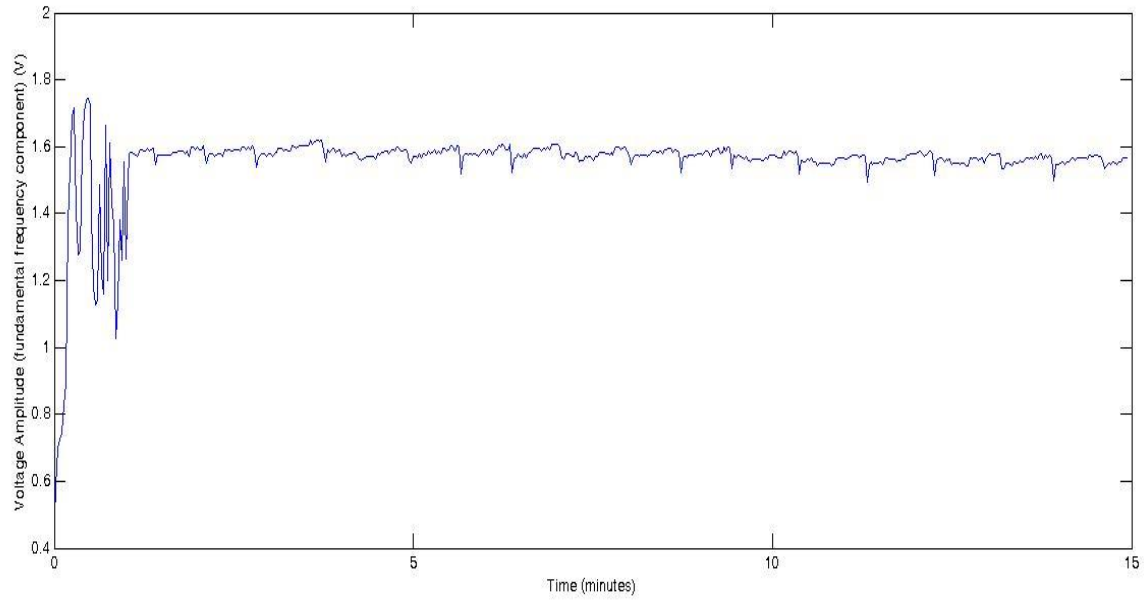

Fig. 6.23: Voltage amplitude (fundamental component)

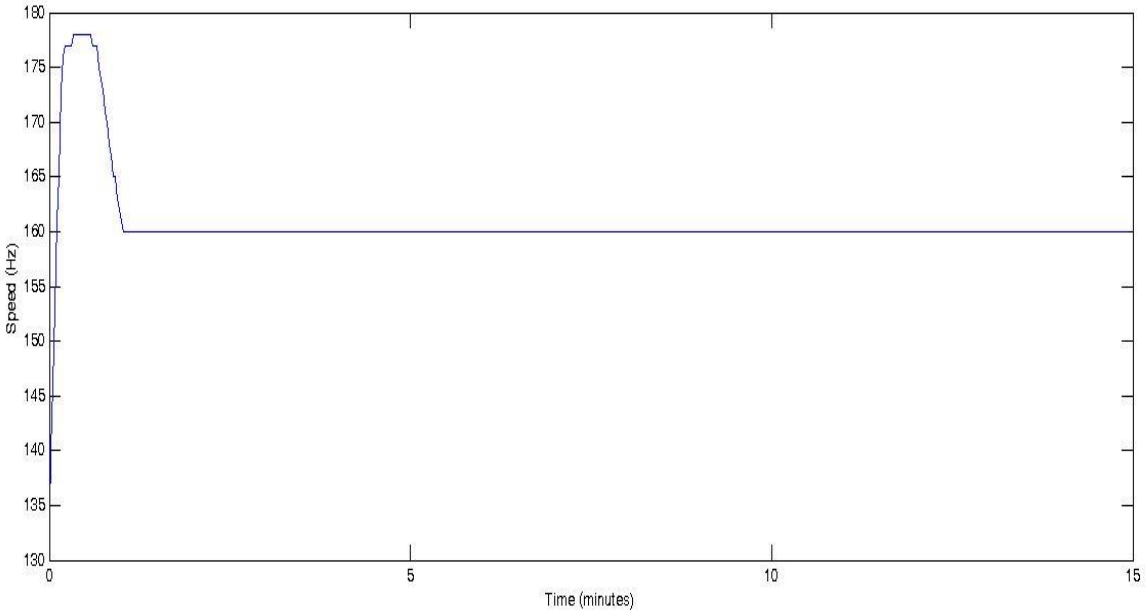

Fig. 6.24: Motor speed (Hz)

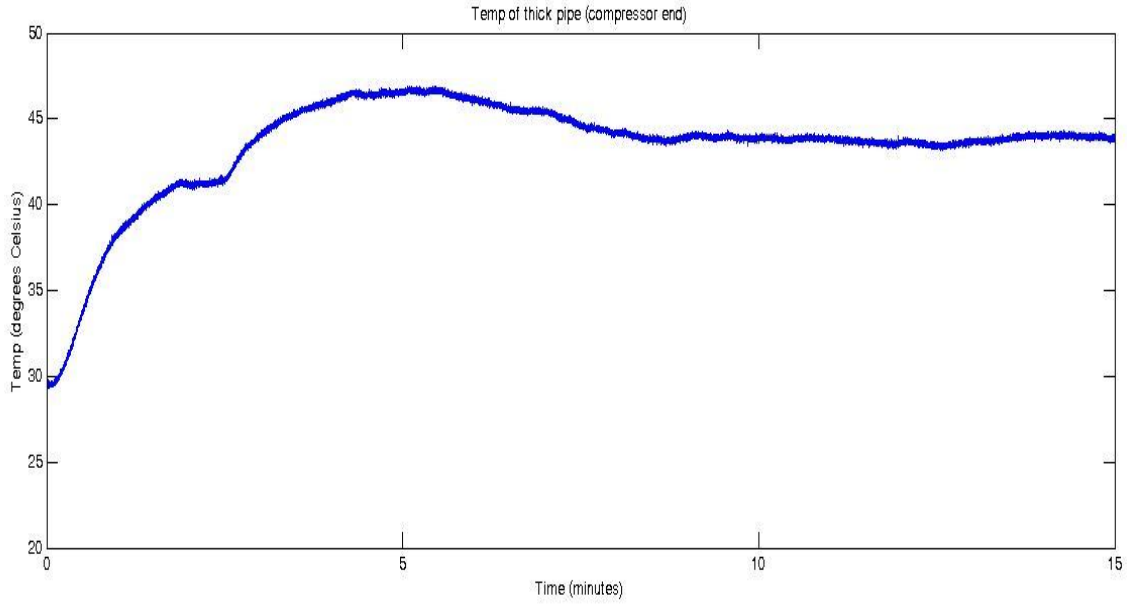

Fig. 6.25: Measured temperature of discharge side (compressor end)

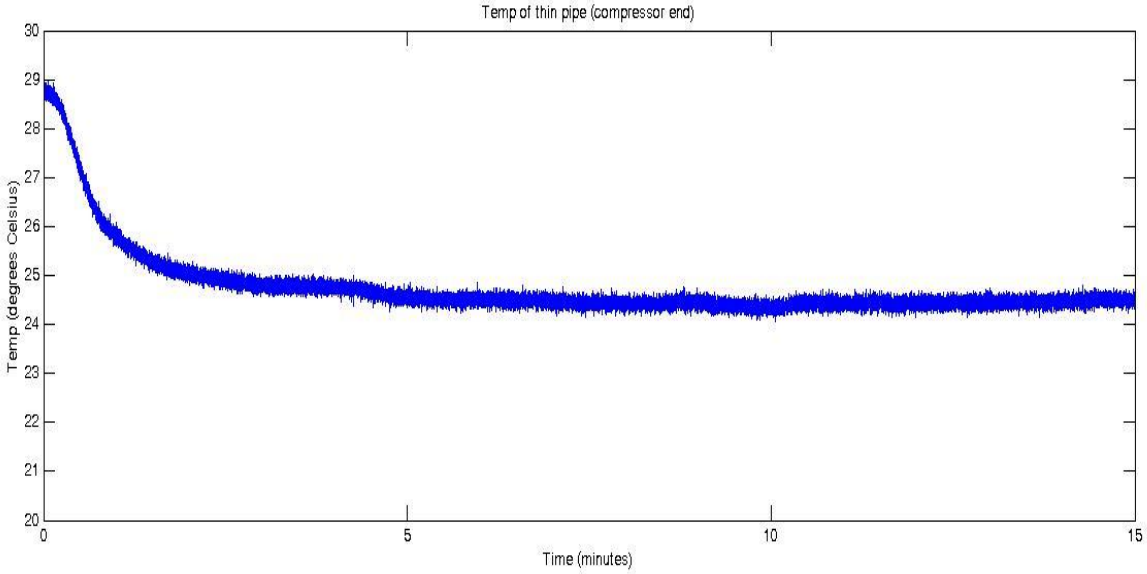

Fig. 6.26: Measured temperature of suction side (compressor end)

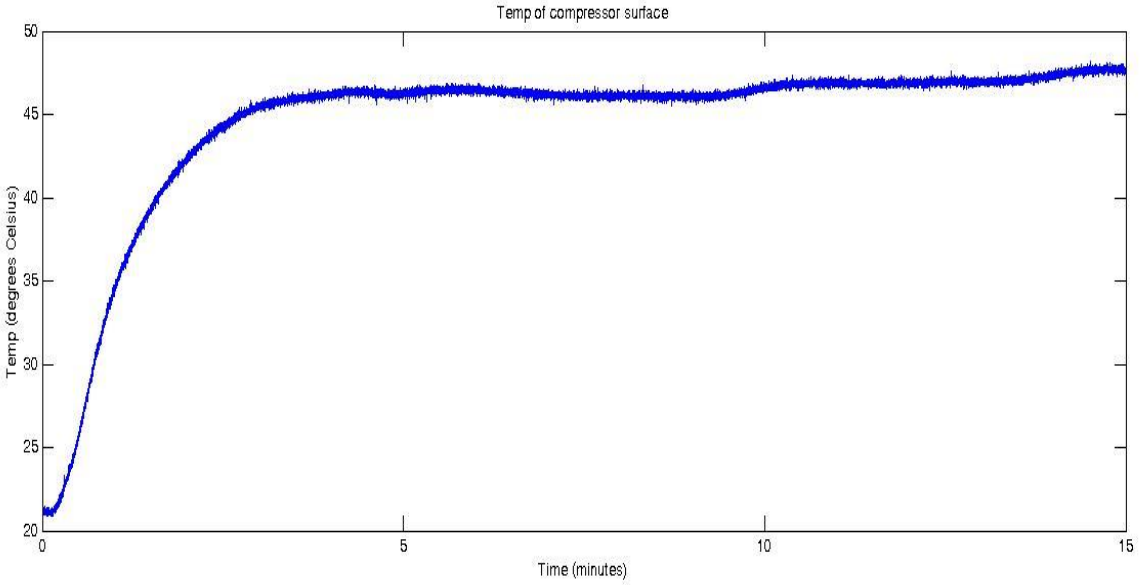

Fig. 6.27: Measured temperature of compressor surface

The measured temperature at the three different points on the compressor are listed in Fig. 6.25-6.27. These real temperature variations are key references for the estimated temperature change of the compressor motor.

In this part, the experiment's fina results are shown in Fig. 6.28-6.29. The final

experiment is conducted following this procedure:

1. Connect all of the voltage, current and temperature sensors to the outdoor unit.
2. Measure the room temperature
3. Take out and weigh all the refrigerant from the system
4. Import back all of the refrigerant to the system
5. Start up the compressor
6. Start recording voltage, current and temperature data using Labview
7. Measure the suction pressure and discharge pressure
8. Stop the system for 30 minutes to cool down the compressor
9. Take α percent of refrigerant out of the system

The steps 5-9 are repeated to obtain all the data at the five different refrigerant levels (100%, 90%, 80%, 70%, 40%).

As mentioned in equation (6.23), the total compression work of the compressor is mainly decided by enthalpy difference. Table 6.4 lists results of the experiment for suction and discharge pressure, measured under different refrigerant charge levels. The discharge pressure is almost constant because of the regulation of the thermal expansion valve. However, the suction pressure decreases with respect to refrigerant level. This increases the pressure difference between the suction port and discharge port. Though there is a decrease in refrigerant mass flow, the enthalpy difference between the inlet and outlet of the compressor increases to increase the compression work.

In Fig. 6.28, the temperature of the compressor surface is measured under different refrigerant levels. The black curve represents the 40% condition and the red curve represents the 100% condition. The rest of the three groups, the data were chosen between the 40% and 100% conditions. For a residential HVAC system, the compressor can operate even under 30% refrigerant level, however, there is a pressure sensor

embedded in this system to shut down the compressor if the refrigerant level is too low, to eliminate a potentially extremely low refrigerant level problem. From a research perspective, system efficiency and stability is the main concern, thus refrigerant levels lower than 40% are not considered. In addition, regulating the refrigerant level must be performed by a professional HVAC technician. Consequently, cost of labor and time is another reason that only five groups of data are recorded in this dissertation.

Table 6.4: Suction pressure and discharge pressure under different refrigerant levels

Refrigerant level	**100%**	**90%**	**80%**	**70%**	**40%**
Suction pressure(psi)	110	108	103	97	45
Discharge pressure (psi)	225	225	225	225	225

In Fig. 6.28, the three curves represent the 70%, 80% and 90% conditions. It is relatively difficult to differentiate these three conditions by estimating the PMSM resistance of the compressor motor. However, it is much easier to interpret the normal condition and 40% condition. In Fig. 6.29, a similar scenario can be observed. Curves of 90% and 80% are intercepted at 2.3 and 10 minutes, which demonstrates the limitation of this method by simply estimating the resistance of the compressor motor. However, the results are still far more positive for the purpose of differentiating normal and undercharged conditions.

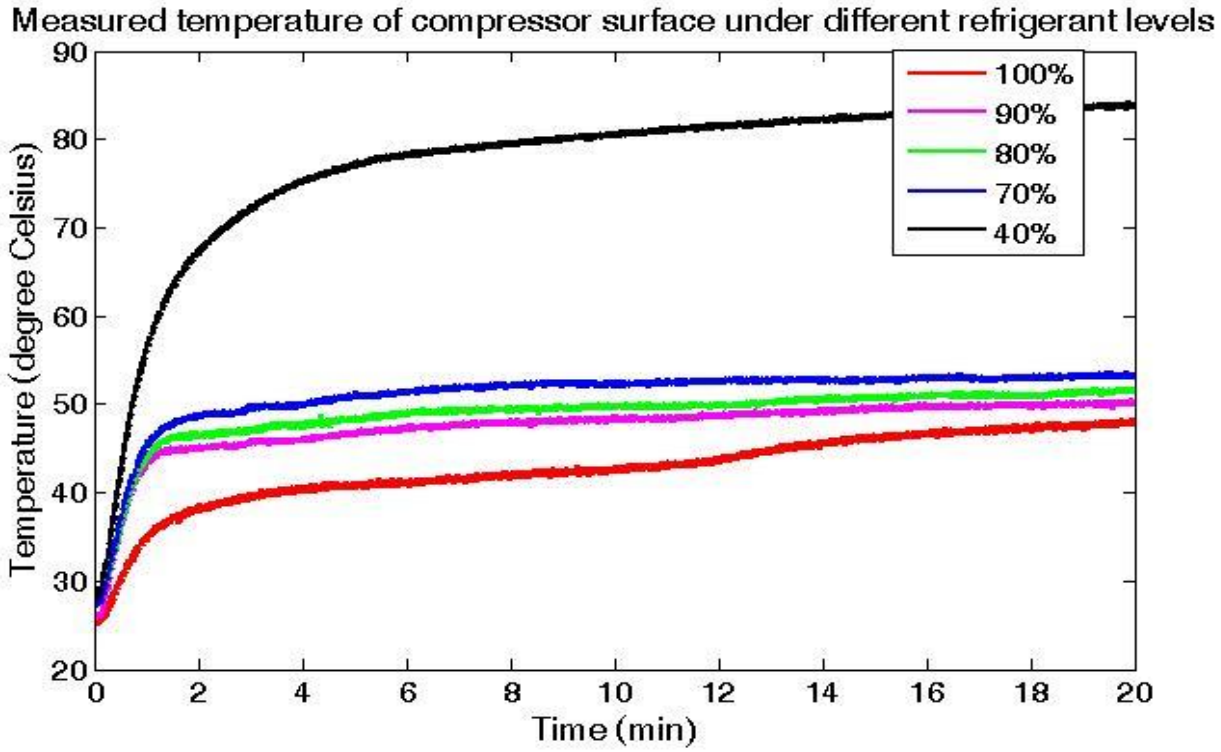

Fig. 6.28: Measured temperature of compressor surface under different refrigerant levels

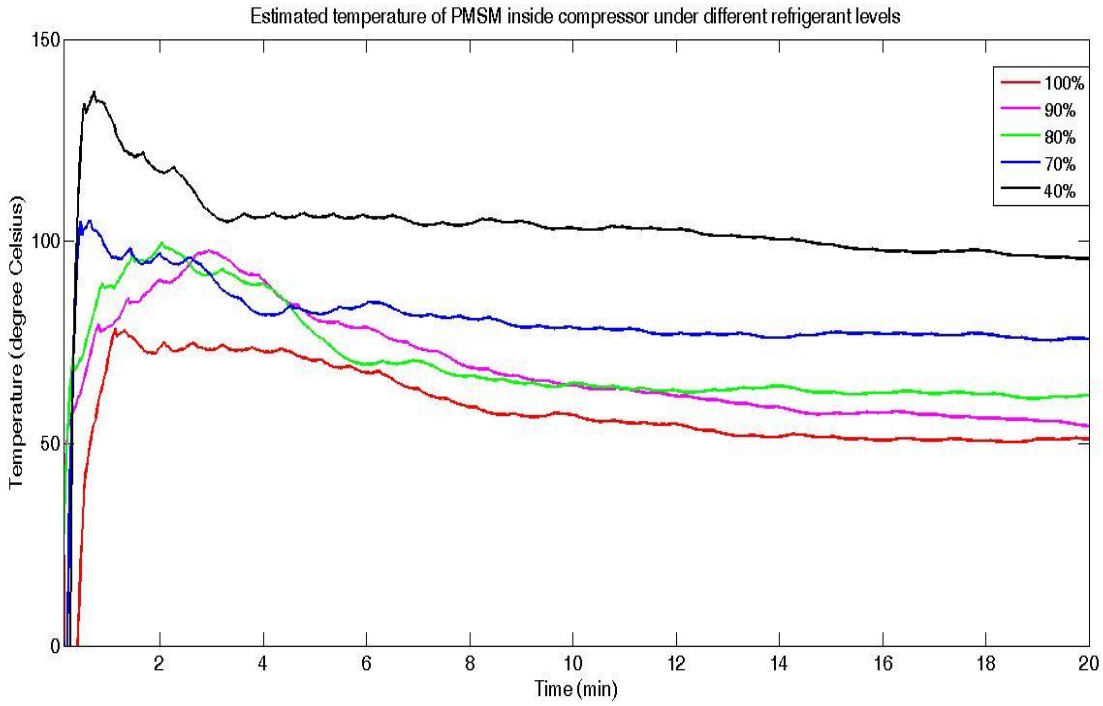

Fig. 6.29: Estimated temperature of PMSM inside compressor under different refrigerant levels

6.5 Refrigerant Estimation Algorithm

From a practical point of view, manufacturers are very interested in adding undercharge detection to the original control algorithm. Based on the theoretical analysis in section 6.2 and the results of the experiment in section 6.4, a detailed refrigerant estimation algorithm in Fig. 6.30 is created to help manufacturers add this new feature to their original control systems. This section focuses on analyzing and designing temperature thresholds, φ, which is determined by many factors, especially room sizes.

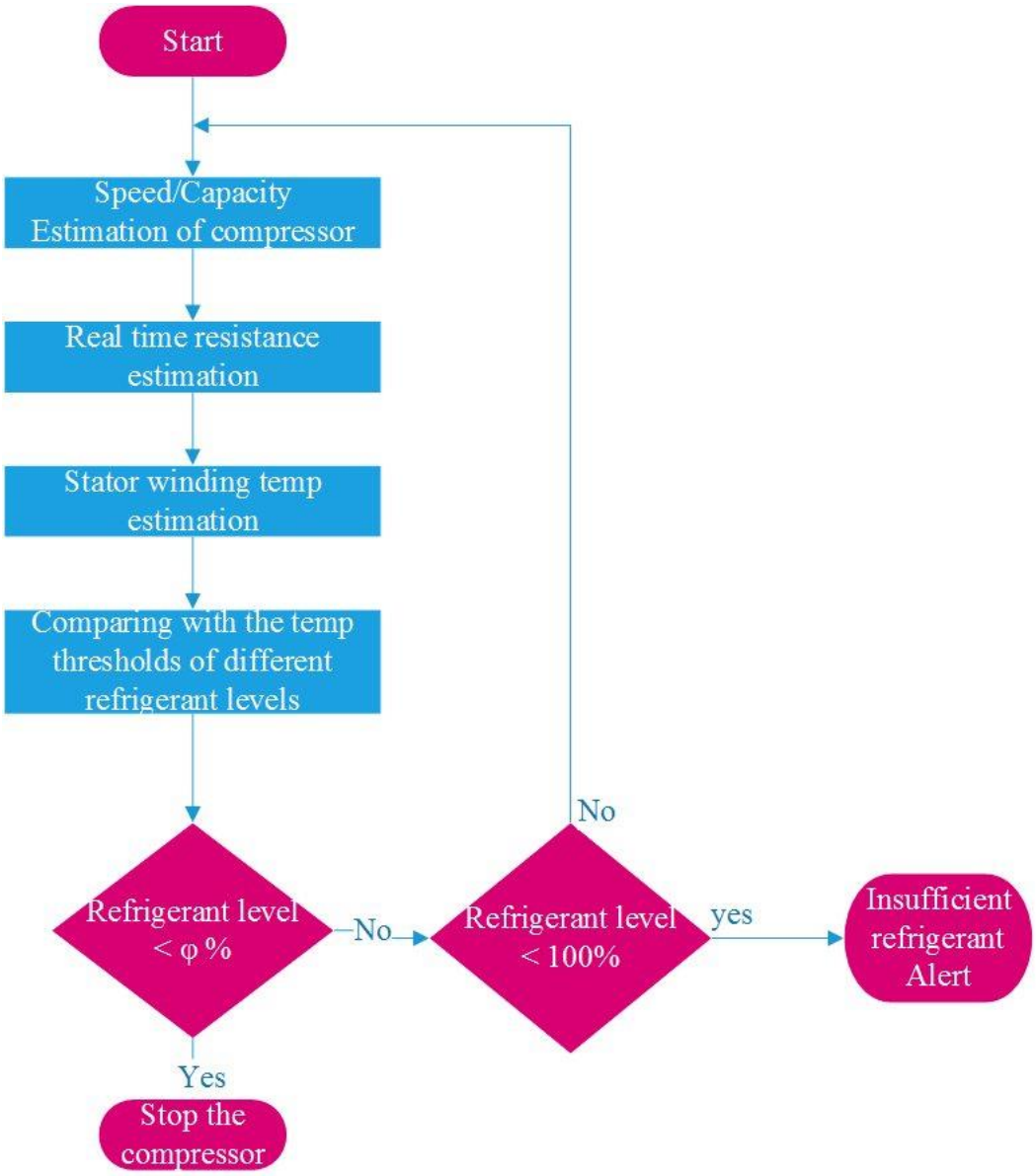

Fig. 6.30: Refrigerant estimation algorithm

Firstly, in Fig. 6.30, speed estimation can be accomplished quickly by applying on FFT to the stator current. Secondly, the RLS method is used to conduct real-time resistance estimation, followed by more straightforward temperature estimation. Thirdly, the estimated temperature is compared with a suitable threshold under different refrigerant levels, to trigger the undercharged alarm if refrigerant levels are insufficient, as shown in Fig. 6.30 where φ is a mean value of the low refrigerant limit, which is largely related to the system itself.

6.5.1 Cooling/Heating Capacity

The compressor capacity is the amount of air that the compressor can pump out. It is a very significant element of an HVAC system, which demonstrates cooling or heating ability. The capacity of the compressor mainly depends on the mass flow rate of the HVAC system. More specifically, the mass flow rate is decided by three important factors: the compressor motor speed, the amount of refrigerant, and the airflow through the evaporator. This relationship is demonstrated in Fig. 6.31. From another perspective, the compressor capacity is influenced by mechanical design factors and application factors. The original design features, such as the number of chambers and the size of the valve, defines the system capacity. On the other hand, capacity is also related to some other application factors, which are determined by the operational conditions such as discharge pressure, sub-cooling, superheating, and type of refrigerant [90][91].

An auto checking system has been implemented in the heat pump to measure the cooling or heating capacity in a real-time mode. Since the undercharged conditions are not considered in this checking system, the only factor related to the capacity is the compressor motor speed. Hence, the capacity shown in the thermostat is actually based on the speed estimation. According to the datasheet of this HVAC system, the original

compressor capacity range is set to 40 ~100%.

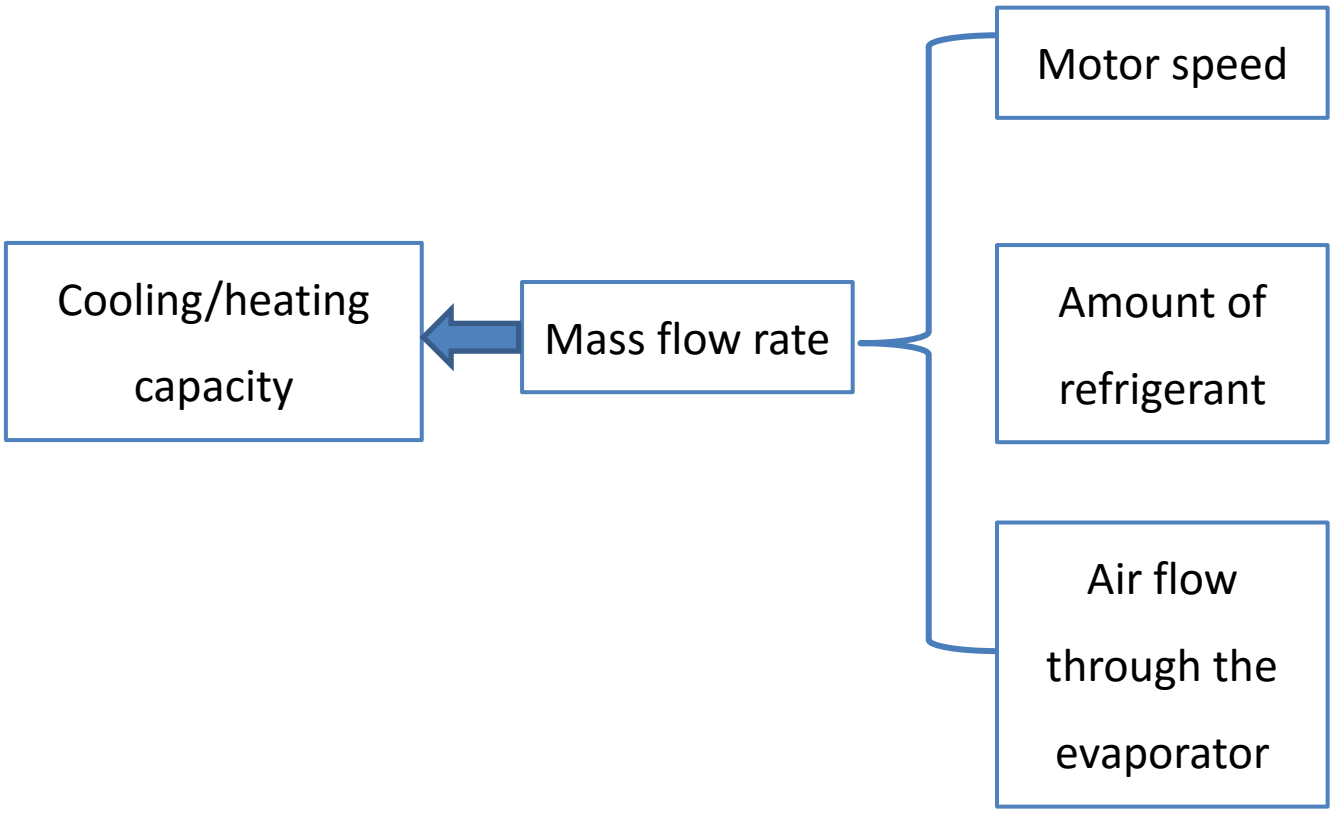

Fig. 6.31：Capacity impact factors

6.5.2 Most Common Torque Load Types

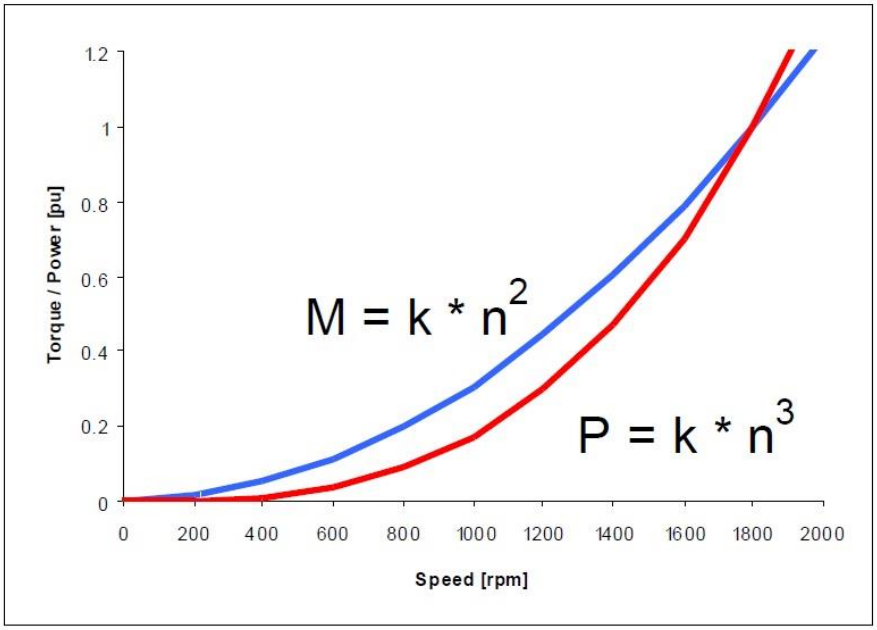

Fig. 6.32: Quadratic torque load type

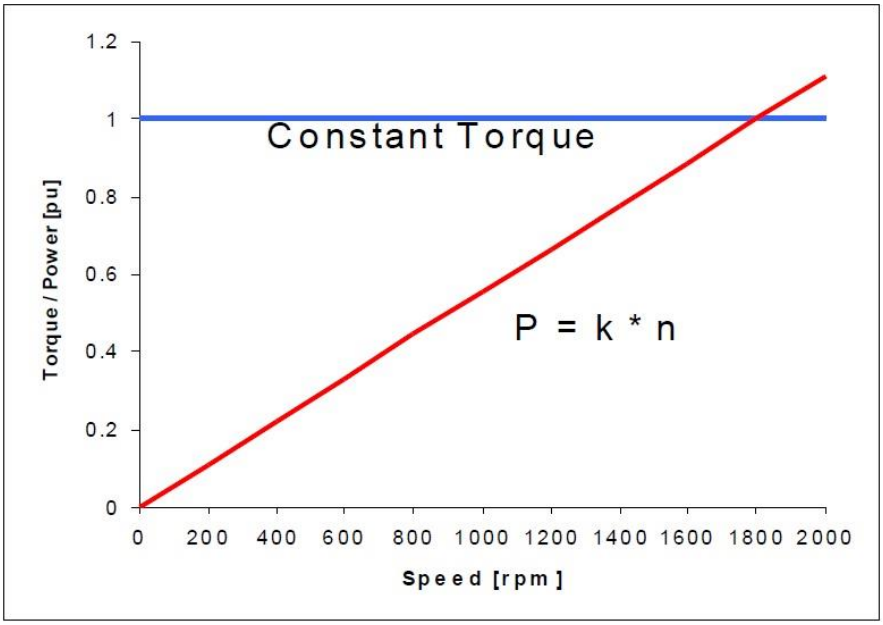

Fig. 6.33: Constant torque load type

Motor loads can be divided into three main categories depending on how their torque requirement varies with their operating speed. The most common load type is

the quadratic torque, as shown in Fig. 6.32. It has several applications, such as use in centrifugal pumps, reciprocating compressors, and fans. The other common load type is constant torque load, which is typical with the handling of fixed volume configurations. The screw/scroll compressors and conveyors are typical applications of constant torque load type. In Fig. 6.33, the red curve represents the power variation with respect to speed. K is a coefficient. The last load type is called a constant power load. The horsepower demanded by the load is constant within the speed range. The speed and torque are inversely proportional to each other. The typical examples of this type of load are center-driven winders and machine tool spindles.

6.5.3 Load Torque vs Capacity

Table 6.5: Load torque and motor speed variation with respect to temperature difference

$\Delta°F =$ room temperature $-$ setting temperature	Capacity percentage	Motor speed	Load torque
8 °F	100%	160Hz	Torque 1
6 °F	80%	140Hz	Torque 1
4 °F	60%	120Hz	Torque 1
...	…	…	…

Further investigation has been conducted to find the reaction of the system under different conditions when temperature setpoint and the actual room temperature are different. The experimental high efficiency HVAC system can automatically regulate the speed as the difference between temperature setpoint and the room temperature varies according to the preset check table. In Table 6.5, a typical example under

cooling mode is given so that motor speed decreases along with the decline of temperature difference. However, the load torque remains stable, since the scroll compressor has a constant torque load.

6.5.4 Power vs Capacity

Table 6.6: Two common initial conditions

Color	Δ°F =room temperature − initial setting temperature	Capacity percentage
Lime	8 degrees	100%
Blue	4 degrees	60%

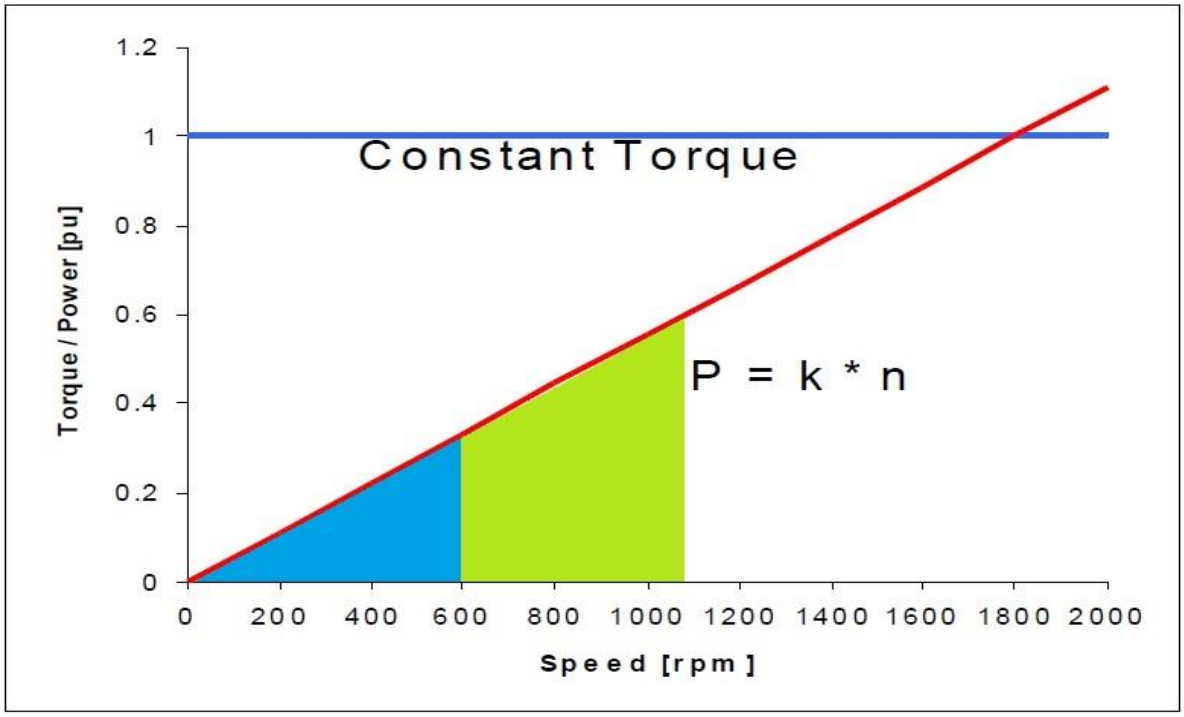

Fig. 6.34: Energy consumption under different initial setting conditions

With more energy being consumed inside the compressor, more heat is produced, so the temperature of the compressor motor increases. Therefore, the energy consumption under two initial conditions are discussed, to find out the impact of the initial temperature setting. In Fig. 6.34, both blue and lime triangles stand for the energy consumed under 100% refrigerant level conditions. Table 6.6 lists two examples of different initial settings. If the initial room temperature is 72°F, and the target temperature is 64°F, the compressor motor speed will be at 100% , which also means that the cooling capacity at the beginning of the cycle is at 100% of its capacity. The speed variation range is 0~100%. If the initial room temperature is 72°F, and the target temperature is 68°F, the compressor motor speed will be at 60%, which also means that the cooling capacity at the beginning of the cycle is at 60% of its capacity. The speed variation range is 0~60%. The compressor power variation curve, shown in Fig. 6.34, explains the relationship between the power and the capacity of the compressor.

6.5.5 Temperature Threshold Settings

Consumers choose HVAC systems because they balance several factors, such as cost, system efficiency, and room size. The most common cooling/heating capacity of a household HVAC system is between 1 to 5 tons. This capacity requirement is largely dependent on room sizes. Suppose there are two rooms, with an area of 2400 ft^2 and 600 ft^2, both of which need a heat pump. A comparative analysis on choosing a suitable temperature threshold is conducted in Fig. 6.35. All of the initial conditions, such as refrigerant level, setting temperature, room temperature, and capacity are the same, with the only difference being room size. The compressors in the two rooms exhibit the same temperature curves for the first 3 minutes. The blue star point in Fig. 6.35 at 3 minutes shows that the capacity starts to decrease in Room 2, which has a

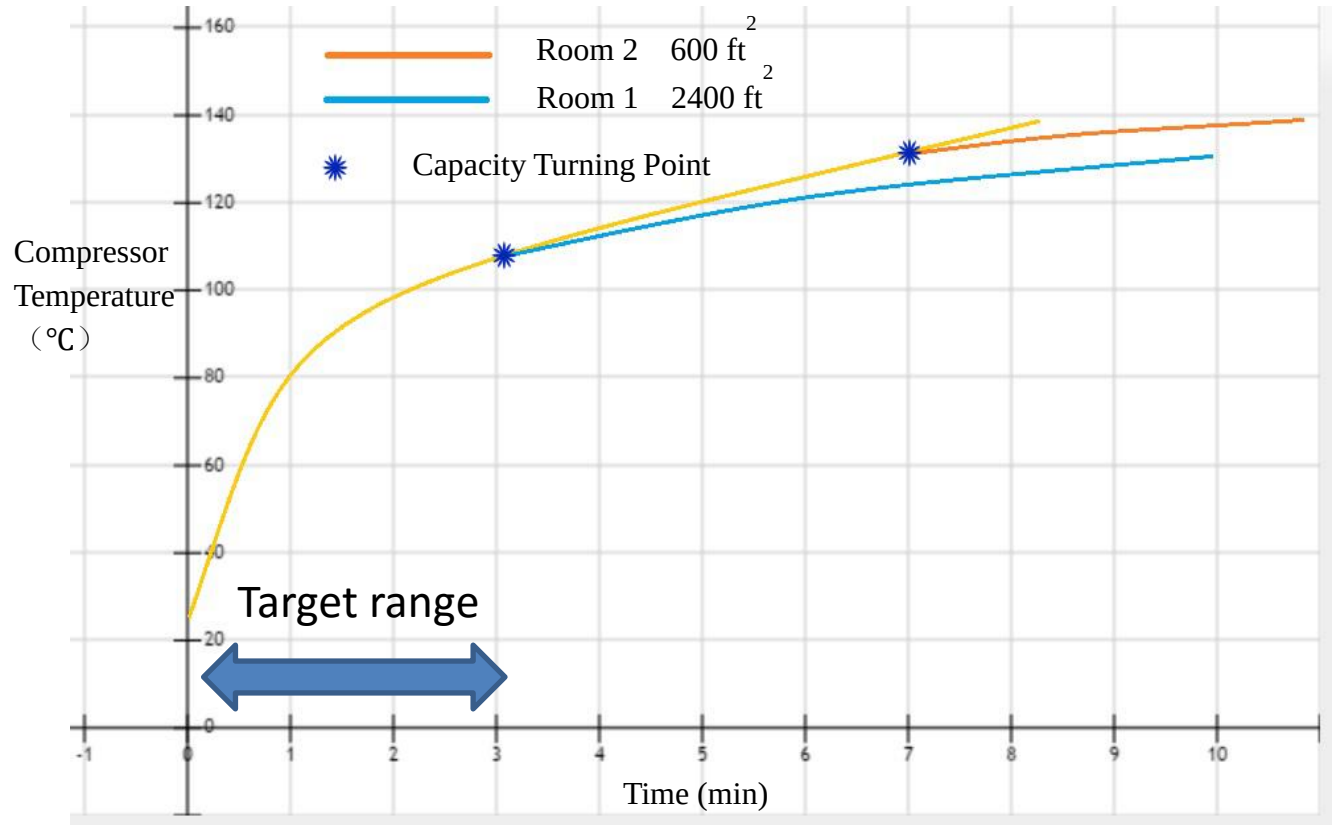

Fig. 6.35: Operation curves for different room sizes

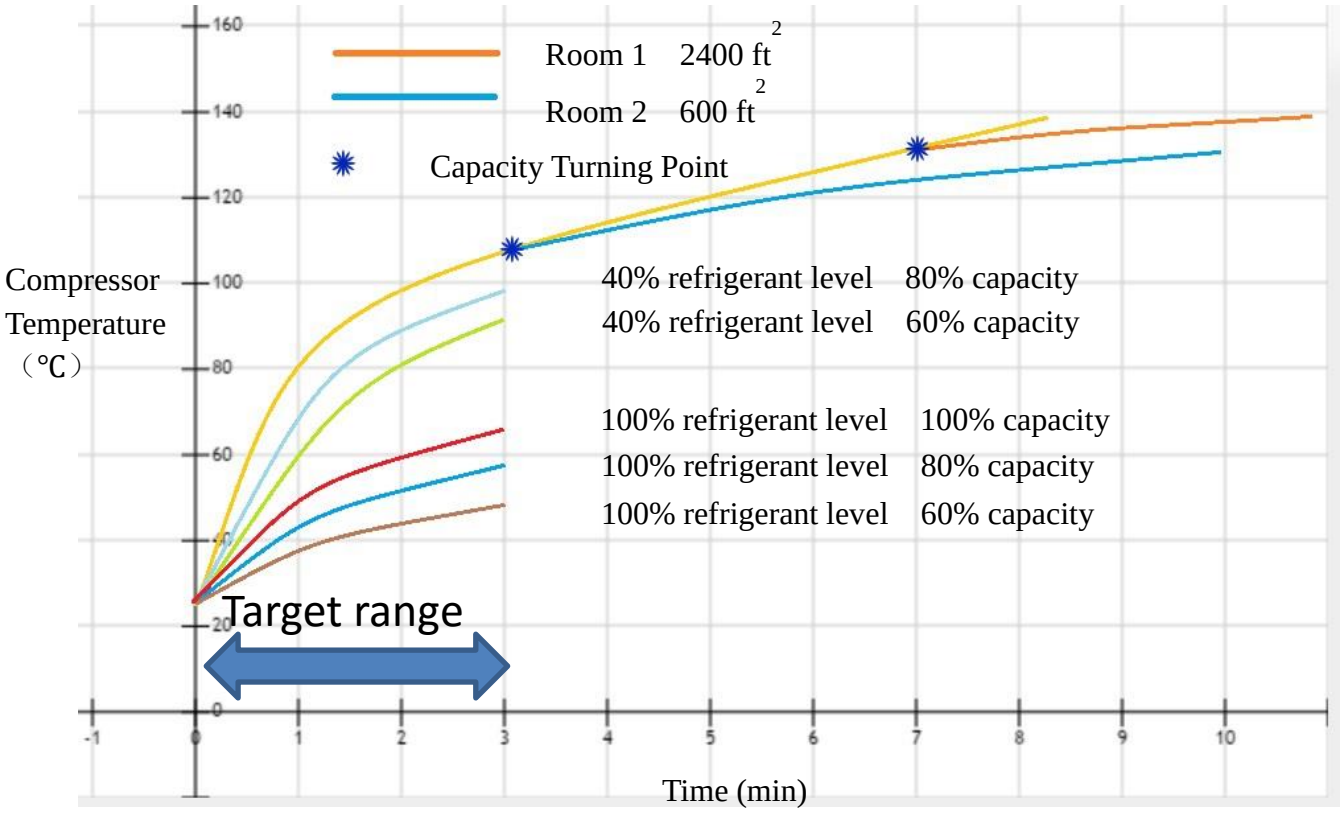

Fig. 6.36: Operation curves for different room sizes and refrigerant levels

smaller area, while the capacity of the compressor in Room 1 stays the same. In addition, the two temperature curves separate at this exact point because of their different capacities at that time. At 7 minutes, the capacity of the compressor in Room 1 is no longer maintained. Fig. 6.35 clearly explains the significant impact of room size on the temperature curve of compressors. In order to differentiate between different refrigerant levels, regardless of room size, the time from 0 to 3 minutes is targeted for further analysis of the temperature threshold.

To go one step further, the target operation curves under different refrigerant levels are considered. For the three curves at 100% refrigerant levels, the slope ratios of these curves are decided by the initial cooling/heating capacity, which is related to the difference between initial setting temperature and room temperature. If a system is undercharged, according to the temperature curves from the experiment, compressor temperature increases. In addition, the temperature gap in Fig. 6.29 between 40% and 100% is huge, and this can be very beneficial in distinguishing between these two conditions.

Several experiments should be conducted in order to gather as much data as possible for use in drawing the temperature threshold curves in Fig. 6.37. One important point which needs to be stated is that the compressor capacity was originally set from 40% to 100%. This gives us the horizontal settings of Fig. 6.37. The undercharged detection can be implemented intermittently once every minute. Furthermore, the amounts of these threshold curves would not be limited if more experiments are conducted.

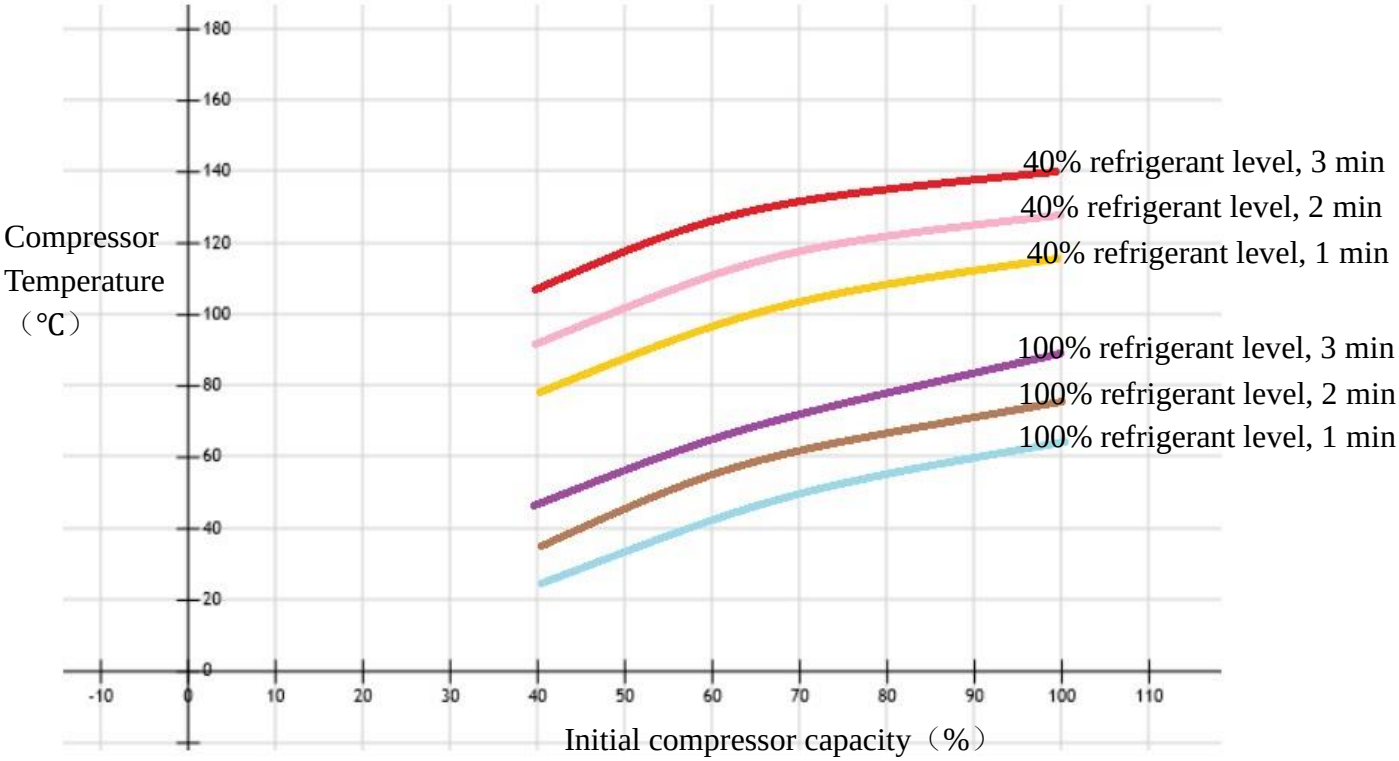

Fig. 6.37: Temperature thresholds for different refrigerant levels

6.6 Conclusions

For each air-conditioning system, a specified amount of refrigerant is required for the system to operate at optimal conditions, in terms of the design discharge and suction pressures. The importance of correct refrigerant charge regarding the amount of refrigerant in an air conditioner affects both the efficiency and capacity of the system. In addition to energy and capacity impacts, incorrect charge can also damage equipment. If the system is overcharged, there is a chance that liquid refrigerant will not completely evaporate and could slug the compressor. If there is too little charge in the system, the low suction line pressure and corresponding saturation temperature of the refrigerant can lead to the formation of ice on the evaporator, which restricts heat transfer, increases airflow resistance, and reduces airflow. This will further reduce air

conditioner performance, and can shorten compressor life. Periodic maintenance of the system can identify and correct the problem. However, in many cases the problem may persist for a long period of time because of poor or no maintenance, resulting in lower system performance and higher energy usage. The traditional method used by technicians is to use temperature sensors and pressure gauges to measure temperature and pressure at suction and discharge ports.

To eliminate the high cost of temperature sensors and pressure gauges, as well as extra labor costs, a new condition monitoring method is proposed based on the relationship between refrigerant level and stator winding resistance. Actually, the cooling capacity is reduced when the refrigerant is insufficient. In order to adjust the temperature with the same requirements as the full charge level, the torque of the compressor is controlled to be higher than rated, thus more energy is being utilized to drive the motor. As the current magnitude is higher, the loss of energy from stator and rotor resistance increases, and more heat is produced inside the motor. Because the stator resistances are assumed to have a linear relationship with temperature, as the time of use increases, the stator winding resistance will bump up. The RLS (recursive square method) estimation method is applied in the research. The RLS is an adaptive filter which recursively finds coefficients that will minimize a weighted linear least squares cost function, relating to the input signals.

To further analyze undercharge problems, one-to-one correspondence of refrigerant levels and compressor motor temperatures is required to set appropriate thresholds of alarm for the HVAC systems. For example, if refrigerant level is 70% of the original settings, the compressor motor temperature can increase to 100°C (normal temperature is 65°C under a refrigerant level of 100%). This thermal dynamic analysis is divided into three steps. The first step is to estimate or measure charge level and mass flow rate. The second step, which is also the key to the whole process, is to calculate

compressor work load. Once a thermal model of the compressor is built, the temperature of some parts of the compressor can be estimated.

The results of the experiment show that the estimated resistance curves under different refrigerant levels can be differentiated. More practically, the estimated temperature gap between normal conditions and 40% conditions are relatively large, which can be easily utilized to implement an undercharged detection algorithm. The specific algorithm is given in detail, and can be universally applied to all models of compressors in HVAC systems, and are independent of room size. The related parameter, which is highly dependent on the compressor model, is the mean value of the low refrigerant limit φ when shutting down the system. Several groups of threshold curves can be measured under different refrigerant levels. It is very intuitive that condition monitoring of refrigerant level can become more accurate if more data is measured to determine the thresholds. The computing capability requirement of DSP for this algorithm is very flexible, and highly dependent on system performance, since the undercharged detection can be implemented intermittently.

CHAPTER 7

CONCLUSIONS, CONTRIBUTIONS AND RECOMMENDATIONS

7.1 Conclusions

7.1.1 Condition Monitoring of Airflow Blockage in Air Handlers

The airflow blockage condition is monitored by merely observing stator current variation. This method can successfully eliminate cost and reliability issues of airflow sensors. For most high efficiency HVAC systems, constant airflow control is a basic function which can continuously control the speed of the fan motor to accommodate the change of the load torque, relating to the pressure change at the inlet or outlet of the air handler. This constant airflow control algorithm is verified under different blockage conditions. Then the main target becomes to estimate airflow variation by detecting fan speed levels. The results of the experiment show that the fundamental frequency increases significantly as the blockage percentage increases. More attention is paid to the amplitude change under different blockage conditions. This can also be utilized to detect the airflow variation, because of load change. However, the speed estimation method is a more straightforward and effective method for an HVAC system, implemented with a constant airflow algorithm.

7.1.2 Condition Monitoring of Unbalanced Loads of Fan Motors in Air Handlers

For most air handlers, the unbalanced load of the blower wheel is created by unevenly distributed contaminants on the blades. In the experiment, the unbalanced load condition is emulated by adding a different number of weights to the inner side

of the blade. The traditional condition monitoring method is to exploit specific characteristic frequency components, which can be used as an index showing unbalanced torque and dynamic eccentricity.

The unbalanced load can create dynamic eccentricity conditions or increase the dynamic eccentricity severity. The main target is to monitor the unevenly distributed contaminants, which can both produce unbalanced conditions, on the blades or a broken blade. Thus, characteristic frequency components of both the unbalanced load conditions and dynamic eccentricity created by the unbalanced loads are observed. Two levels of unbalanced load conditions are examined, with one and two weights added to the inner side of one blade. Experiment results show very clearly that 2/3 and 4/3 of fundamental frequency components increase significantly with respect to the unbalanced load severity, while 1/3 and 5/3 of fundamental frequency components also increase due to dynamic eccentricity. Moreover, since the air handler is running in a relatively stationary mode, with three fixed preset speed levels most of the time, the unbalanced load detection is conducted under constant speed conditions without any speed level change. For the non-stationary condition, the Time-Frequency/Time-Scale Methods can be utilized to detect the faults.

A new stray flux spectrum condition monitoring method is proposed to increase reliability in detecting an unbalanced load condition. The stray flux of an electrical machine is a residual and an undesirable effect which does not participate in the process of generating electromagnetic torque. A high accuracy external flux sensor is used to detect unbalanced load. When the load is unbalanced, the magnetic field of the BLDC motor is not a perfect circle, so additional stray flux appears outside the motor. For a BLDC motor, the rotational harmonics reflecting the asymmetry of the field can be $2f_e$, because an unbalanced load produces even harmonics in the system. Introducing another high accuracy sensor increases the total cost of the system, so this

is mainly applicable for an HVAC system that requires a higher reliability and is of greater importance, for example an HVAC system for a data center.

7.1.3 Condition Monitoring of Static Eccentricity of BLDC Motors in Air Handlers

The fault diagnosis of BLDC motors becomes an essential problem because of the wide range of applications of BLDC (brushless DC) motors. It is known that asymmetries in three-phase BLDC motors may arise for several reasons, such as load fluctuations, unbalanced supply voltages, and static eccentricities. Static eccentricity detection for BLDC motors is relatively difficult compared with dynamic eccentricity. With BLDC motors, the relative permeability of a magnet is equal to that of the air, leading to relatively large air gaps in BLDC motors. Hence, any physical shift causing air gap length change has a negligible effect on flux distribution. Most of the previous research on detecting static eccentricity focuses on the negative sequence current change of BLDC motors.

An improved method for detecting static eccentricity is proposed based on the comparison between the positive sequence current and the negative sequence current. Compared to the traditional method, which only focuses on the change of negative sequences of fundamental frequency current, the method proposed could be more reliable, since the effect of load fluctuations can be largely eliminated. According to the results of the experiment, this method is very effective in detecting severe static eccentricity conditions in this 1/2 HP three phase, six pole and eighteen slot BLDC motor. However, further research on this method can be conducted for all kinds of BLDC motors with different structures and power ratings.

7.1.4 Condition Monitoring of the Refrigerant Level in Refrigeration Systems

For each air-conditioning system, a specified amount of refrigerant is required

for the system to operate at optimal conditions in terms of the design discharge and suction pressures. The importance of correct refrigerant charge for the amount of refrigerant in an air conditioner should be noted, as it affects both the efficiency and capacity of the system. In addition to energy and capacity impacts, incorrect charge can also damage equipment. If the system is overcharged, there is a chance that liquid refrigerant will not completely evaporate, and could slug the compressor. If there is too little charge in the system, the low suction line pressure and corresponding saturation temperature of the refrigerant can lead to ice formation on the evaporator, which restricts heat transfer, increases airflow resistance, and reduces airflow. This will further reduce air conditioner performance and can shorten compressor life. Periodic maintenance of the system can identify and correct the problem. However, in many cases, the problem may persist for a long period of time because of poor or no maintenance, resulting in lower system performance and higher energy usage. The traditional method used by technicians is to use temperature sensors and pressure gauges to measure temperature and pressure at suction and discharge ports.

To eliminate the high cost of temperature sensors and pressure gauges, as well as extra labor costs, a new condition monitoring method is proposed based on the relationship between refrigerant level and stator winding resistance. Cooling capacity is reduced when refrigerant is insufficient. In order to adjust the temperature with the same requirement as the full charge level, the torque of the compressor is controlled to a higher level than it is rated for, thus more energy is utilized to drive the motor. As the current magnitude is higher, loss of energy on the stator and rotor resistance increases, and more heat is produced inside the motor. Because the stator resistances are assumed to have a linear relationship with temperature, as the time of use increase, the stator winding resistance will bump up. The RLS (recursive square method) estimation method is applied in the research. The RLS is an adaptive filter which recursively finds the coefficients that minimize a weighted linear least squares cost function, relating to

the input signals.

To further analyze the undercharge problem, one-to-one correspondence of refrigerant level and compressor motor temperature is required to set appropriate thresholds of alarm for HVAC systems. For example, if refrigerant level is 70% of the original settings, the compressor motor temperature can increase to 100°C (normal temperature is 65°C for a refrigerant level under 100%). This thermal dynamic analysis is divided into three steps. The first step is to estimate or measure charge level and mass flow rate. The second step, which is also crucial to the entire process, is to calculate compressor work load. Once a thermal model of compressor is built, the temperature of some parts of the compressor can be estimated.

The results of the experiment show that the estimated resistance curves under different refrigerant levels can be differentiated. More practically, the estimated temperature gap between normal conditions and 40% conditions are relatively large, and can be easily utilized to implement an undercharged detection algorithm. The specific algorithm is given in detail, and can be universal for all models of compressors in HVAC systems, and is independent of room size. The related parameter, which is highly dependent on the compressor model, is the mean value of the low refrigerant limit φ when shutting down the system. Several groups of threshold curves can be measured under different refrigerant levels. It is very intuitive that the condition monitoring of the refrigerant level can be more accurate if more data is measured to obtain the thresholds. The requirement of the computing capability of DSP for this algorithm is very flexible and is highly dependent on system performance, since the undercharged detection can be implemented intermittently.

7.2 Contributions

The contributions of this study are listed as follows:

- A literature study and investigation into the condition monitoring of faults in the air handlers and outdoor units of HVAC systems such as airflow blockage, unbalanced load of BLDC fan motors, static eccentricity of BLDC fan motors and online estimation of PMSM resistance. In addition, a literature review of stray flux detection in induction machines is presented in detail. The development and application of the stray flux detection method is compared with stator current detection, considering stator insulation failure, bearing faults, eccentricity and broken rotor bar/end-ring. Since there is limited research regarding stray flux detection in BLDC motors and the stray flux method is used mostly for induction machines, its potential application for PMSM and BLDC is included.

- A current based condition monitoring method is established to detect airflow blockage in an air handler. The airflow blockage condition is monitored by merely observing stator current variation. This method can successfully eliminate the cost and reliability issues of airflow sensors. For the relevant HVAC systems, which have constant airflow control, this fault diagnostic method would be very easy and it would be a straightforward process to add it to the original control algorithm.

- A new stray flux spectrum condition monitoring method is proposed to increase the reliability in detecting an unbalanced load condition. The stray flux of an electrical machine is a residual and undesirable effect which does not participate in the process of generating electromagnetic torque. A high accuracy external flux sensor is used to detect unbalanced load. Introducing another high accuracy sensor increases the total cost of the system, so this is mainly applicable to an HVAC

system which requires higher reliability and is of greater importance, for example an HVAC system in a data center.

- Detecting static eccentricity in BLDC motors is relatively difficult compared to detecting dynamic eccentricity. Most of the previous research on detecting static eccentricity focuses on the negative sequence current changes in BLDC motors. An improved method in detecting static eccentricity is proposed based on the comparison between positive sequence current and negative sequence current. Compared to the traditional method, which only focuses on the change of negative sequences of fundamental frequency current, the method proposed could be more reliable, since the effect of load fluctuations can be largely eliminated. According to the experiment results, this method is very effective in detecting severe static eccentricity conditions in a 1/2 HP three phase, six pole and eighteen slot BLDC motor. However, further research on this method can be conducted for all kinds of BLDC motors with different structures and power ratings.

- A current-based nonintrusive condition monitoring method is established for refrigerant level detection. This method can eliminate the high cost of temperature sensors and pressure gauges, as well as the extra labor costs of periodic examinations. A thermal model of the compressor is analyzed under insufficient refrigerant level conditions to explore the mathematical relationship between refrigerant level and stator winding resistance. The recursive least square (RLS) method is implemented to estimate the winding resistance.

- An offline back-EMF constant detection method is proposed specifically for PMSM motors in compressors. It utilizes the circumstance that the PMSM inside the scroll compressor runs backwards for a short time after shutting off the power supply, so that the internal pressures are equalized. At that time, the terminal voltage equals to the back-EMF in the circuit which can help to calculate the

back-EMF constant. The momentary reversal of direction of the scrolls has few effects on the compressor stability and lifespan. This is also a very normal condition which produces some noise when shutting down the system.

- A systematical algorithm of condition monitoring refrigerant levels is developed. The estimated temperature gap between normal conditions and 40% conditions is relatively large, and thus can be easily utilized to implement an undercharged hazard alarm. The specific algorithm is given in detail, and can be universally applied for all models of compressors in HVAC systems, and is independent of room sizes. Moreover, the refrigerant level detection is conducted under different cooling capacity conditions, which means the effect of compressor motor speed variation is considered. This condition monitoring method can be very accurate if enough data is measured to acquire the temperature thresholds.

7.3 Recommendations

7.3.1 Condition Monitoring of Multi-Faults in Outdoor Unit

There are several faults that can occur with an outdoor unit of an HVAC system, and they can exist individually or in any combination. The four main parts of outdoor units, including condensers, evaporators, expansion valves and compressors, can all suffer different faults. For the compressor, refrigerant can be undercharged or overcharged. The thermal expansion valve can possibly become stuck or defective after a long run. Condenser and evaporator fouling is another common problem which can happen from time to time. However, these individual problems are not that difficult to handle compared with a combination of different faults, which creates a multitude of symptoms. For example, a problem with a liquid line restriction or non-condensable

contaminants in the system can lead to a false diagnosis of refrigerant charge. Many service technicians often become confused when the liquid line becomes restricted in the refrigeration system. This is because the symptoms often look like an undercharge of refrigerant. The difficulty of using condition monitoring to detect multiple faults that are interconnected is the main concern of the system in the future.

7.3.2 Design a Sensor-less Constant Airflow Control Method for Blower Wheels of Air Handlers

It has been shown in previous studies that the efficiency of a heating or cooling system will improve significantly when the air flow rate through the heat exchanging unit is maintained at a constant level. Recently, constant air flow rate control has become an important criterion for appliance manufacturers in selecting blower drives, due to the increasing government regulations on the system efficiency of air-moving appliances. Besides the advantage of higher system efficiency, constant air flow rate control can also provide better temperature and humidity control, and raise the comfort level of the residents. A number of research efforts have been directed toward the development of a constant air flow rate controller for blowers in residential HVAC systems. In general, to control air flow rate to a set point, regardless of load variation, the motor must vary its speed according to the air pressure in the duct work. Thus, a variable-speed drive equipped with air pressure sensors in the duct work is generally needed to realize the control. However, this approach is not practical from a cost and reliability point of view, as the pressure sensors increase cost and reduce reliability of the whole system. So, the project will aim to develop a simple but effective method to control the air flow rate of an inverter-driven blower.

Since the original control board and converters are provided by Carrier, some of the research will be limited. So, it will be useful to build the controller and converters or

use another ac unit that is at GT. Although there are some constant airflow control methods used in the industry, it is still quite important and valuable to build a new algorithm which is more accurate for the BLDC fan motor. On the other hand, having a custom control board will become more necessary to study faults in parts of the controller, such as the inverter.

7.3.3 Noise Issue in Air Handlers with BLDC Fan Motors

Noise levels in household appliances are attracting increased attention from manufacturers and customers. Legislation is becoming stricter on acceptable noise levels, and low noise is a major marketing point for many products. Currently, many appliance manufacturers are favoring the use of brushless direct-current (BLDC) motors or PMSMs for compressors in refrigerators and air conditioners, and in applications for circulation fans because of their higher efficiency, high power density, low weight, and low cost in comparison with AC induction motors or other variable-speed drives. These motors are especially advantageous for fan applications, because of their wide speed range, easy speed controllability, high efficiency, and long lifetime expectancy. However, permanent magnetic motors are disadvantageous from a vibration and noise point of view, caused by the commutation in the trapezoidal drive and cogging torque.

In practice, it is desirable for a PMSM to have a sinusoidal back-EMF waveform and BLDC motor to have a trapezoidal back-EMF waveform, in order to minimize the torque ripple and maximize the efficiency and torque capability. The goal is to find a new method to reduce the torque ripple of a permanent magnetic motor with a sinusoidal back-emf wave using sensor-less trapezoidal control. In some previous research, sensored direct torque control has been applied to a BLDC drive, and its utility has been validated by simulations and measurements on two permanent

magnetic motors which have very different back-EMF waveforms. It has been shown that DTC is capable of instantaneous torque control and, thereby, of reducing torque pulsations. The sensorless DTC and conventional current control will be compared in future research as well based on the torque ripple reduction and rapid torque response.

APPENDIX A: STATOR RESISTANCE ESTIMATION USING RLS METHOD

Matlab code:

```
%initialization
p=length(Xmax1);
f=Xmax1(1:p);

k1=10/(2)^0.5;
k2=2^0.5;
I=Ymax1(1:p)*k1;     % peak to rms
Ur=135*Ymax2(1:p)*k2;   % peak to rms
Vpeak/Vsensor_peak=380/2.8=135

N=length(f);

ramda=0.9999;
deltaT=0.02;

a=1000;
Pc=a*repmat(eye(2),1,N);
theta=zeros(N,2);
Z=zeros(2,N);
U=zeros(1,N);

for n=1:N;
U(n)= Ur(n)/3^0.5-0.077*(1-0.01)*2*pi*f(n);
end
Z=[(I)',(U)']';

for n=1:(N-1)
%RLS
Pc(1:2,2*n+1:2*n+2)=1/ramda*(Pc(1:2,2*n-1:2*n)-Pc(1:2,2*n-1:2*
n)*Z(:,n)*(ramda+(Z(:,n))'*Pc(1:2,2*n-1:2*n)*Z(:,n))^-1*(Z(:,n
))'*Pc(1:2,2*n-1:2*n));
%I(n+1)=A(n)*I(n)+B(n)*U(n);
theta(n+1,:)= theta(n,:)+
(I(n+1)-theta(n,:)*Z(:,n))*(Z(:,n))'*Pc(1:2,2*n-1:2*n);
```

```
end

A=theta(:,1);
B=theta(:,2);

L=deltaT./B;
R=(ones(N,1)-A)./B;

%temperature estimation
R0=2;    %measured resistance under normal temperature
k=225;
T0=25;   %normal temperature
T=R/R0*(T0+k)-k;
figure(2);
plot(T(3:end));
hold on
%ylim([0 100]);
```

APPENDIX B: TECHNICAL PARAMETERS OF INDOOR AND OUTDOOR UNIT

B1. Fan motor

- Genteq ECM 3.0 BLDC motor
- 120V/ 240V AC single-phase input, 50/60Hz
- Designed for direct-drive blower applications in residential systems up to 5-tons
- Variable speed operation from 200 -1300 rpm and a high speed option at 200-1800 rpm

B3. Outdoor unit

- Variable speed compressor with capacity range from 40--100%
- Air cooled Inverter variable speed drive
- 2 control wires to outdoor unit
- High pressure switch

REFERENCES

[1] https://www.trane.com/residential/en/resources/glossary/what-is-a-heat-pump.html

[2] http://www.seai.ie/Your_Business/Sustainable_Energy_Awards/Shortlist_2014/Summaries_of_Shortlisted_Projects/category3.html.

[3] L. Pérez-Lombard, J. Ortiz, and C. Pout, “A review on building’s energy consumption information,” Energy Build., vol. 40, no. 3, pp. 394–398, 2008

[4] Reliability and Functional Availability of HVAC Systems, Sonn Myrefelt

[5] D. He, C. Jiang, R. G. Harley, T. G. Habetler and R. Ding, "A new electrical method on airflow fault detection of air handling unit (AHU)," *Power Systems Conference (PSC), 2015 Clemson University*, Clemson, SC, 2015, pp. 1-5.

[6] https://highperformancehvac.com/heat-pump-components/

[7] http://highperformancehvac.com/common-problems-air-handlers/

[8] https://en.wikipedia.org/wiki/Condition_monitoring

[9] S. Nandi, H. A. Toliyat and X. Li, "Condition monitoring and fault diagnosis of electrical motors-a review," in *IEEE Transactions on Energy Conversion*, vol. 20, no. 4, pp. 719-729, Dec. 2005.

[10] ASHRAE, "ASHRAE Handbook: Fundamentals," ed. Atlanta, GA,, 2001

[11] P. Francisco and L. Palmiter, "Field evaluation of a new device to measure air handler flow," ASHRAE Transactions, vol. 109, pp. 403-412, 2003.

[12] K. R. D. Westphalen, and J. Brodrick, "Duct leakage fault detection," ASHRAE Journal, vol. 47, pp. 56-58, August 2005.

[13] R. W. Cox, "Minimally intrusive strategies for fault detection and energy monitoring," Ph D, Massachusetts Institute of Technology, 2006.

[14] M. H. F. D. S. a. D. J. Oldham, "The development of a rapid single spectrum method for determining the blockage characteristics of a finite length duct," Journal of Sound and Vibration, vol. 243, pp. 625-640, June 2001.

[15] C. R. Laughman, "Fault detection methods for vapor-compression air conditioners using electrical measurements," Ph D, Massachusetts Institute of Technology, 2008.

[16] S. Rajagopalan, J. M. Aller, J. A. Restrepo, T. G. Habetler, and R. G. Harley, “Analytic-wavelet-ridge-based detection of dynamic eccentricity in brushless direct current (BLDC) motors functioning under dynamic operating conditions,” IEEE Trans. Ind. Electron., vol. 54, no. 3, pp. 1410–1419, Jun. 2007.

[17] Satish Rajagopalan; le Roux, W.; Habetler, T.G.; Harley, R.G., "Diagnosis of

potential rotor faults in brushless DC machines," in *Power Electronics, Machines and Drives, 2004. (PEMD 2004). Second International Conference on (Conf. Publ. No. 498)* , vol.2, no., pp.668-673 Vol.2, March 31 2004-April 2 2004

[18] Kral, C.; Habetler, T.G.; Harley, R.G., "Detection of mechanical imbalances of induction machines without spectral analysis of time-domain signals," in *Industry Applications, IEEE Transactions on* , vol.40, no.4, pp.1101-1106, July-Aug. 2004

[19] Obaid, R.R.; Habetler, T.G., "Effect of load on detecting mechanical faults in small induction motors," in *Diagnostics for Electric Machines, Power Electronics and Drives, 2003. SDEMPED 2003. 4th IEEE International Symposium on* , vol., no., pp.307-311, 24-26 Aug. 2003

[20] Henao, H.; Demian, C.; Capolino, G.-A., "A frequency-domain detection of stator winding faults in induction machines using an external flux sensor," in *Industry Applications, IEEE Transactions on* , vol.39, no.5, pp.1272-1279, Sept.-Oct. 2003

[21] Khmais Bacha, Humberto Henao, Moncef Gossa, Gérard-André Capolino, Induction machine fault detection using stray flux EMF measurement and neural network-based decision, Electric Power Systems Research, Volume 78, Issue 7, July 2008, Pages 1247-1255, ISSN 0378-7796

[22] Vitek, O.; Janda, M.; Hajek, V.; Bauer, P., "Detection of eccentricity and bearings fault using stray flux monitoring," in *Diagnostics for Electric Machines, Power Electronics & Drives (SDEMPED), 2011 IEEE International Symposium on* , vol., no., pp.456-461, 5-8 Sept. 2011

[23] Rastegar Fatemi, S.M.J.; Henao, H.; Capolino, G.A., "The Effect of the Mechanical Behavior on the Stray Flux in an Induction Machine Based Electromechanical System," in *Diagnostics for Electric Machines, Power Electronics and Drives, 2007. SDEMPED 2007. IEEE International Symposium on* , vol., no., pp.155-160, 6-8 Sept. 2007

[24] C. Jiang, T. G. Habetler and W. p. Cao, "Improved condition monitoring of the faulty blower wheel driven by brushless DC motor in air handler unit (AHU)," *2016 IEEE Energy Conversion Congress and Exposition (ECCE)*, Milwaukee, WI, 2016, pp. 1-5.

[25] Satish Rajagopalan, “detection of rotor and load faults in brushless dc motors operating under stationary and non-stationary conditions,” PhD, Georgia Institute of Technology, 2006

[26] L. Wu, B. Lu, X. Huang, T. G. Habetler, and R. G. Harley, “Improved online condition monitoring using static eccentricity-induced negative sequence current

information in induction machines," in Proc. 32nd IEEE IECON, Nov. 2005, pp. 1737–1742.

[27] Shakouhi, S.M. ; Mohamadian, M. ; Afjei, S.E, "control of BLDC motor in presence of static rotor eccentricity," in Electrical Machines and Power Electronics and 2011 Electromotion Joint Conference (ACEMP). 2011, pp. 43–48.

[28] C. Jiang and T. G. Habetler, "Static eccentricity fault detection of the BLDC motor inside the air handler unit (AHU)," *2015 IEEE International Electric Machines & Drives Conference (IEMDC)*, Coeur d'Alene, ID, 2015, pp. 1473-1476.

[29] Kexin Yang, Taizhi Liu, Rui Zhang, Dae-Hyun Kim, Linda Milor, Front-end of line and middle-of-line time-dependent dielectric breakdown reliability simulator for logic circuits, Microelectronics Reliability, 2017, ISSN 0026-2714.

[30] K. Yang and L. Milor, "Impact of stress acceleration on mixed-signal gate oxide lifetime," *2015 IEEE 20th International Mixed-Signals Testing Workshop (IMSTW)*, Paris, 2015, pp. 1-6.

[31] T. Liu, C. C. Chen, J. Wu and L. Milor, "SRAM stability analysis for different cache configurations due to Bias Temperature Instability and Hot Carrier Injection," *2016 IEEE 34th International Conference on Computer Design (ICCD)*, Scottsdale, AZ, 2016, pp. 225-232.

[32] T. Liu; C. C. Chen; L. Milor, "Comprehensive Reliability-Aware Statistical Timing Analysis Using a Unified Gate-Delay Model for Microprocessors," in *IEEE Transactions on Emerging Topics in Computing*, vol.PP, no.99, pp.1-1

[33] Sang-Bin Lee, Thomas G. Habetler, "An online stator winding resistance estimation technique for temperature monitoring of line-connected induction machines", *IEEE Trans. Ind. Appl.*, vol. 39, no. 3, May. 2014

[34] Nikola Z. Popov, Slobodan N. Vukosavic, "Motor temperature monitoring based on impedance estimation at PWM frequencies," *IEEE Trans. Energy Conv.*, vol. 29, no. 1, pp. 215-223, Mar. 2014.

[35] X. Jiang, Z. Zhang, P.Sun Z., 'Estimation of Temperature Rise in Stator Winding and Rotor Magnet of PMSM Based on EKF', 3rd International Conference on Computer and Electrical Engineering ICCEE, 2010

[36] T. Huber, W. Peters and J. Böcker, "Monitoring critical temperatures in permanent magnet synchronous motors using low-order thermal models," *Power Electronics Conference (IPEC-Hiroshima 2014 - ECCE-ASIA), 2014 International*, Hiroshima, 2014, pp. 1508-1515.

[37] T. Goktas; M. Zafarani; K. W. Lee; B. Akin; T. Sculley, "A Comprehensive

Analysis of Magnet Defect Fault Monitoring Through Leakage Flux," in *IEEE Transactions on Magnetics* , vol.PP, no.99, pp.1-1

[38] P.J. Tavner, P. Hammond, J. Penman, “Contribution to the study of leakage fields at the ends of rotating electrical machines”, IEE, Vol. 125, N°12, 1978, pp.1339-1349.

[39] R. Romary, R. Pusca, J. P. Lecointe and J. F. Brudny, "Electrical machines fault diagnosis by stray flux analysis," 2013 IEEE Workshop on Electrical Machines Design, Control and Diagnosis (WEMDCD), Paris, 2013, pp. 247-256.

[40] O. Chadebec, J.L. Coulomb, V. Leconte, J.P. Bongiraud, G. Cauffet, “Modeling of static magnetic anomaly created by iron plates”. IEEE Trans. on magnetics, Vol. 36, N°4, pp. 667-671, July 2000.

[41] Y. Du, T.C. Cheng, A.S. Farag, “Principles of power-frequency magnetic field shielding with flat sheets in a source of long conductors”. IEEE Trans. on Electromagnetic compatibility, Vol. 38, N°3, pp. 450-459, August 1996

[42] A. Canova, A. Manzin, M. Tartaglia, “Evaluation of different analytical and semi-analytical methods for the design of ELF magnetic field shields”, IEEE Trans. on Industry Applications, vol. 38, N°3, pp. 788-796, May/June 2002.

[43] P. Moreno, R.G. Olsen, “A simple theory for optimizing finite width ELF magnetic field shielding for minimum dependence on source orientations”, IEEE Trans. on Electromagnetic Compatibility, vol. 39, N°4, pp. 340-348, Nov. 1997.

[44] G. Le Coat, A. Foggia, J. Bongiraud and P. Le Thiec, "Electromagnetic signature of induction machines," in IEEE Transactions on Energy Conversion, vol. 14, no. 3, pp. 628-632, Sep 1999. doi: 10.1109/60.790926

[45] V. P. Bui, O. Chadebec, L. L. Rouve and J. L. Coulomb, "Fast Models to Predict the Magnetic Stray Field Created by Faulty Electrical Machines," 2007 IEEE International Electric Machines & Drives Conference, Antalya, 2007, pp. 1594-1598.

[46] H. Henao, G. A. Capolino and C. Martis, "On the stray flux analysis for the detection of the three-phase induction machine faults," 38th IAS Annual Meeting on Conference Record of the Industry Applications Conference, 2003., 2003, pp. 1368-1373.

[47] V. Kokko, “Condition monitoring of squirrel-cage motors by axial magnetic flux measurements,” M.S. thesis, Dept. Elect. Eng., Optoelectron. Meas., Univ. Oulu, Oulu, Finland, 2006.

[48] L. Frosini, C. Harlişca and L. Szabó, "Induction Machine Bearing Fault Detection by Means of Statistical Processing of the Stray Flux Measurement," in IEEE Transactions on Industrial Electronics, vol. 62, no. 3, pp. 1846-1854, March 2015.

[49] R Chandralekha and D Jayanthi, “Diagnosis of Faults in Three Phase Induction Motor using Neuro Fuzzy Logic,” International Journal of Applied Engineering Research ISSN 0973-4562 Volume 11, Number 8 (2016) pp 5735-5740

[50] Khmais Bacha, Humberto Henao, Moncef Gossa, Gérard-André Capolino, Induction machine fault detection using stray flux EMF measurement and neural network-based decision, Electric Power Systems Research, Volume 78, Issue 7, July 2008, Pages 1247-1255, ISSN 0378-7796,

[51] T. Ghanbari and A. Farjah, "A Magnetic Leakage Flux-Based Approach for Fault Diagnosis in Electrical Machines," in IEEE Sensors Journal, vol. 14, no. 9, pp. 2981-2988, Sept. 2014. doi: 10.1109/JSEN.2014.2319175

[52] J. M. Corres, J. Bravo, F. J. Arregui, and I. R. Matias, “Unbalance and harmonics detection in induction motors using an optical fiber sensor,” IEEE Sensors J., vol. 6, no. 3, pp. 605–612, Jun. 2006.

[53] J. G. Mueller and T. G. Pratt, “A radio frequency polarimetric sensor for rotating machine analysis,” IEEE Sensors J., vol. 13, no. 12, pp. 4866–4873, Dec. 2013.

[54] T. Goktas; M. Zafarani; K. W. Lee; B. Akin; T. Sculley, "A Comprehensive Analysis of Magnet Defect Fault Monitoring Through Leakage Flux," in *IEEE Transactions on Magnetics* , vol.PP, no.99, pp.1-1

[55] M. Riera-Guasp, J. Antonino-Daviu, and G. Capolino,"Advances in electrical machine, power electronic and drive condition monitoring and fault detection: state of the art," IEEE Transactions on Industrial Electronics, Vol. 62, No. 3, pp.1746-1759, March 2015.

[56] Zheng Liu, W. Cao, P. H. Huang, G. Y. Tian and J. L. Kirtley, "Non-invasive winding fault detection for induction machines based on stray flux magnetic sensors," 2016 IEEE Power and Energy Society General Meeting (PESGM), Boston, MA, 2016, pp. 1-6.

[57] J. W. Wilson, G. Y. Tian, and S. Barrans, "Residual magnetic field sensing for stress measurement," Sensors and Actuators A: Physical, Vol. 135, pp. 381-387, 2007.

[58] L. Frosini, A. Borin, L. Girometta and G. Venchi, "A novel approach to detect short circuits in low voltage induction motor by stray flux measurement," 2012 XXth International Conference on Electrical Machines, Marseille, 2012, pp. 1538-1544.

[59] V. Fireteanu, P. Lombard and A. I. Constantin, "Detection of a short-circuit fault in the stator winding of induction motors through neighboring magnetic field harmonics," 2014 International Conference on Electrical Machines (ICEM), Berlin, 2014, pp. 1555-1561.

[60] Motor Reliability Working Group, "Report of Large Motor Reliability Survey of Industrial and Commercial Installations," Part I, II. IEEE Transactions on Industry Applications, vol. IA-21, pp. 853-872, 1985.

[61] Negrea, M.D., "Electromagnetic flux monitoring for detecting faults in electrical machines," Helsinki University of Technology, Laboratory of Electromechanics, Helsinky, Finland, 2006. ISBN 951-22-8477-4

[62] F. Immovilli, A. Bellini, R. Rubini, C. Tassoni, "Diagnosis of Bearing Faults in Induction Machines by Vibration or Current Signals: A Critical Comparison," IEEE Transactions on Industry Applications, vol. 46, No.4, pp. 1350 – 1359, Jul./Aug. 2010.

[63] O. Vitek, M. Janda, V. Hajek and P. Bauer, "Detection of eccentricity and bearings fault using stray flux monitoring," 8th IEEE Symposium on Diagnostics for Electrical Machines, Power Electronics & Drives, Bologna, 2011, pp. 456-461.

[64] D. Morinigo-Sotelo, O. Duque-Perez, L. A. Garcia-Escudero, and M. Perez-Alonso, "Bearing lubrication assessment using an statistical analysis of the stator current spectrum," in Proceedings of the XIX International Conference on Electrical Machines (ICEM' 2010) Rome (Italy), 2010, pp. 1-6.

[65] R. Hoppler and R.A. Errath, "Motor bearings, not just a piece of metal," in Proceedings of the IEEE Cement Industry Technical Conference Record, Charleston (USA), 2007, pp. 214-233.

[66] R.R. Schoen, T.G. Habetler, F. Kamran, R.G. Bartfield, "Motor bearing damage detection using stator current monitoring," IEEE Transactions on Industry Applications, vol. 31, No.6, pp. 1274 – 1279, Nov./Dec. 1995.

[67] C. Harlişca, L. Szabó, L. Frosini and A. Albini, "Diagnosis of rolling bearings faults in electric machines through stray magnetic flux monitoring," 2013 8TH INTERNATIONAL SYMPOSIUM ON ADVANCED TOPICS IN ELECTRICAL ENGINEERING (ATEE), Bucharest, 2013, pp. 1-6.

[68] V. Kokko "Condition monitoring of squirrel-cage motors by axial magnetic flux measurements" Doctoral dissertation, University of Oulu (2003).

[69] F. Zidat et al. "Non invasive sensors for monitoring the efficiency of acelectrical rotating machines", Sensors, 10, pp. 7874-7895, (2010).

[70]M. Gomez-Parra et al., "2009 ECCE — predictive maintenance techniques to determine dirt in railway traction motors using radial stray flux analysis," 2009 IEEE Energy Conversion Congress and Exposition, San Jose, CA, 2009, pp. 248-255.

[71]R Chandralekha and D Jayanthi, “Diagnosis of Faults in Three Phase Induction Motor using Neuro Fuzzy Logic,” International Journal of Applied Engineering Research ISSN 0973-4562 Volume 11, Number 8 (2016) pp 5735-5740

[72]P. Ferrari, A. Mariscotti, A. Motta and P. Pozzobon, "Electromagnetic emissions from electrical rotating machinery," in IEEE Transactions on Energy Conversion, vol. 16, no. 1, pp. 68-73, Mar 2001.

[73]S. Nandi, S. Ahmed and H.A. Toliyat, “Detection of rotor slot and other eccentricity related harmonics in a three phase induction motor with different rotor cages,” IEEE Transactions on Energy Conversion. Vol. 16, pp. 253-260, 2001

[74]Mohamed Salah, Khmais Bacha, Abdelkader Chaari, An improved spectral analysis of the stray flux component for the detection of air-gap irregularities in squirrel cage motors, ISA Transactions, Volume 53, Issue 3, May 2014, Pages 816-826, ISSN 0019-0578

[75]O. Vitek, M. Janda and V. Hajek, "Effects of eccentricity on external magnetic field of induction machine," Melecon 2010 - 2010 15th IEEE Mediterranean Electrotechnical Conference, Valletta, 2010, pp. 939-943.

[76]H. Wang, X. Bao, C. Di and Z. Cheng, "Detection of eccentricity fault using slot leakage flux monitoring," 2015 9th International Conference on Power Electronics and ECCE Asia (ICPE-ECCE Asia), Seoul, 2015, pp. 2188-2193.

[77]Ielyzaveta ISHKOVA, Ondřej VÍTEK, “Detection and classification of faults in induction motor by means of motor current signature analysis and stray flux monitoring”, PRZEGLĄD ELEKTROTECHNICZNY, ISSN 0033-2097, R. 92 NR 4/2016

[78]Sheng-Ming Yang, "A constant air flow rate control of blower for residential applications," in *IEEE Transactions on Industry Applications*, vol. 34, no. 2, pp. 263-267, Mar/Apr 1998.

[79]Henao, H.; Demian, C.; Capolino, G.-A., "A frequency-domain detection of stator winding faults in induction machines using an external flux sensor," in *Industry Applications, IEEE Transactions on* , vol.39, no.5, pp.1272-1279, Sept.-Oct. 2003

[80]Salah, M.; Bacha, K.; Chaari, A., "Load torque effect on diagnosis techniques consistency for detection of mechanical unbalance," in *Control, Decision and*

Information Technologies (CoDIT), 2013 International Conference on , vol., no., pp.770-775, 6-8 May 2013

[81] Measure Guideline: Air Conditioner Diagnostics, Maintenance, and Replacement, D. Springer and B. Dakin PE Alliance for Residential Building Innovation (ARBI),2013

[82] Goswami, D.Y.; Ek, G.; Leung, M.; Jotshi, C.K.; Sherif, S.A.; Colacino, F., "Effect of refrigerant charge on the performance of air-conditioning systems," *Energy Conversion Engineering Conference, 1997. IECEC-97., Proceedings of the 32nd Intersociety* , vol.3, no., pp.1635,1640 vol.3, 27 Jul-1 Aug 1997

[83] R. Raber, Spektralmethode zur Fehlerfriiherkennung in warmetechnischen Anlagen," Diss. ETH Nr. 12234, 1997

[84] J. J. Gertler, "Fault Detection and Diagnosis in Engineering Systems," Marcel Dekker, 1998.

[85] T. M. Rossi and J. E. Braun, "A Statistical, Rule-Based Fault Detection and Diagnostic Method for Vapour Compression Air Condition*ers,"* HVAC&R Research, Vol. 3, No. 1, pp. 19-37, 1997.

[86] R. J. Patton, F. J. Uppal, C. J. Lopez-Toribio, ''Soft Computing Approaches to Fault Diagnosis for Dynamic Systems: A Survey," Preprints of 4" IFAC SAFEPROCESS Svmuosium, Vol. 1, pp. 298-3 11,2000.

[87] R. H. J. Welch and G. W. Younkin, "How temperature affects a servomotor's electrical and mechanical time constants," *Industry Applications Conference, 2002. 37th IAS Annual Meeting. Conference Record of the*, Pittsburgh, PA, USA, 2002, pp. 1041-1046 vol.2.

[88] Marco C. Diniz, Evandro L.L. Pereira, Cesar J. Deschamps, A lumped-parameter thermal model for scroll compressors including the solution for the temperature distribution along the scroll wraps, International Journal of Refrigeration, Volume 53, 2015, Pages 184-194, ISSN 0140-7007

[89] http://www.hvacrinfo.com/scroll_trouble.htm

[90] http://hvacronline.co.za/index.php/more/regular-contributors/selele-mashilo/1655 refrigeration-compressor-capacity

[91] Impacts of Refrigerant Charge on Air Conditioner and Heat Pump Performance, Woohyun Kim, James E. Braun, *Purdue University, International Refrigeration and Air Conditioning Conference*